Flow properties of 3He in dilute 3He-4He mixtures at temperatures between 10 and 150 mK

FLOW PROPERTIES OF ^{3}He IN DILUTE ^{3}He-^{4}He MIXTURES AT TEMPERATURES BETWEEN 10 AND 150 mK

C.A.M. CASTELIJNS

FLOW PROPERTIES OF ^{3}He IN DILUTE ^{3}He-^{4}He MIXTURES AT TEMPERATURES BETWEEN 10 AND 150 mK

PROEFSCHRIFT

DOOR

CORNELIS ADRIANUS MARCELLUS CASTELIJNS

GEBOREN TE TILBURG

Dit proefschrift is goedgekeurd door de promotoren
Prof. Dr. H.M. Gijsman en Prof. Dr. W. van Haeringen.
co-promotor: Dr. A.T.A.M. de Waele.

Aan mijn moeder
Aan Marian

CONTENTS

I   INTRODUCTION

1.1   *Short review*

In low temperature physics cooling produced by dilution of
^{3}He into a ^{3}He-^{4}He mixture plays an important role. This technique
was first proposed in 1951 by London (Lon51) and further
elaborated by London, Clarke and Mendoza in 1962 (Lon62). In 1964
the first dilution refrigerator was built by Das, de Bruyn Ouboter
and Taconis in Leiden (Das64). Nowadays, dilution refrigerators
are used in large numbers for many purposes. They provide the
possibility of reaching temperatures in the millikelvin region
continuously and they are an indispensable pre-cooling stage for
nuclear demagnetization. The theory, most commonly used for
describing the flow properties of ^{3}He in the dilute side of a
dilution refrigerator, is based on the assumption that the ^{3}He
particles move without mutual friction in the superfluid ^{4}He, and
thus the ^{4}He II can be treated as a vacuum.

At the Department of Physics at the Eindhoven University of
Technology, a refrigeration technique with a multiple mixing
chamber system was developed. Most of the experiments were
performed in a dilution refrigerator with a high ^{3}He circulation
rate (>1 mmol/s), built in 1978 (Wae76, Wae77, Wae78, Coo81).
During this period discrepancies between the experiments and the
theoretically expected behaviour of the dilution refrigerator
showed up (Coo81, section 7.10). These led to the presumption that
the flow properties of ^{3}He moving through ^{4}He II were not fully
described by the model in which mutual friction between the ^{3}He
and its superfluid ^{4}He background is neglected (Wae82, Coo82).
Therefore, an investigation was started on the flow phenomena in
the mixing chamber and in the dilute side of a ^{3}He circulating
dilution refrigerator (Wae83, Cas85). In this thesis these
experiments will be described. Empirical relations concerning the
flow properties of ^{3}He moving through superfluid ^{4}He are derived
and a first step towards a theoretical description of the observed
phenomena is given.

1

1.2 *Dilution refrigeration*

In figure 1.2.1 the phase diagram of ^{3}He-^{4}He mixtures at saturated vapour pressure is given in a T-x plane, where x is the molar concentration of ^{3}He, and T the temperature in kelvin.
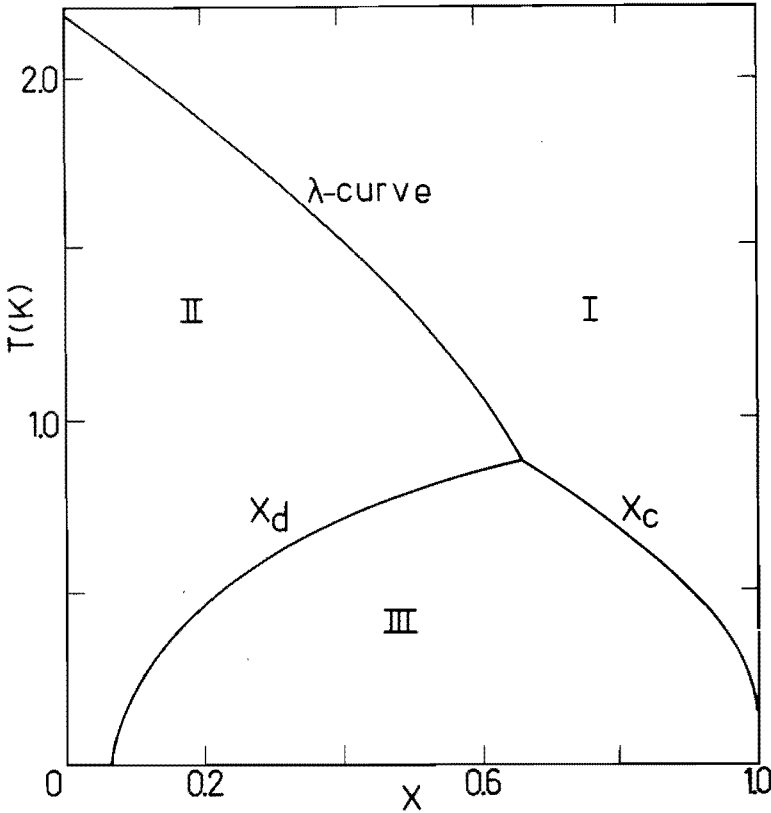
Fig. 1.2.1   The phase diagram of ^{3}He-^{4}He mixtures at saturated vapour pressure. Below 0.87 K phase separation occurs (region III). The λ-curve separates the normal region (I) from the superfluid region (II).

This diagram is characterized by two curves: the λ-curve and the coexistence curve. The λ-curve separates the regions where the ^{4}He is normal (I) c.q. superfluid (II). This curve intersects the T-axis at a value of 2.17 K, the λ-point of pure ^{4}He.

2

The coexistence curve encloses the two-phase region of
^{3}He-^{4}He mixtures (III). When ^{3}He is added to ^{4}He, at a constant
temperature below 0.87 K, the concentration of ^{3}He cannot be
raised unlimited. At the point where the ^{3}He concentration would
exceed the value given by the left side of the coexistence curve,
phase separation occurs. The liquid consists of two phases with
different composition. One phase is poor of ^{3}He and has a
concentration x_d, given by the left hand side of the coexistence
curve. The other phase is ^{3}He rich and has a concentration x_c
given by the right side of the coexistence curve. The phase with
the higher ^{3}He molar concentration (the so-called concentrated
phase) has the lower density and floats on top of the phase with
the low ^{3}He concentration (the dilute phase). At temperatures
below 100 mK the concentrated phase consists of almost pure ^{3}He.
On the other hand, even at the lowest temperatures, up to 6.6% ^{3}He
can be dissolved into ^{4}He (Wat69, Gho79). This will be elucidated
in section 1.3 when the energy distributions of the particles in
the two phases are considered. When, starting from equilibrium,
^{3}He is extracted from the dilute phase, ^{3}He from the concentrated
phase will cross the phase boundary and thus restore the
concentration in the dilute mixture. Since the ^{3}He molar entropy
in the dilute phase is larger than the molar entropy in the
concentrated phase at the same temperature, the dilution of ^{3}He
will result in cooling.

In a dilution refrigerator this phenomenon is used to produce
continuous cooling in the millikelvin range. The phase separated
mixture is contained in a vessel called the mixing chamber. The
dilute phase in the mixing chamber is connected to the liquid in
the so-called still, which is a container partially filled with a
liquid 1% ^{3}He solution at a temperature of about 0.7 K, in
equilibrium with its vapour. Vapour is removed from the still,
using a pumping system at room temperature. Since the ^{3}He
concentration in the vapour outweighs the ^{4}He concentration by a
factor of about 30, nearly pure ^{3}He is extracted. This extraction
is compensated by an equal amount of ^{3}He dissolving from the
concentrated into the dilute phase in the mixing chamber. In order
to establish continuous cooling the ^{3}He extracted from the still,

is recondensed and returned to the concentrated phase in the mixing chamber. The enthalpy balance for the mixing chamber is given by:

$$\dot{Q}_m = \dot{n}_3(H_{3_d} - H_{3_c}),$$ 1.2.1.

here $\dot{Q}_m$ is the heating power on the mixing chamber, $\dot{n}_3$ the molar rate of ^{3}He passing the phase boundary, and H_{3_d} and H_{3_c} the molar ^{3}He enthalpies of the dilute and the concentrated phases respectively. Substituting the low temperature limiting values for H_{3_d} and H_{3_c} the cooling power reads:

$$\dot{Q}_m = \dot{n}_3(92.95T_m^2 - 11.4T_i^2),$$ 1.2.2.

where T_m is the temperature in the mixing chamber, equal to the temperature at the phase boundary, and T_i the temperature of the ^{3}He entering the mixing chamber. When $\dot{Q}_m=0$, and excluding the physical irrelevant solutions $(T_m,T_i)\leq0$ and $\dot{n}_3=0$, a steady state is reached when $T_m=0.36T_i$. Thus, for reaching low mixing chamber temperatures, it is necessary to precool the incoming ^{3}He effectively.

Only a very brief and simplified description of a dilution refrigerator was given here. In the following chapters a more profound consideration will be given. The subject of dilution refrigeration is treated in a number of books and papers (e.g. Lou74, Bet76, Fro78, Hae79a, Hae79b, Tac82).

1.3 _Dilute ^{3}He-^{4}He mixtures below 0.5 kelvin_

In figure 1.2.1 it was indicated that the ^{4}He component in the dilute phase is superfluid. The ^{4}He particles have zero spin and are bosons. At temperatures below 0.5 K the ^{4}He is practically in its ground state. The number of thermal excitations (phonons and rotons) is negligible and the superfluid ^{4}He is often described as thermally inert. For calculating the thermodynamic properties of the total mixture the ^{4}He background gives no

4

significant contribution. In this way it can be regarded as a vacuum. The ^{3}He particles have spin 1/2 and therefore it is tempting to describe a dilute mixture according to the ideal Fermi gas theory. Experiments show that this can be done, provided one introduces a gas of non-interacting Fermi particles with the same number density as the ^{3}He particles, but with an effective mass m^* which is about 2.5 times the bare mass of a ^{3}He atom. These Fermi particles are usually called the ^{3}He-quasiparticles. The concentrated phase of ^{3}He at low temperatures can be treated as a Fermi liquid in a similar way.

In equilibrium the ^{3}He chemical potentials of the two phases are equal, hence

$$\mu_{3_c} = \mu_{3_d} \quad , \qquad\qquad 1.3.1.$$

where μ_{3_c} and μ_{3_d} are the ^{3}He molar chemical potentials in the concentrated and the dilute phases respectively. At zero temperature, μ_{3_c} can be set equal to a potential energy $-E_c o$, plus the molar Fermi energy of the concentrated phase RT_{Fc}:

$$\mu_{3_c} = -E_c o + RT_{Fc} \quad . \qquad\qquad 1.3.2.$$

In this thesis μ_{3_c} at zero temperature is chosen as the zero point of the ^{3}He chemical potential scale. For a dilute mixture of ^{3}He concentration x the chemical potential can be written in a similar way taking into account that the potential energy $-E_d o$ and the Fermi temperature T_{Fd} are concentration dependent

$$\mu_{3_d}(x) = -E_d o(x) + RT_{Fd}(x) \quad . \qquad\qquad 1.3.3.$$

In figure 1.3.1 a diagram representing μ_3 versus x is shown. For concentrations below 6.6% it shows that $\mu_{3_d} < \mu_{3_c}$ and it is energetically favourable for a ^{3}He atom to be in the dilute phase rather than in the concentrated phase. This means that ^{3}He will dissolve into the dilute mixture until $\mu_{3_d} = \mu_{3_c}$.
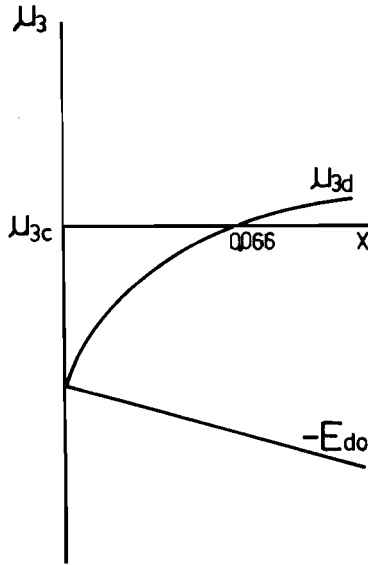
Fig. 1.3.1. The ^{3}He molar chemical potential as a function of
the ^{3}He concentration x, at zero temperature. For
x=0.066 the chemical potential of the concentrated
phase equals the chemical potential of the dilute
phase.

A mixture of ^{3}He in ^{4}He shows a behaviour different from pure
^{4}He II. A small addition of ^{3}He has a large influence on some
physical properties. For instance the thermal conductivity of a
dilute mixture is much smaller than the conductivity of pure ^{4}He
below the lambda point. This is caused by the fact that, in
contrast with the normal ^{4}He component in the two fluid model, the
^{3}He atoms cannot be transformed to the superfluid state and thus
impede the counterflow of normal ^{4}He atoms which is responsible
for the large thermal conductivity in pure ^{4}He II. Furthermore,
because of their Fermi character, the ^{3}He quasiparticles cannot
all be in the same single particle state, but they fill the energy
levels up to the Fermi-sphere. Thermal activity is caused by the
particles occupying the energy levels in an energy band of width
kT near the Fermi-sphere. When the temperature of a Fermi gas is

raised from zero to T kelvin, the increase in internal energy of the gas will approximately be $k^2T^2D(E_F)$, where $D(E_F)$ is the density of states near the Fermi surface. From this it follows that the specific heat of the Fermi-system is linear in T. The specific heat of ^{4}He at very low temperatures is determined by the phonon contribution, and is proportional to T^3. Therefore, the ^{3}He entropy outweighs the ^{4}He contribution at low temperatures. Quantities like thermal conductivity and viscosity of the mixture have a temperature dependence according to the Fermi particle model as well.

II   THEORETICAL CONSIDERATIONS

2.1   *Introduction*

In this chapter some theoretical considerations about ^{4}He II
and dilute mixtures of ^{3}He and ^{4}He are given. In section 2.2 the
so-called mechanical-vacuum model will be discussed. The
properties of a ^{3}He flow through superfluid ^{4}He, as present in a
dilution refrigerator, are usually described according to this
model. In section 2.3 a short description of superfluid turbulence
in ^{4}He II will be given. This subject is of importance for the
interpretation of the experimental results described in this
thesis.

2.2   *The mechanical-vacuum model*

Pure liquid ^{4}He, at temperatures below the lambda point, is
usually described in the framework of the two-fluid model (Lan59,
Kha65, Wil67, Put74, McC84). In this model it is assumed that the
liquid behaves as if it consists of two components: the normal
fluid component and the superfluid component. The total fluid
density ρ is the sum of the normal component density ρ_n and the
superfluid component density ρ_s. The two fluids are completely
intermingling. For not too high relative velocities the two
components can move without mutual friction. The superfluid
component carries no entropy. It exhibits neither viscosity nor
turbulence. The latter property can be specified by requiring
$\vec{\nabla} \times \vec{v}_s = 0$ in the bulk liquid, where $\vec{v}_s$ is the velocity of the
superfluid. The entropy content of the liquid is carried by the
normal component. This component has a viscosity unequal to zero.

Landau and Pomeranchuk (Lan48) and Khalatnikov (Kha65) showed
that impurities in ^{4}He II can be treated in the same way as the
normal component in the liquid. At low temperatures (T<500 mK)
thermal excitations in the ^{4}He are negligible. As long as the
velocity of the impurities is smaller than the velocity of sound
no phonons can be created. For roton excitation the velocity of

the particles must exceed the so-called Landau critical velocity
v_L. This velocity corresponds with the slope of the tangent near
the local minimum of the ^{4}He dispersion curve (see figure 2.2.1).
This local minimum is well described by $E = \Delta + (p-p_0)^2/(2\mu_r)$.
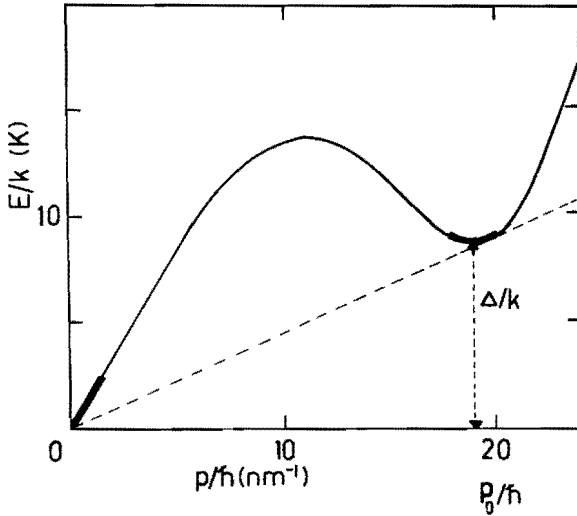
Fig. 2.2.1   *The dispersion curve for elementary exitations in*
He II. The thickened regions of the curve indicate
the states of phonon and roton exitations.
The slope of the dashed line corresponds to the
Landau critical velocity for roton creation.

The quantities Δ, p_0 and μ_r are known as roton parameters and
represent respectively energy, momentum, and effective mass of a
roton. From the laws of energy and momentum conservation it can be
deduced that in good approximation $v_L = \Delta/p_0$. Thus there exists a
critical velocity below which no dissipative interactions can
occur between the moving (quasi)particle and the ^{4}He background.
    Dilute mixtures of ^{3}He and ^{4}He at very low temperatures are
often described within the mechanical-vacuum (MV) model (Whe68a,
Whe68b). In this model the ^{4}He, which consists of superfluid only,
is treated as a vacuum in which the ^{3}He quasiparticles can move
without friction. Starting from the assumptions that no critical

velocities are exceeded and that the ^{4}He can be treated as a
vacuum, the thermodynamic and hydrodynamic equations for dilute
mixtures can be given. Here we will derive these equations for a
system consisting of a cylindrical tube connecting two reservoirs
containing diluted ^{3}He-^{4}He mixtures. The ^{3}He is moving through the
tube from one reservoir to the other. In practice the first
reservoir is the mixing chamber of a dilution refrigerator, and
the connecting tube a flow impedance installed at the exit of this
mixing chamber. The second reservoir can be an experimental room
on top of the mixing chamber or some other part in the
refrigerator such as the dilute side of the heat exchangers or the
still. From some general assumptions the acceleration of the

superfluid ^{4}He component $(\partial\vec{v}_s/\partial t)$ can be shown to be related to
the gradient in the molar ^{4}He chemical potential μ_4 according to
(And66, Kha65, Wil67):

$$M_4(\partial\vec{v}_s/\partial t) = -\vec{\nabla}\mu_4 \ , \qquad\qquad 2.2.1.$$

where M_4 is the ^{4}He molar weight. Therefore, in the steady state
$\vec{\nabla}\mu_4=\vec{0}$. Hence, the chemical potential of the ^{4}He is constant
everywhere in the dilute side of the system. This is one of the
basic relations for the MV-model. In case of pure ^{4}He, the
chemical potential is a function of pressure and temperature. In a
mixture it depends on the concentration of the ^{3}He as well. The
dependence between the molar chemical potentials of both
components is given by the Gibbs-Duhem relation (Gug85)

$$xd\mu_3 + (1-x)d\mu_4 = -S_m dT + V_m dp \ . \qquad\qquad 2.2.2.$$

where S_m and V_m are the entropy and volume per mole mixture, p is
the pressure and μ_3 is the molar chemical potential for ^{3}He.
    In our case, when the entropy of the ^{4}He component can be
neglected, and no net ^{4}He flow is assumed, the law of energy
conservation for a steady flow of ^{3}He through ^{4}He II in a
restricted geometry (flow impedance) reads (Whe68a, Ebn71, Hae79a,
Hae79b, Kue85)

$$\dot{n}_3 \mu_3 + \dot{n}_3 TS_F + \dot{Q} = \text{constant} , \qquad 2.2.3.$$

where $\dot{n}_3$ is the ^{3}He molar flow rate, $\dot{Q}$ is the heat flow rate, and S_F is the molar entropy of the ^{3}He. The molar ^{3}He entropy has been given the index F because it equals the entropy of an ideal Fermi gas at the same quasiparticle density as the mixture and with an effective quasiparticle mass m^* (Kue85). Equation (2.2.3.) can be written as an enthalpy conservation law by introducing

$$H_3^{OS} = \mu_3 + TS_F . \qquad 2.2.4.$$

This enthalpy is called the osmotic enthalpy in accordance with Ebner and Edwards (Ebn71). This term is equal to the enthalpy H_3^* introduced in (Cas85) and the term H_3 as used by Radebaugh (Rad67). With Eq.(2.2.3.) this results in

$$\dot{n}_3 H_3^{OS} + \dot{Q} = \text{constant}. \qquad 2.2.5.$$

At very low temperatures the contribution of the ^{4}He to the entropy of the mixture can be neglected. Hence,

$$S_m = xS_F . \qquad 2.2.6.$$

Combination of Eqs.(2.2.1.) - (2.2.6.) yields:

$$\dot{n}_3 TdS_F + \dot{n}_3 V_3 dp + d\dot{Q} = 0 , \qquad 2.2.7.$$

where $V_3 = V_m/x$ is the volume of a mixture containing one mole ^{3}He. For cylindrical flow channels and no external heat load, the heat flow $\dot{Q}$ is given by the heat conduction in the liquid:

$$\dot{Q} = - \frac{\pi D^2}{4} \kappa \frac{dT}{d\ell} , \qquad 2.2.8.$$

where κ is the thermal conductivity of the liquid, ℓ the distance

12

from the tube entrance, and D is the diameter of the tube. A possible conduction through the wall of the tube is not taken into account here.

Dilute mixtures are viscous and thus will give a pressure drop when flowing through a channel. In our experiments the Reynolds number is usually on the order of 300 or less. Hence, the flow in the tube will be laminar. For a cylindrical tube the pressure drop is then given by

$$dp = - \eta \dot{n}_3 V_3 \left[\frac{128}{\pi D^4}\right] d\ell \ , \qquad\qquad 2.2.9.$$

where η is the viscosity of the liquid. The radial distribution of the ^{3}He molar flow rate density as a function of the distance r from the tube axis is given by

$$j_3(r) = \frac{8\dot{n}_3}{\pi D^4}(D^2 - 4r^2) \ . \qquad\qquad 2.2.10.$$

At very low temperatures and for ^{3}He concentrations close to the concentration of a saturated mixture at absolute zero, x_0, one can approximate S_F, η, κ, and the specific heat per mole ^{3}He, C_d, by their low temperature values (Cas85) given by:

$$S_F = C_d = C_0 T \qquad (C_0 = 104 \ J/molK^2),$$
$$\kappa = \kappa_0/T \qquad (\kappa_0 = 3\times10^{-4} \ W/m),$$
$$\eta = \eta_0/T^2 \qquad (\eta_0 = 5\times10^{-8} \ sPaK^2).$$

Substitution of these values in Eqs.(2.2.7.), (2.2.8.), and (2.2.9.) leads to a differential equation for the T-ℓ relationship, which can be written in a dimensionless form by introducing the dimensionless parameters τ and λ according to

$$\tau = T/T_0 \qquad\qquad 2.2.11.$$

and

$$\lambda = \ell/L_0 \ , \qquad\qquad 2.2.12.$$

in which L_0 and T_0 are given by

$$L_o = \frac{\pi}{2} \left[\frac{\kappa_o{}^2}{128 C_o \eta_o V_3{}^2} \right]^{1/3} \frac{D^{8/3}}{\dot{n}_3} , \qquad\qquad 2.2.13.$$

$$T_o = \left[\frac{128 \eta_o V_3{}^2 \kappa_o}{C_o{}^2} \right]^{1/6} D^{-1/3} . \qquad\qquad 2.2.14.$$

The dimensionless differential equation for the T-ℓ relationship then reads

$$\frac{d\tau^2}{d\lambda} - \frac{1}{\tau^2} - \frac{d}{d\lambda}\left[\frac{1}{\tau}\frac{d\tau}{d\lambda}\right] = 0 . \qquad\qquad 2.2.15.$$

The solutions of this differential equation are described by Van Haeringen (Hae80). His analysis shows that at higher temperatures ($T > T_o$), in the main part of long tubes (length $L \gg L_o$), the term corresponding with the thermal conductivity can be neglected. In these cases Eq.(2.2.15.) reduces to

$$\frac{d\tau^2}{d\lambda} - \frac{1}{\tau^2} = 0 . \qquad\qquad 2.2.16.$$

Integration of Eq.(2.2.16.) and substitution of τ and λ by T and ℓ gives

$$T^4 = T_m{}^4 \left[1 + \frac{128\ell}{\pi D^4} \frac{4V_3{}^2 \eta_o}{C_o T_m{}^4} \dot{n}_3 \right] . \qquad\qquad 2.2.17.$$

where T_m is the temperature at the tube entrance. Substitution of Eq.(2.2.17.) in Eq.(2.2.9.) leads to an expression for the pressure drop over the impedance as a function of temperature

$$p = p_m - \frac{C_o}{2V_3}(T^2 - T_m^2) , \qquad\qquad 2.2.18.$$

where p_m is the pressure at the entrance of the flow impedance. Equation (2.2.18.) is also found by integration of Eq.(2.2.7.) in

14

case the heat flow $\dot{Q}$ can be neglected. From the fact that in the steady state $\Delta\mu_4=0$, and that the fountain pressure is negligible at low temperatures follows:

$$p - \Pi = \text{constant}. \qquad\qquad 2.2.19.$$

where Π is the osmotic pressure of the mixture. In the low temperature limit the osmotic pressure for ^{3}He concentrations close to saturation $(x{\approx}x_m)$ is given by (Kue85)

$$\Pi(x,T) = 2209 + 45.0{\times}10^3(x{-}x_m) + 81.7{\times}10^3 T^2 . \qquad 2.2.20.$$

Combination of Eqs.(2.2.18.), (2.2.19.) and (2.2.20.) yields an expression for the relationship between x and T reading

$$T^2 = T_m^2 - b(x{-}x_m) , \qquad\qquad 2.2.21.$$

where b is a constant with a value of $0.2\ \text{K}^2$. In (Cas85) it is shown that Eq.(2.2.21.) equals the expression for osmotic enthalpy conservation. Combining Eqs.(2.2.17.) and (2.2.21.) gives an expression for the concentration profile in the tube:

$$x = x_m - \frac{T_m^2}{b}\left[\left[1 + \frac{128\ell}{\pi D^4}\frac{4V_3{}^2\eta_0}{C_0 T_m{}^4}\,\dot{n}_3\right]^{\frac{1}{2}} - 1\right] . \qquad 2.2.22.$$

Relations (2.2.10.), (2.2.17-18.) and (2.2.22.) form a complete set of equations from which the j_3, T, p, and x profiles in the tube can be calculated from $\dot{n}_3$, T_m, and the tube dimensions, in case of a ^{3}He flow under the conditions of the MV-model.

2.3 *Turbulence in superfluid helium*

Although the main part of this work concerns dilute mixtures, a closer look at turbulence in pure ^{4}He II is useful for a better understanding of the experimental results to be discussed in the following chapters. In this paragraph an introduction on this

subject will be given.

The equations of motion, in somewhat simplified form, for both components in ^{4}He II can be derived (Kha65, Wil67) resulting in:

$$\rho_n \left[\frac{\partial \vec{\upsilon}_n}{\partial t}\right] + \rho_n (\vec{\upsilon}_n \cdot \vec{\nabla}) \vec{\upsilon}_n = \eta_n \nabla^2 \vec{\upsilon}_n - \frac{\rho_n}{\rho} \vec{\nabla} p - \rho_s \left[\frac{S}{M_4}\right] \vec{\nabla} T \ , \qquad 2.3.1.$$

$$\rho_s \left[\frac{\partial \vec{\upsilon}_s}{\partial t}\right] + \rho_s (\vec{\upsilon}_s \cdot \vec{\nabla}) \vec{\upsilon}_s = - \frac{\rho_s}{\rho} \vec{\nabla} p + \rho_s \left[\frac{S}{M_4}\right] \vec{\nabla} T \ , \qquad 2.3.2.$$

where $\vec{\upsilon}_n$ and $\vec{\upsilon}_s$ are the velocities of the normal and the superfuid components respectively, S the molar entropy and M_4 the molar weight of the liquid. In the steady state the left side terms of both equations can be set equal to zero, when neglecting quadratic terms in the velocities. Summation of Eqs.(2.3.1.) and (2.3.2.) yields the pressure gradient, equal to the viscous force acting on the normal fluid component:

$$\vec{\nabla} p = \eta_n \nabla^2 \vec{\upsilon}_n \ . \qquad 2.3.3.$$

Equation (2.3.2.) gives the London equation for the fountain pressure

$$\vec{\nabla} p = \frac{\rho S}{M_4} \vec{\nabla} T \ . \qquad 2.3.4.$$

The equations of motion given above are valid in a region of not too high velocities. Flow experiments show discrepancies when large velocities are involved. The first experiments showing this effect were performed by Gorter and Mellink (Gor49) in thermal counterflow. From these experiments can be concluded that an interaction between the normal and superfluid components is present, giving rise to a considerably larger temperature difference over the flow tube. The interaction occurs above a certain critical velocity, dependent on the size of the flow channels in use. The critical velocities involved are smaller than

16

those necessary for creating thermal excitations, the Landau critical velocities (see figure 2.2.1). The extra force arising in the supercritical region seems to be a frictional force between the two components. This mutual frictional force density, $\vec{F}_{sn}$, appears to be proportional to the cube of the relative velocities between the two components in the liquid. Gorter and Mellink introduced the relation

$$\vec{F}_{sn} = A_{sn}\rho_n\rho_s(\vec{v}_s-\vec{v}_n)^3 \; , \qquad\qquad 2.3.5.$$

where A_{sn} is the Gorter-Mellink constant. In the presence of this force, the equation of motion for the superfluid component is given by:

$$\rho_s\left[\frac{\partial\vec{v}_s}{\partial t}\right] + \rho_s(\vec{v}_s.\vec{\nabla})\vec{v}_s = -\frac{\rho_s}{\rho}\vec{\nabla}p + \rho_s\left[\frac{S}{M_4}\right]\vec{\nabla}T - \vec{F}_{sn} \; . \qquad 2.3.6.$$

In the steady state the left side terms, when averaged over a not infinitely small volume in the liquid, can be set equal to zero, yielding

$$\vec{\nabla}\mu_4 = -V_{4_s}\vec{F}_{sn} \; , \qquad\qquad 2.3.7.$$

where V_{4_s} is the volume of the liquid containing one mol of superfluid. Considering an axial flow through a long cylindrical tube, as in our experiments, and assuming that μ_4 is constant in a plane perpendicular to the axis, Eq.(2.3.7.) gives

$$\frac{d\mu_4}{d\ell} = -V_{4_s}F_{sn} \; , \qquad\qquad 2.3.8.$$

where F_{sn} represents the magnitude of the vector $\vec{F}_{sn}$ and ℓ is the distance from the tube entrance.

The flow phenomena in the supercritical region suggest that in the supercritical region vorticity in the superfluid is created. However, the superfluid velocity field satisfies $\vec{\nabla}\times\vec{v}_s=0$

and applying Stokes' theorem yields that the circulation K_c = $\oint \vec{\upsilon}_s.d\vec{\ell}$ will be zero for any reducible closed circuit (simply connected region) in the liquid. In case of a singular region inside the integral contour, in which there is no superfluid, rotation is not excluded. Therefore, turbulence in superfluid [4]He can be described with vortices, which are often depicted as vacuum cores around which the superfluid is circulating with a velocity the magnitude of which is inversely proportional to the distance to the core. Unlike ordinary vorticity, in [4]He the circulation is quantized. The quantization of circulation can be understood by taking into account the macroscopic wave function of the [4]He II condensate (Lon54):

$$\Psi(\vec{r}) = \Psi_0(\vec{r})e^{iS(\vec{r})} \; , \qquad\qquad 2.3.9.$$

where $\vec{r}$ is the location and $S(\vec{r})$ the phase of the wave function. For the momentum operator $\vec{p}$ holds

$$\vec{p}\Psi = -i\hbar\vec{\nabla}\psi \; . \qquad\qquad 2.3.10.$$

This equation may be interpreted in terms of the motion of one atom of superfluid

$$\vec{p} = m_4\vec{\upsilon}_s \; , \qquad\qquad 2.3.11.$$

where m_4 is the bare mass of a [4]He atom.
Combination of Eqs.(2.3.10.) and (2.3.11.) gives an expression for the superfluid velocity

$$\vec{\upsilon}_s = \frac{\hbar}{m_4}\vec{\nabla}S \; . \qquad\qquad 2.3.12.$$

For the circulation K_c of a vortex core we now get:

$$K_c = \frac{\hbar}{m_4}\Delta S \ , \qquad\qquad\qquad 2.3.13.$$

where ΔS is the change in phase of the wave function going round
the loop. The phase only can change by $2n\pi$,where n is an integer,
without changing the wave function. From this it follows that K_c
can be set equal to nh/m_4. Thus the circulation is quantized in
units of h/m_4. Experiments (Vin61, Ray64) showed that the
magnitude of the quantum of circulation in ^{4}He II is equal to h/m_4
(n=1).

The picture one has of mutual friction now is that above some
critical relative velocity vortices are created. Under the
influence of their velocity field and interaction with the normal
component in the fluid, these vortices are moving in space,
forming a random configuration. This random configuration is
usually called a vortex tangle. The normal component in the fluid
is scattered by this vortex tangle which results in dissipative
effects in addition to the viscous forces already present. An
extensive treatment of superfluid turbulence is given by Tough
(Tou82).

III EXPERIMENTAL SET-UP

3.1 *The ³He circulating dilution refrigerator*

The experiments described in this thesis are performed in a
^{3}He circulating dilution refrigerator with a maximum ^{3}He flow rate
of about 2.5 mmol/s. This machine has been described earlier
(Wae80, Coo81).
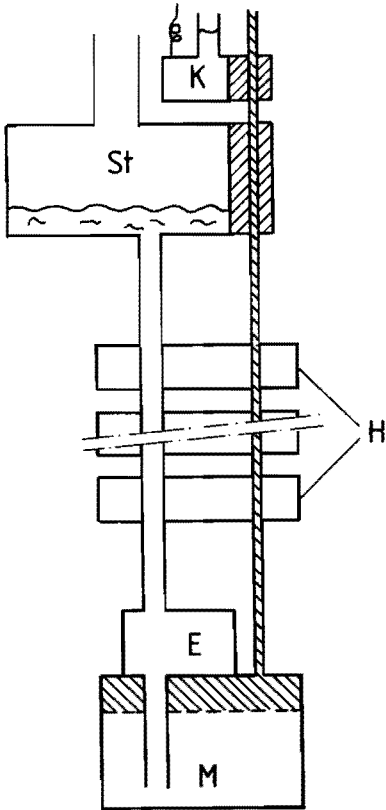
Fig. 3.1.1

Schematic drawing of the
low-temperature part of the
dilution refrigerator used in
our experiments.
M: mixing chamber;
E: experimental space;
K: 1K plate;
St: still;
H: heat exchangers.

The dilution refrigerator is contained in a cryostat in which four
spaces can be distinguished, namely: a space with superisolation
at permanent vacuum, a liquid nitrogen container, a second vacuum
space, and a liquid helium container. The low-temperature part of
the dilution refrigerator is mounted in a vacuum chamber (height
815 mm, inner diameter 215 mm). In this vacuum chamber a copper

radiation shield, surrounding the mixing chamber, can be installed. This shield is thermally grounded to the heat exchanger second nearest to the mixing chamber and has a temperature of approximately 100 mK during operation of the refrigerator. In figure 3.1.1 a schematic drawing of the low-temperature part of the dilution refrigerator is given.

The 1-kelvin plate (K) is made of copper. A continuous flow of ^{4}He is supplied to the 1K bath through a constriction, connected to the liquid in the ^{4}He cryostat. Pumping this 1K bath with a mechanical pump establishes a continuous cooling power extracting the heat released by the condensation of the ^{3}He gas which enters the refrigerator (DeL71). The 1K bath consumes about 0.3 liter LHe/h.

The still (St) has a volume of about 0.65 liter. The still is pumped by a system which consists of a booster pump (Edwards 18B3) and a mechanical backing pump (Edwards ES4000). This pumping system is designed for a ^{3}He circulation rate of 4 mmol/s. However, an orifice at the entrance of the pumping tube, reducing the ^{4}He film flow, limits the maximum circulation rate to the value of 2.5 mmol/s mentioned before (Coo81).

In the refrigerator ten step heat exchangers (H) of the Niinikoski type (Nii71) are installed. They consist of a copper body in which two large channels are drilled. These channels are filled with sintered copper sponges except for some smaller open channels in order to reduce the flow impedance. The sinter sponges are made of copper powder, with an average grain size of 5 μm (type FL, Norddeutsche Affinerie, Hamburg) has been used. The surface area of the sponges varies from about 0.15 m^2 in the heat exchanger near to the still, up to 5.5 m^2 in the exchanger close to the mixing chamber.

The mixing chamber (M) usually consists of a stainless steel cylinder with an experimental space (E) on top. The bottom of E is connected with the dilute exit tube of the mixing chamber. The top of E is connected to the dilute side of the heat exchangers. The mixing chamber and the experimental space will be described in more detail in the next section.

The ^{3}He leaving the still is returned to the refrigerator, by

way of a gas handling system at room temperature. The circulating gas is purified in a charcoal trap at liquid nitrogen temperature before entering the dilution refrigerator. The circulation flow rate is measured with a flowmeter (Hastings EALL-100P) placed in the gas handling system. This flowmeter measures the total molar circulation rate, $\dot{n}_t$, which is the sum of the ^{3}He circulation rate, $\dot{n}_3$, and the ^{4}He circulation rate $\dot{n}_4$:

$$\dot{n}_t = \dot{n}_3 + \dot{n}_4. \qquad\qquad 3.1.1.$$

The total circulation rate can be varied between 0.13 and 2.5 mmol/s by varying the heating power $\dot{Q}_s$ supplied to the still. The ^{4}He flow rate $\dot{n}_4$ was typically 3% of $\dot{n}_t$ (see section 4.2).

In order to reduce vibrational heating, the cryostat is suspended from a 6000 kg concrete block mounted on air springs. All pumping and filling tubes at room temperature are connected to the refrigerator and cryostat by flexible stainless steel bellows. In the continuous-mode experiments heat leaks are negligible. The minimum temperature is limited by the performance of the heat exchangers and is, with a single mixing chamber, about 10 mK.

3.2   *The single mixing chamber with experimental space*

A schematic drawing of the mixing chamber M, used in most of the experiments reported in this thesis, is given in figure 3.2.1. The mixing chamber is made of stainless steel and has a cylindrical shape. It has an inner height of 78 mm and an inner diameter of 38 mm. An experimental space E is part of the top of the mixing chamber. This space has an inner height of 34 mm and an inner diameter of 30 mm. The concentrated ^{3}He enters the mixing chamber at the top via a tube with an inner diameter of 1.8 mm. The temperature T_i of the incoming ^{3}He can be varied by means of a heating power $\dot{Q}_i$, supplied by a heater placed between the concentrated side of the last heat exchanger and the entrance of the mixing chamber. This heater consists of a copper body with a copper-powder sintered surface with a total area of 0.5 m^2. In

this way a good thermal contact between the liquid and the heater body is established, and the body temperature can be kept low.
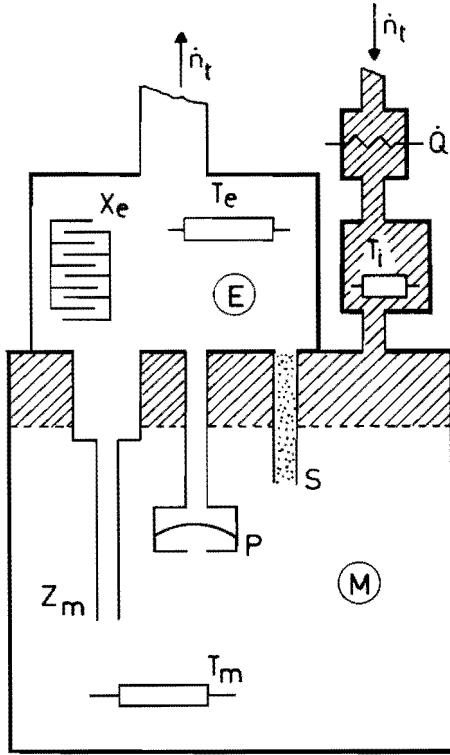
Fig. 3.2.1   Schematic drawing of the mixing chamber M and experimental space E. Between M and E a flow resistance Z_m, a superleak S, and a differential pressure gauge P can be installed.
Temperatures T_i, T_m, and T_e are usually measured by calibrated Speer carbon resistors. The ^{3}He concentration x_e in E is measured with an air capacitor. Temperature T_i can be varied with a heater $\dot{Q}_i$ at the entrance tube.

In order to avoid losses of heat through the tubing, a second sintered copper sponge heat exchanger is placed between the heater and the mixing chamber (Coo81). The temperature of the incoming ^{3}He is measured with a resistance thermometer installed at the

24

entrance of the mixing chamber. The ^{3}He leaves the mixing chamber through the dilute exit tube Z_m, and enters the experimental space E at the bottom. The upper side of E is connected with the dilute side of the heat exchangers by way of a cupro-nickel tube with an inner diameter of 4.8 mm and a length of 250 mm. The exit tube Z_m usually is the flow impedance under investigation. In general, the flow impedances studied are cylindrical tubes of length L and inner diameter D with L >> D. The lengths varied from 5 mm to 1.4 m; the diameters from 0.3 to 2.3 mm. During certain experiments (e.g. the calibration of the thermometers in E), Z_m consisted of a short tube with a relatively large diameter (D=5 mm). This situation will be referred to as $Z_m=0$.

In addition to the flow impedance it is possible to install a superleak S and a pressure cell P between M and E parallel to Z_m.

In nonadiabatic flow experiments a heating power $\dot{Q}_z$ is supplied to the liquid flowing from M to E. The heater used in these experiments consists of a copper body with a copper-powder sinter sponge (surface area 1 m^2) in order to keep the body temperature low. Twelve parallel channels (inner diameter 2 mm, length 23 mm) in the sinter sponge provide a passage for the flowing ^{3}He with practically zero flow resistance. The body of the heater is placed in a cylindrical araldite holder in order to protect the heater wire (manganin 50 μm), and to establish a thermal resistance between the heater and the liquid in the mixing chamber.

When a nonzero flow impedance is installed, the temperature T_e in E can be substantially higher than the mixing chamber temperature T_m. Therefore, in principle heat flows from E to M. However, the thermal contact between the liquids in E and M is negligible in our temperature region, due to the high Kapitza resistance and the poor thermal conductivity of the liquid in Z_m. Hence, the direct influence of T_e on T_m is negligible. This will be shown later when the experimental results are discussed (section 4.4). The heat flow towards E via the connecting tube with the heat exchangers is negligible too.

As stated before, the temperature T_i can be raised by supplying a heating power $\dot{Q}_i$. However, when T_i is raised above 500 mK the vapour pressure of the liquid exceeds the pressure in the heater and the liquid will be boiling. When this occurs, the dilution refrigerator fails to operate properly. Therefore, in the experiments reported here, T_i is limited to values below 500 mK, and, as a consequence, T_m to values smaller than 150 mK.

3.3 *Thermometry*

In our experiments various types of thermometers are used, namely: superconductive fixed point devices, cerium magnesium nitrate (CMN) thermometers and carbon resistance thermometers. In this section these three types of thermometers will be described.

The superconductive fixed point device, SRM768, is described by Schooley et al. (Sch80). It contains samples of $AuIn_2$, $AuAl_2$, Ir, Be and W, with superconducting transition temperatures at 205.00, 162.60, 99.05, 22.35, and 15.23 mK respectively. The fixed point device is placed in the liquid in the mixing chamber. It is screened from external magnetic fields by a metal cylinder with a high magnetic permeability (μ-metal). The superconducting transitions are detected with a lock-in amplifier (PAR 126), generating an AC current of 10 μA rms at a frequency of 329 Hz through the primary coil. Because of its large volume the device is only installed in the mixing chamber during the calibration of the other thermometers in use. During some experiments a second SRM768 fixed point device was at our disposal. This device was kindly lent to us by the "Natuurkundig Laboratorium der N.V. Philips' Gloeilampenfabrieken". With this fixed point device we were able to calibrate the thermometers measuring T_i and T_m simultaneously.

The CMN thermometer is also placed in the liquid in the mixing chamber. It is calibrated against the superconducting fixed point device. In figure 3.3.1 a schematic drawing of the CMN thermometer is given.
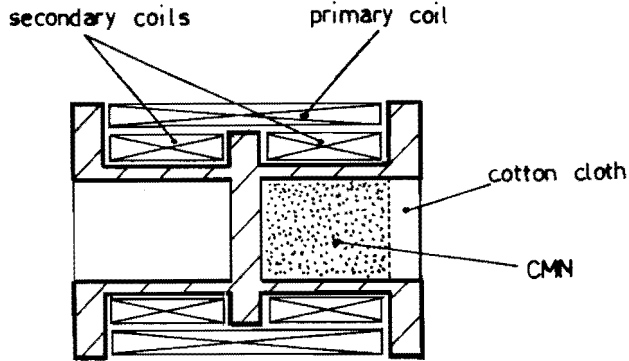
Fig. 3.3.1   Schematic drawing of the CMN-thermometer. On the
              araldite holder (length 20 mm, outer diameter 10 mm),
              a primary coil and a (compensated) secondary coil are
              wound. The CMN-salt fills half the holder and is
              secured by a cotton cloth.

The thermometer consists of an araldite coil holder on which a
primary coil (1320 windings of 50 µm NbTi wire in a CuNi-matrix)
and a secondary coil (50 µm Cu wire) are wound. The secondary coil
consists of two parts of 1650 windings each, both covering one
half of the length of the holder. One part is wound clockwise, the
other part counter-clockwise. When there is no CMN in the coil
holder, the signal induced in the right half of the secondary coil
will be compensated by the left half of the coil. In this way a
good reduction of the empty-coil signal is obtained. Furthermore,
a compensated pair of coils gives a reduction of the background
noise. The powdered CMN (75 mg; grain size smaller than 20 µm) in
the coil holder fills one half of the secondary coil. As a result
the induced voltage generated in the secondary coil is mainly due
to the susceptibility of the CMN. The CMN thermometer is operated
with a PAR 128A lock-in amplifier generating an AC current of
10 µA rms at a frequency of 129 Hz through the primary coil. The
induced voltages in the secondary coil are on the order of several
microvolts. The signal-to-noise ratio is on the order of 100. In
figure 3.3.2 a typical example of the CMN calibration is given.

    In the dilution refrigerator several resistance thermometers
are installed because of their ease in operation and their small

dimensions. In the low temperature part of the refrigerator carbon resistance thermometers of the Speer type are used. They are calibrated against the fixed point device and the CMN thermometer. The resistance values are measured with a resistance bridge (IT VS-2) with an excitation voltage of 30 or 100 μV. The Speer resistance thermometer in the experimental space E was calibrated while $Z_m=0$, in which case $T_e=T_m$.
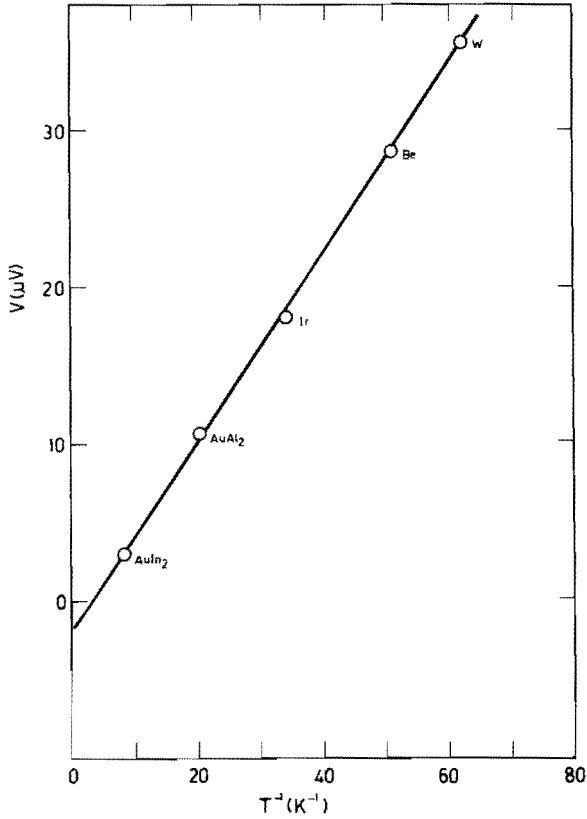

Fig. 3.3.2. A typical example of the CMN-thermometer calibration. The induced voltage in the secondary coil is plotted versus the inverse temperature. The circles indicate the different transition temperatures of the superconductive fixed point device.

3.4 *³He concentrations*

The ^{3}He concentration, x_e, of the mixture in E is determined
by way of a capacitive technique, using the property that the
relative dielectric constant ϵ_r of a ^{3}He-^{4}He mixture is, by good
approximation, a linear function of x (Kie76) according to:

$$\epsilon_r = 1.0572 - 0.0166x \ . \hspace{2cm} 3.4.1.$$

In E an air capacitor, consisting of 23 plates with a clear
distance of 0.2 mm, is placed. The nominal capacitance value is
32 pF. The capacitance is measured using a bridge (General Radio
1615A) and a lock-in amplifier (PAR 5101) as null detector. The
capacitor is calibrated by measuring the capacitance in vacuum, in
pure ^{4}He, and in a 6.6% mixture. The latter value is obtained in
experiments with $Z_m=0$ or from the extrapolation of the measured
x_e-$\dot{n}_t$ dependences to zero flow rate. With this technique the ^{3}He
concentration can be determined within 0.05%.

The ^{3}He concentration in the mixing chamber, x_m, is
calculated from the measured temperature T_m and the relation for
the phase separation line (Kue85)

$$x_m = 0.066 + 0.506T_m^2 - 0.249T_m^3 + 18.2T_m^4 - 74.2T_m^5. \hspace{1cm} 3.4.2.$$

This relation is confirmed by measuring x_e in experiments with
$Z_m=0$ in which case $x_e=x_m$.

3.5 *Pressure changes*

Pressure differences between M and E are measured with the
pressure gauge depicted in figure 3.5.1. It consists of two spaces
in an araldite holder (inner height: 7 mm; inner diameter: 14 mm),
separated by a 25 μm thick Kapton foil. The thermal expansion
coefficient of the Kapton foil is smaller than that of the
araldite body. This would result in a rumpling of the foil when
the pressure gauge is cooled down. Therefore, the foil has been
stretched at room temperature with a ring (see figure 3.5.1).
Chromium support layers and silver top layers are deposited onto

one side of the foil and onto an opposite surface of the gauge
body. The distance between the two siver layers, equal to the
height of the lower space in the gauge, is approximately 1 mm. The
capacitive coupling between the two silver layers, measured with a
capacitance bridge, is of the order of 2.5 pF and is a function of
the pressure difference across the foil.
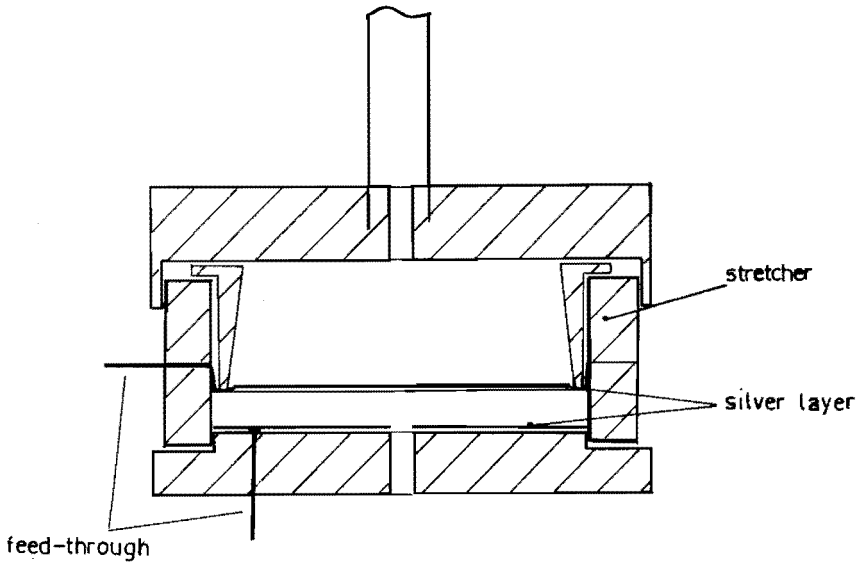
Fig. 3.5.1   Schematic drawing of the pressure gauge. The
             different parts are glued together with Stycast 1266.
             The free space between the two silver layers is about
             1 mm.

The gauge is calibrated in a [4]He cryostat against the hydrostatic
pressure head of a [4]He liquid column, for pressures between 0 and
300 Pa. The capacitance is measured with a capacitance bridge. The
calibration is 480±30 aF/Pa; the resolution 0.2 Pa.

     Pressure differences over Z_m are measured with the set-up
depicted in figure 3.2.1. The pressure gauge is installed in the
mixing chamber in such a way that the lower chamber of the gauge
is in connection with the dilute phase in M, while the upper
chamber is connected to E via a 3 cm long tube with an inner
diameter of 1.8 mm. In this way the dielectric, filling the space

30

between the two silver layers, is a saturated dilute mixture.

The measured pressure differences between M and E can be disturbed by systematic errors. The most probable errors will be discussed here. In the situation of ^{3}He flow there will be a ^{3}He concentration drop over Z_m as will be shown in section 4.3. As a result the concentrations in M, E, and the upper chamber of the pressure gauge will be different. Therefore, there will be a density gradient in the liquid, causing a hydrostatic pressure difference over the pressure gauge. Calculation of this hydrostatic pressure difference shows that it is on the order of 1 Pa. During the experiments, the temperature T_m varies between 10 and 150 mK. The capacitance of the gauge is a function of the dielectric constant of the mixture filling the lower space of the gauge. The ^{3}He concentration of this mixture will vary from 6.6% at 10 mK to 8.0% at 150 mK, resulting in a variation of ϵ_r of -0.02%. With a value of 2.5 pF for the capacitance of the pressure gauge, this variation in ϵ_r will result in a capacitance change of -580 aF. As the gauge has a sensitivity of 480 aF/Pa, an error of about 1 Pa in the pressure measurements is made, when no correction for the change in concentration is made.

3.6 Osmotic pressure

The values of the osmotic pressures Π_e and Π_m of the mixtures in E and M respectively, are calculated from the measured temperatures and concentrations (Kue85). The osmotic pressure in the still is measured with a so-called London device (Lon68). In figure 3.6.1 a schematic drawing of the London device is given. It consists of a CuNi tube (length L: 9 cm; inner diameter D: 3.8 mm) closed at one end. The open end is connected with the liquid in the still. At the closed end of the tube a heater is installed. Two resistance thermometers (Th$_1$ and Th$_2$) are placed at a respective distance of L/4 and L/2 from the heater. With a heating power $\dot{Q}_{ld}$ the temperature of the liquid in the device near the heater is increased. This results in a decrease of the ^{3}He concentration in this part of the liquid because the sum of the osmotic pressure and the fountain pressure must remain constant. A

further increase of $\dot{Q}_{ld}$ will result in a further increase of the
temperature and decrease of the ^{3}He concentration, until no ^{3}He is
left in this part of the London device and only ^{4}He is present
there. The temperature of the liquid in this region of pure ^{4}He
will be such that the fountain pressure of the ^{4}He is balanced by
the osmotic pressure plus the fountain pressure in the still.
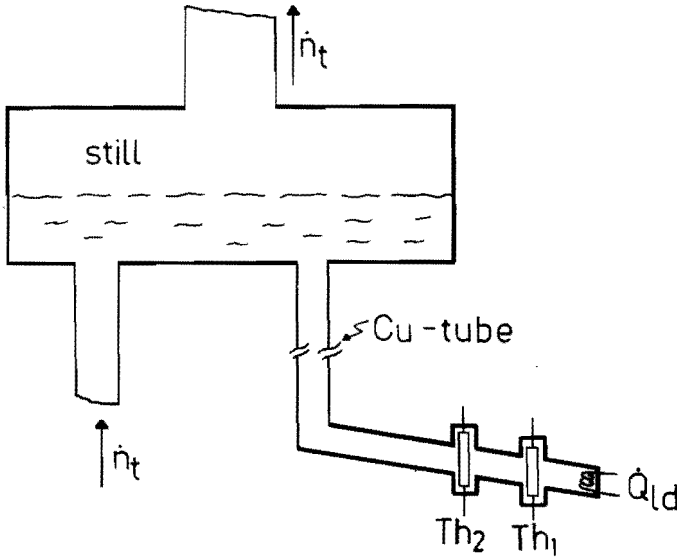
Fig. 3.6.1   Schematic drawing of the London device. The device is
made of cupro-nickel and connected to the still via a
16 cm long copper tube. The thermometers, Th_1 and
Th_2, are of the Allen-Bradley and Speer type
respectively.

The temperature of the warm liquid will no longer rise with $\dot{Q}_{ld}$
(see figure 3.6.2), and an increase of $\dot{Q}_{ld}$ results in an expansion
of the region of pure ^{4}He II in the device and an increase of the
temperature gradient near the still side. Since the thermal
conductivity of pure ^{4}He II is orders of magnitude larger than in
mixtures, the point where the region of pure ^{4}He covers both the
thermometers is indicated by a disappearance of a temperature
difference between these two thermometers.

32

Under normal operating conditions the temperature in the still is about 0.7 K. Therefore, the fountain pressure in the still is negligibly small and Π_s can be set equal to the fountain pressure given by the temperature at the warm end of the London device.
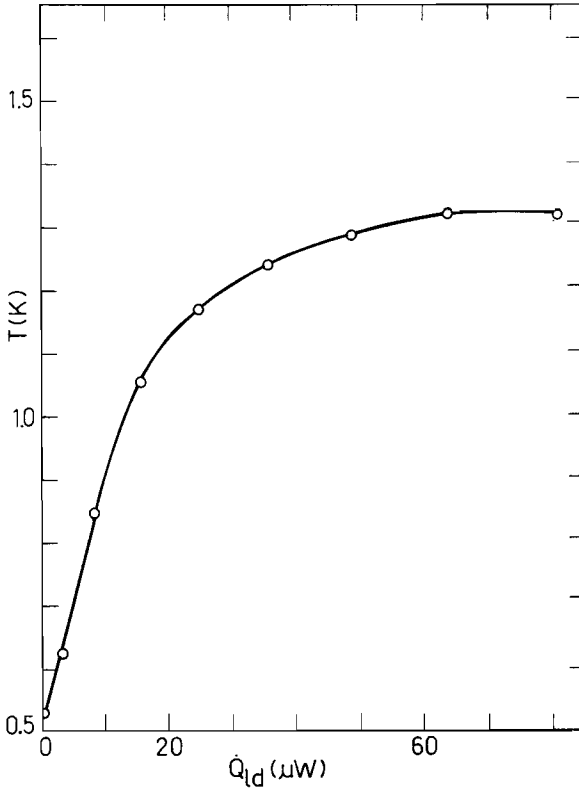
Fig. 3.6.2   *The temperature of the liquid in the London device, measured with Th_2, as a function of the supplied heating power $\dot{Q}_{ld}$. For $\dot{Q}_{ld} > 60$ μW the temperature of the liquid is constant.*

In our case the London device is operated with a $\dot{Q}_{ld}$ of 100 μW. This heat load is small compared to other heat loads on the still, and therefore does not influence the operation of the dilution refrigerator. As the temperature in the London device rises to about 1.3 K (see figure 3.6.2), the liquid will start boiling when

the hydrostatic pressure difference between the still and the
London device is smaller than the vapour pressure of the pure ^{4}He
at the warm end of the device. At a temperature of 1.3 K this
vapour pressure is about 170 Pa. Therefore, the London device is
attached to the still by a 16 cm long vertical tube, giving a
hydrostatic pressurehead of approximately 230 Pa. In order to
retain a good thermal contact between the still and the London
device, a copper tube is used. Since boiling of the liquid is not
completely excluded (the ^{4}He vapour pressure at 1.4 K is about
290 Pa), the London device is installed slightly tilted so that
the heater is situated at the lowest position. In the event of
boiling, gas bubbles can escape to the still, preventing the
situation that the heater becomes thermally isolated from the
liquid.

The resistance thermometers in the London device
(Allen-Bradley, 56 Ω, 1/2 W; Speer, 220 Ω, 1/2 W) are calibrated
with an accuracy of 25 mK against the vapour pressure of pure ^{4}He.
Due to the strong temperature dependence of the fountain pressure
($dp_f/dT \simeq 13$ kPa/K at T=1.3 K), Π_s can only be determined with an
accuracy of a few times 100 Pa. The uncertainty of the calibration
is removed to some extent by shifting the calibration curve
slightly in such a way that the measured fountain pressure is
equal to Π_e at low circulation flow rates. This is justified by
the fact that the difference between Π_s and Π_e will be very small
because the pressure difference between E and the still is
negligible at low flow rates, and in both compartments the
fountain pressure is nearly zero. With the London device osmotic
pressure changes as small as 10 Pa can be measured.

34

IV EXPERIMENTAL RESULTS

4.1 _Introduction_

In this chapter experimental results will be discussed. In each section a specific flow property is considered. The first five sections give information about adiabatic flow experiments. In section 4.2 we will discuss the dependence of the circulation rate of the refrigerator on the heating power supplied to the still. In sections 4.3 and 4.4 the temperature and ^{3}He-concentration differences across a flow impedance are given. Measurements performed _inside_ a flow impedance Z_m are presented in section 4.5. In section 4.6 pressure and osmotic pressure measurements are discussed. In the final section 4.7 results are given for nonadiabatic flow experiments.

Most of the experiments are performed with the mixing chamber as depicted in figure 3.2.1. The installed flow impedance Z_m usually consists of a cylindrical tube, either commercially available CuNi tubing, or made of german silver. It must be noted that the values for L and D given in this thesis have an accuracy of about 0.05 mm.

4.2 _Circulation flow rates_

A $\dot{n}_t$-$\dot{Q}_s$ dependence for Z_m=0

The total circulation flow rate $\dot{n}_t$ is dependent on the heating power $\dot{Q}_s$ supplied to the still, and also on the flow resistance Z_m in the dilute exhaust tube of the mixing chamber. In figure 4.2.1 plots are given of $\dot{n}_t$ versus $\dot{Q}_s$ in cases of Z_m=0. In this figure the results of two experiments are depicted. The squares represent the $\dot{n}_t$-$\dot{Q}_s$ dependence, measured in the situation that the only connection between the dilute mixtures in the mixing chamber and the still is established by the dilute side of the heat exchangers. Under this circumstance a kink occurs in the $\dot{n}_t$-$\dot{Q}_s$ curve when the flow rate is 0.92 mmol/s.
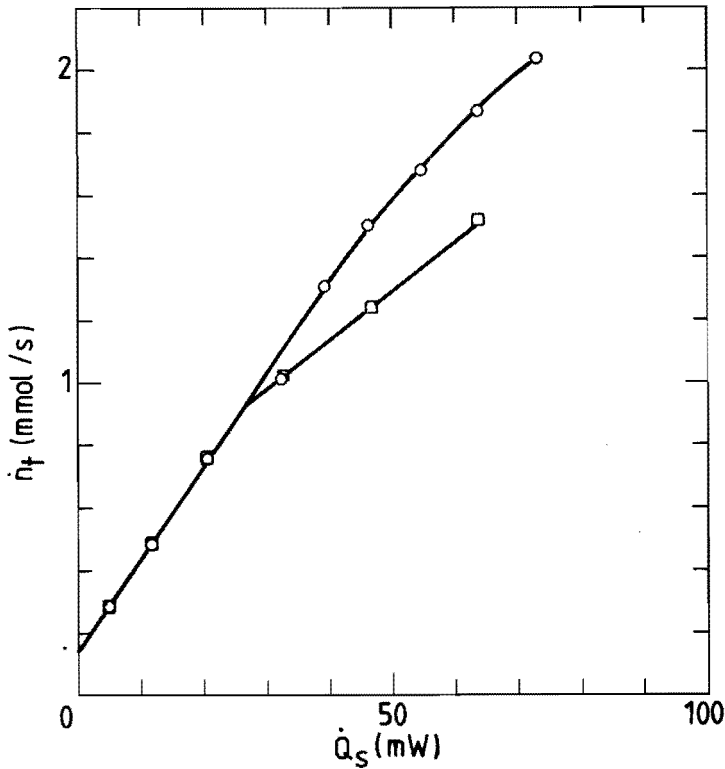
Fig. 4.2.1   Measured $\dot{n}_t$-$\dot{Q}_s$ dependences with (o) and without (□)
a superleak S parallel to the dilute side of the
heat exchangers. In both cases Z_m=0.

For circulation rates below this value $d\dot{Q}_s/d\dot{n}_t$=33 J/mol; for
higher flows $d\dot{Q}_s/d\dot{n}_t$=74 J/mol. The circles represent the flow rate
dependence in case of a superleak shunt along the dilute side of
the heat exchangers (see figure 4.2.2.), as was proposed by G.M.
Coops. In this situation no kink appears and $d\dot{Q}_s/d\dot{n}_t$ equals the
value of 33 J/mol over a much wider range.
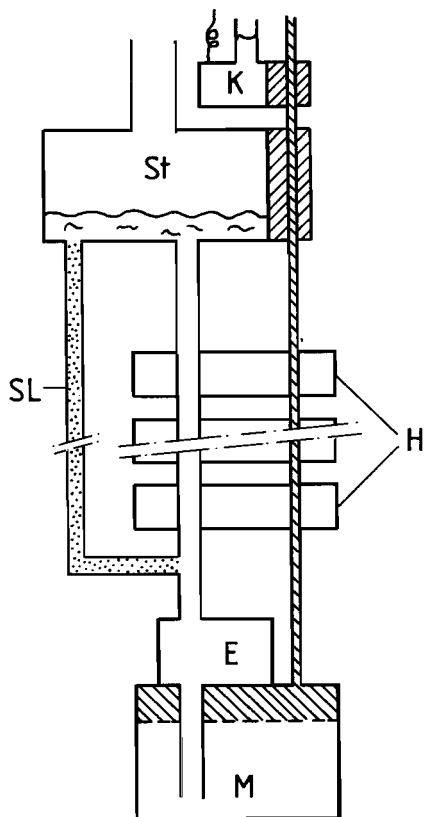
Fig. 4.2.2
The low-temperature part of the
dilution refrigerator. The
dilute side of the heat
exchangers is shunted by the
superleak SL.

The presence of the kink in the absence of a superleak shunt can be explained as follows: at low flow rates an increase of $\dot{Q}_s$ leads mainly to an increase of $\dot{n}_3$ and hardly influences the fraction of ^{4}He in the circulating mixture. The slope of the $\dot{n}_t$-$\dot{Q}_s$ curve then corresponds to the latent heat of evaporation of ^{3}He. At high flow rates ($\dot{n}_t > 0.92$ mmol/s) an increase of $\dot{Q}_s$ no longer establishes an increase of $\dot{n}_3$, but merely increases the amount of ^{4}He evaporated from the liquid in the still. The slope of the $\dot{n}_t$-$\dot{Q}_s$ curve now corresponds to the latent heat of evaporation of ^{4}He. Apparently, at circulation rates corresponding to the kink and higher, the ^{3}He concentration in the liquid in the still has dropped to a very low level, due to a flow resistance somewhere in

the dilute channel. This idea is supported by the analysis of the
vapour extracted from the still with a mass spectrometer, showing
a sharp increase of the ^{4}He concentration at high flow rates. With
a superleak shunt parallel to the dilute side of the heat

exchangers (SL//H) the kink in the $\dot{n}_t - \dot{Q}_s$ curve disappears,
indicating a reduction of the effective flow resistance of the
dilute channel by this superleak (Coo82, Wae82). As ^{3}He can not
pass superleaks, the reduction of the effective flow impedance
must be due to a change of the ^{4}He flow inside the dilute channel.
However, if the ^{4}He could be treated as a vacuum, a change in ^{4}He
flow would have no effect on the ^{3}He. Therefore, the reduction of
the effective flow impedance is an indication for the existence of
a mutual interaction between superfluid ^{4}He and ^{3}He particles
moving through this superfluid.

In order to extend the ^{3}He flow rate region of our machine to
values larger than 0.92 mmol/s, all further experiments are
performed with SL//H, unless mentioned otherwise. In this situation

an appreciable amount of ^{4}He is circulated when $\dot{n}_t > 1.5$ mmol/s, due

to the temperature rise in the still. For smaller flow rates $\dot{n}_3$

equals $\dot{n}_t$ within 6%.

B $\underline{\dot{n}_t - \dot{Q}_s \text{ dependence for } Z_m \neq 0}$

The dependence of the $\dot{n}_t - \dot{Q}_s$ characteristic on the flow
impedance Z_m is depicted in figure 4.2.3. It must be noted that
Z_m, installed between M and E, is not shunted by the superleak
parallel to the dilute side of the heat exchangers (see figures
3.2.1 and 4.2.2). For large flow resistances (large L, small D), a

kink in the $\dot{n}_t - \dot{Q}_s$ curve is observed at a critical flow rate $\dot{n}_{tc}$,
similar to the kink shown in figure 4.2.1. For small flow

resistances the kink is less pronounced. The value of $\dot{n}_{tc}$
decreases with increasing values of L and decreasing values of D.
Special attention must be paid to curves 1, 6, and 7. Curve 1

corresponds to the condition $Z_m=0$. Curve 6 gives the $\dot{n}_t - \dot{Q}_s$

dependence for a relatively large Z_m (L=23 mm, D=0.8 mm); $\dot{n}_{tc}$ has a value of about 0.3 mmol/s. Curve 7 corresponds to the same Z_m which is shunted by a superleak (S//Z_m), giving the same $\dot{n}_t$-$\dot{Q}_s$ dependence as for Z_m=0.
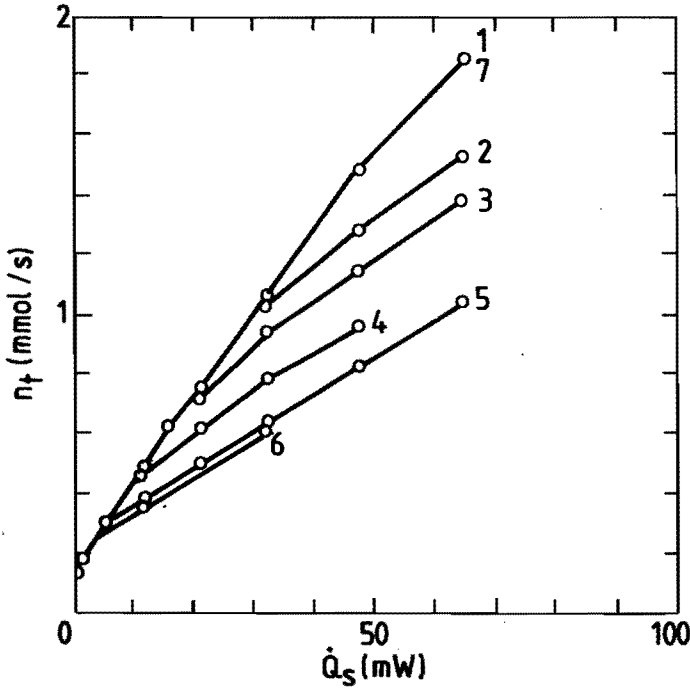
Fig. 4.2.3   *Measured $\dot{n}_t$-$\dot{Q}_s$ dependences with a superleak shunt across the heat exchangers (S//H) for different sizes of Z_m (L and D given in mm): 1, Z_m=0; 2, L=23, D=1.6; 3, L=80, D=1.6; 4, L=700, D=1.6; 5, L=1400, D=1.6; 6, L=23, D=0.8; 7, L=23, D=0.8, with superleak shunt S//Z_m.*

When Z_m is not shunted by a superleak, large amounts of ^{4}He are circulated for $\dot{n}_t \gg \dot{n}_{tc}$. The experiments performed under this condition show that the flow properties of the ^{3}He component, as reported in this thesis, are not very sensitive to ^{4}He circulation rates up to 50%. In the remaining part of this thesis only the

results of experiments in which the ^{4}He circulation rate is less than 6% of the total circulation rate ($\dot{n}_t < \min(\dot{n}_{tc}$, 1.5 mmol/s)) will be presented.

4.3 ^{3}He concentrations

The ^{3}He concentrations x_e and x_m of the dilute mixtures in E and M respectively, are determined according to the methods described in section 3.4. The difference in ^{3}He concentration across Z_m is defined by: $\Delta x = x_m - x_e$. The change in concentration depends on the circumstance whether Z_m is shunted by a superleak or not. First the results in case of no superleak shunt will be discussed.

A $\Delta x - T_m$ dependence

In figure 4.3.1 some typical $x_e - T_m$ dependences are given for two sizes of Z_m and different values of $\dot{n}_t$, in the situation of adiabatic flow ($\dot{Q}_z = 0$). This figure shows that Δx is practically independent of T_m, but varies with $\dot{n}_t$ and Z_m.

B $\Delta x - \dot{n}_t$ dependence

In figure 4.3.2 some typical results of $x_e - \dot{n}_t$ measurements are given, for different sizes of Z_m. During these measurements no extra heat is supplied to the liquid, neither at the entrance of the mixing chamber ($\dot{Q}_i = 0$), nor between M and E ($\dot{Q}_z = 0$). Under these circumstances in general the mixing chamber cools down to temperatures below 20 mK. As a consequence $x_m \approx 0.066$. Figure 4.3.2 shows that for given Z_m, x_e decreases with increasing flow rate. Curve 4 corresponds to the same Z_m as curve 6 in figure 4.2.3, and in both curves a kink shows up at $\dot{n}_t = 0.3$ mmol/s. For $\dot{n}_t > 0.3$ mmol/s, x_e has a practically constant value of 1.3%. Apparently such a low x_e causes a very low ^{3}He concentration in the liquid in the still, resulting in a high ^{4}He concentration in the vapour in the still (see section 4.2).

40
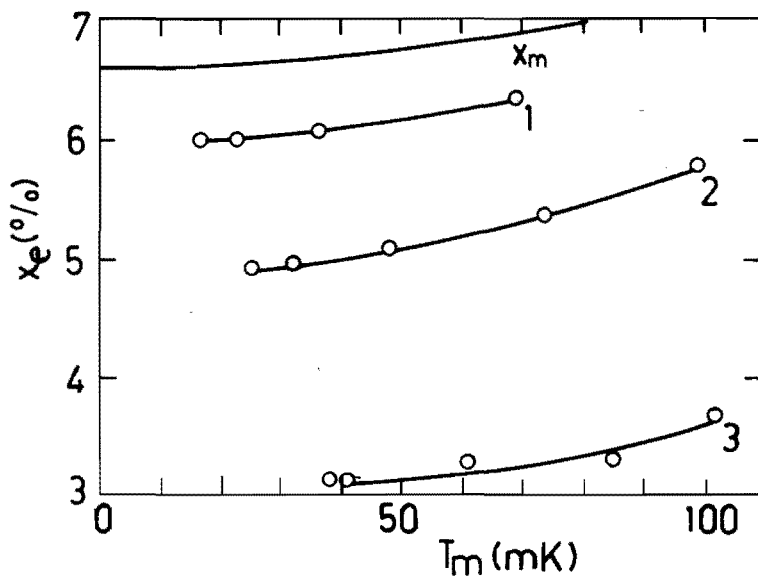
Fig. 4.3.1   Measured x_e-T_m dependences for $\dot{Q}_z$=0 for two

sizes (mm) of Z_m and different values of $\dot{n}_t$ (mmol/s):

1, L=23, D=1.6, $\dot{n}_t$=0.51;

2, L=23, D=1.6, $\dot{n}_t$=0.76; and

3, L=23, D=1.2, $\dot{n}_t$=0.71.

The curve labeled x_m represents the x_m-T_m

relationship calculated with Eq.(3.4.2.).
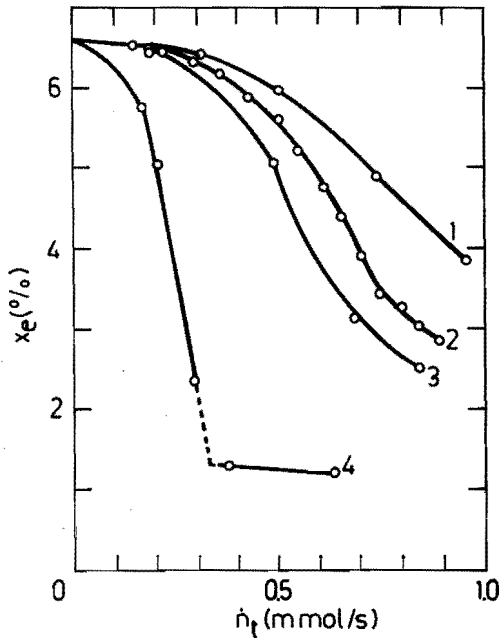
Fig. 4.3.2   Measured x_e-$\dot{n}_t$ dependences for $\dot{Q}_i$=$\dot{Q}_z$=0 for four
             different sizes (mm) of Z_m: 1, L=23, D=1.6; 2,
             L=10.5, D=1.2; 3, L=23, D=1.2; and 4, L=23, D=0.8.
             The lines connecting the points are to guide
             the eye only.

Double-logarithmic plots of Δx vs. $\dot{n}_t$, as given in figure 4.3.3, show that

$$\Delta x = \beta(L,D)\dot{n}_t^{\alpha} ,$$ 4.3.1.

where α is a constant with an empirical value of 2.8 ± 0.4, independent of L, D, $\dot{n}_t$, and T_m. The parameter $\beta(L,D)$ depends on L and D, but is independent of $\dot{n}_t$ and T_m.
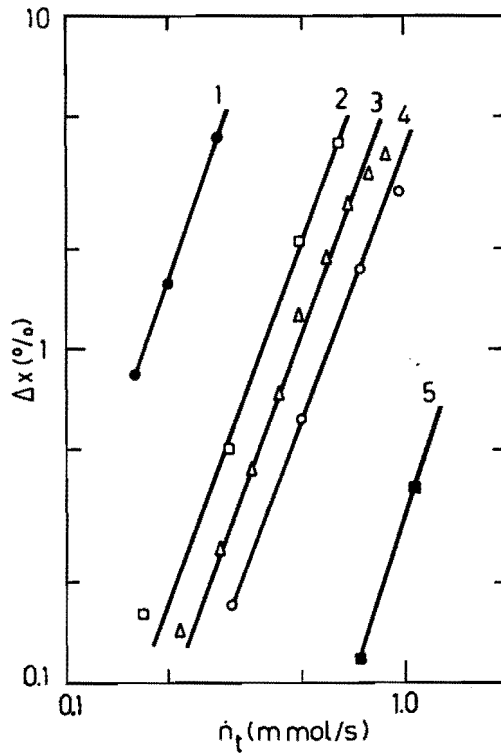
Fig. 4.3.3   Measured Δx–$\dot{n}_t$ dependences for $\dot{Q}_i=\dot{Q}_z=0$ for 5 different tube sizes (mm): 1, L=23, D=0.8; 2, L=130, D=1.6; 3, L=10.5, D=1.2; 4, L=23, D=1.6; and 5, L=23, D=2.3. The straight lines represent Δx–$\dot{n}_t$ dependences of the form Δx~n_t^{α}

C   Δx-L dependence

The concentration x_e as a function of L is examined by using several individual tubes with different lengths. However, the most accurate results are obtained with the set-up depicted in figure 4.3.4. In this experiment Z_m has a inner diameter of 1.6 mm and a total length of 130 mm.
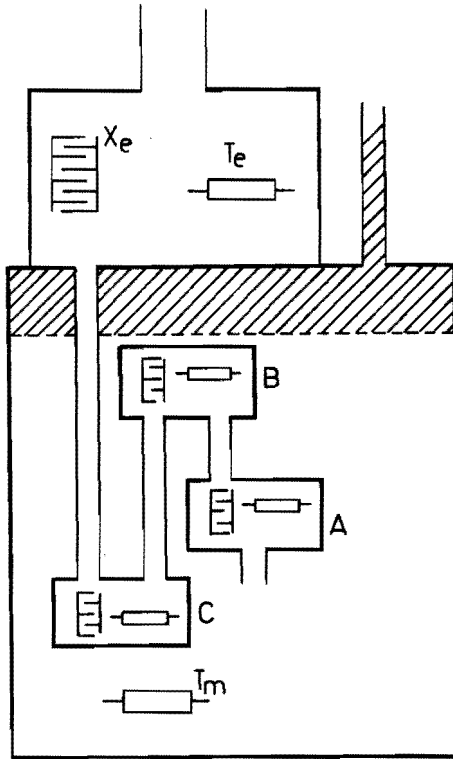
Fig. 4.3.4   Experimental set-up for x-L measurements. In spaces A, B, and C, temperature and ^{3}He concentration were measured. The connecting tubes had equal diameters (D=1.6mm). The lengths were 8, 15, 37, and 70 mm, respectively.

This flow impedance is cut in four pieces with respective lengths of 8, 15, 37, and 70 mm. The pieces are connected by experimental

spaces A, B, and C, in which x and T are measured.

In figure 4.3.5 the ^{3}He concentration x is plotted versus L for

different values of $\dot{n}_t$, and a linear x-L dependence is found

$$\Delta x \sim L. \qquad\qquad 4.3.2.$$
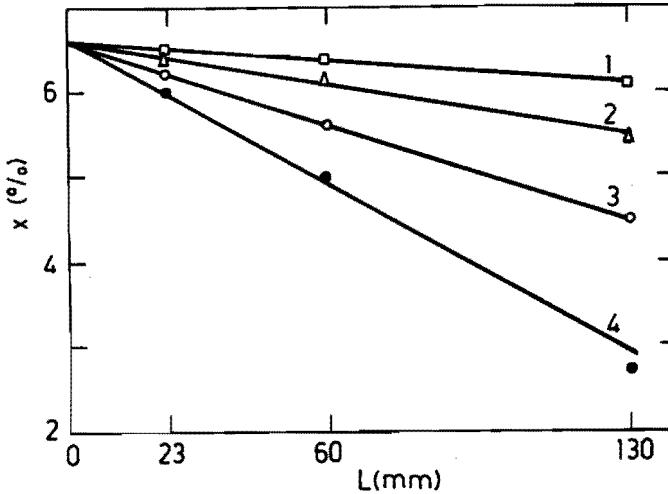
Fig. 4.3.5   Measured x-L dependences for four different flow

rates (mmol/s): 1, $\dot{n}_t$=0.31; 2, $\dot{n}_t$=0.38; 3, $\dot{n}_t$=0.49;

4,$\dot{n}_t$=0.64. The values of x and T are measured at L=0,

23, 60, and 130 mm respectively, (see figure 4.3.4).

D   Δx-D dependence

In order to examine the relation between Δx and the tube

diameter D, $\dot{n}_t$ vs. D is measured, for constant values of Δx and

flow impedances with a length of 23 mm. Typical results are given

in figure 4.3.6, showing that for constant Δx holds

$$\dot{n}_t \sim D^2. \qquad\qquad 4.3.3.$$
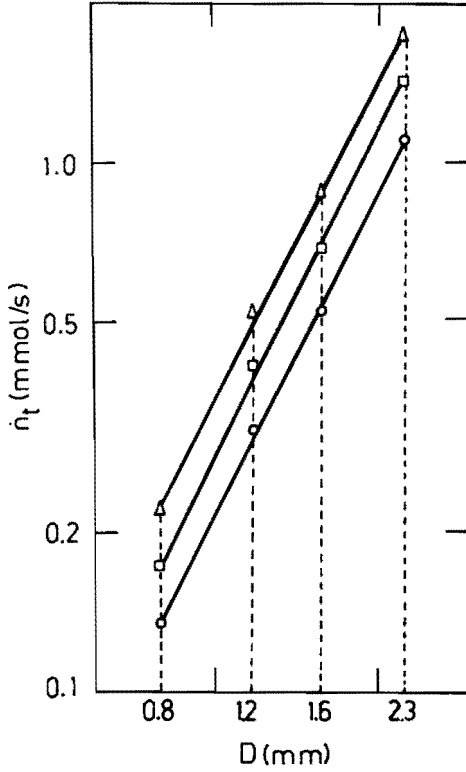
Fig. 4.3.6   Measured circulation flow rate $\dot{n}_t$ as a function of
the diameter D for flow impedances with L=23 mm, for
three different values of the concentration drop:
(△), Δx=0.02; (▫), Δx=0.01; (○), Δx=0.005. The
connecting lines show the relation $\dot{n}_t \sim D^2$.

Combination of Eqs.(4.3.1) – (4.3.3.) results in

$$\Delta x = \gamma L \left[\frac{\dot{n}_t}{D^2} \right]^\alpha , \qquad\qquad 4.3.4.$$

where γ is a constant, independent of $\dot{n}_t$, L, D, and T_m. Defining
an average flow rate density over the cross-sectional surface area

46

in the tube

$$j_t = \frac{4\dot{n}_t}{\pi D^2} \; , \qquad\qquad 4.3.5.$$

yields

$$\Delta x = \gamma' L j_t^\alpha \simeq \gamma'' L j_3^\alpha \; , \qquad\qquad 4.3.6.$$

taking into account that $\dot{n}_t$ contains on the average 3% ^{4}He. For
$\alpha=2.8$ the parameter γ'' has a numerical value of $(40\pm3)\times10^{-9}$
(SI units).

Equation (4.3.6.) suggests that the change in concentration
over Z_m depends on the ^{3}He flow rate density and the length of the
flow impedance only. The fact that the concentration drop is
independent on the shape of the cross-sectional surface area has
been confirmed in a series of experiments with 3 types of flow
impedances, all with the same surface area of 2 mm^2 and length
23 mm. These flow impedances are: (i) a single tube with D=1.6 mm,
(ii) 9 parallel tubes with D=0.5 mm, and (iii) 28 parallel tubes
with D=0.3 mm. In figure 4.3.7 the results for these experiments
are given, confirming that the cross-sectional surface area of the
tube is of major importance on the $\Delta x-\dot{n}_t$ dependence. However,
later on it will be shown that flow and temperature regimes exist
in which the geometry of Z_m influences the flow properties of the
dilute mixture (see sections 4.4 and 5.2).

E   Critical flow rate
When $x_e=0$, Eq.(4.3.6.) leads to a theoretical maximum value
j_c of j_3 given by

$$j_c = \left[\frac{x_m}{\gamma'' L} \right]^{1/\alpha} \; . \qquad\qquad 4.3.7.$$
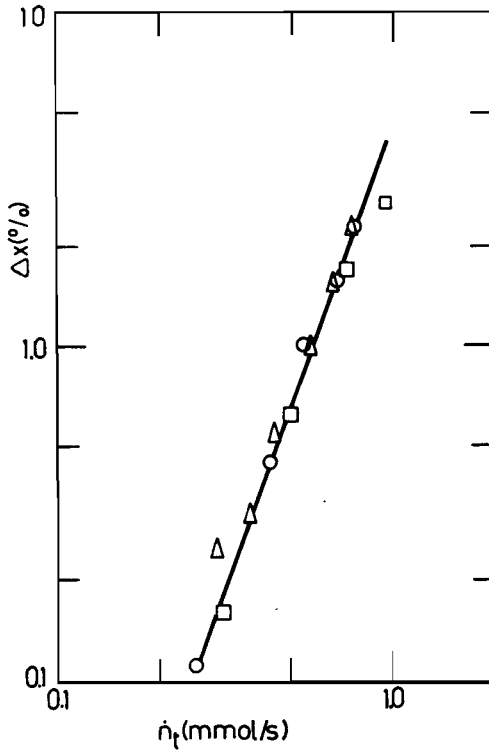
Fig. 4.3.7   Measured Δx-$\dot{n}_t$ dependences for three different types
of Z_m, with $L=23$ mm and equal surface area A:
($\circ$), 28 parallel tubes with $D=0.3$ mm; ($\triangle$), 9 parallel
tubes with $D=0.5$ mm; ($\square$), 1 tube with $D=1.6$ mm.
The data shows that Δx does not change with D when
A is kept constant.

This critical [3]He flow-rate density is the origin of the critical
flow rate $\dot{n}_{tc}$ which shows up in the $\dot{n}_t$-$\dot{Q}_s$ curves as discussed in
section 4.2. For our machine a critical flow rate will be reached
for values slightly less then those given by Eq.(4.3.7.), because
the minimum value of x_e is about 1.3%, as can be concluded from
curve 4 in figure 4.3.2.

F   Superleak shunt

Up to now only experiments have been discussed in which Z_m was not shunted by a superleak. Measurements with $S//Z_m$ show that under this circumstance the concentration drop is much smaller than for non-shunted Z_m, and is in good agreement with the expression for Δx according to the MV-model (Eq.(2.2.22.)). Again, the installation of a superleak has an influence on the ^{3}He flow properties.

4.4 *Temperatures*

The temperatures in the mixing chamber (T_m), in the experimental space (T_e), and at the entrance of the mixing chamber (T_i), are measured in the stationairy situation, at different flow rates and for different flow impedances. First the experiments with no superleak shunt across Z_m will be discussed.

A   T-ṅ$_t$ dependence

A typical example of the dependence of the temperatures on the circulation rate is given in figure 4.4.1. In this figure data is presented for an impedance with L=10.5 mm and D=1.2 mm, and for $\dot{Q}_i$=0. From figure 4.4.1 it can be deduced that the ratio T_i/T_m is almost independent of the flow rate and of T_e. This illustrates that there is no heat load to the mixing chamber $(T_i \simeq 2.8\ T_m)$. Hence, even for high values of T_e, the heat flow from E to M is negligible as stated in section 3.2. Furthermore, it is shown that for low circulation flow rates T_e is nearly equal to T_m, while for high flow rates T_e becomes almost equal to T_i.

The temperature T_e is determined by the mixing chamber temperature T_m and the temperature increase due to dissipation in Z_m. The ^{3}He enters the dilute side of the heat exchangers with this temperature T_e. In the temperature regime, in which our experiments are performed, the thermal resistance in the heat exchanger next to the mixing chamber is mainly determined by the so-called Kapitza resistance. The heat flow in this heat exchanger is thus proportional to $T_i^4 - T_e^4$, so T_i is a function of T_e. When $T_e^4 \ll T_i^4$ the effect of T_e on T_i is very small. However, when T_e is

comparable with T_i, an increase of T_e will result in an increase of T_i, because T_e always has to be smaller than T_i. In our machine T_e is always smaller than $0.9T_i$. In combination with $T_i=2.8T_m$, this results in $T_e \leq 2.5T_m$. When $T_e \simeq 2.5T_m$, the temperature increase in Z_m is nearly equal to the temperature decrease from T_i to T_m in the mixing chamber. This situation will be referred to as the "high dissipation limit".
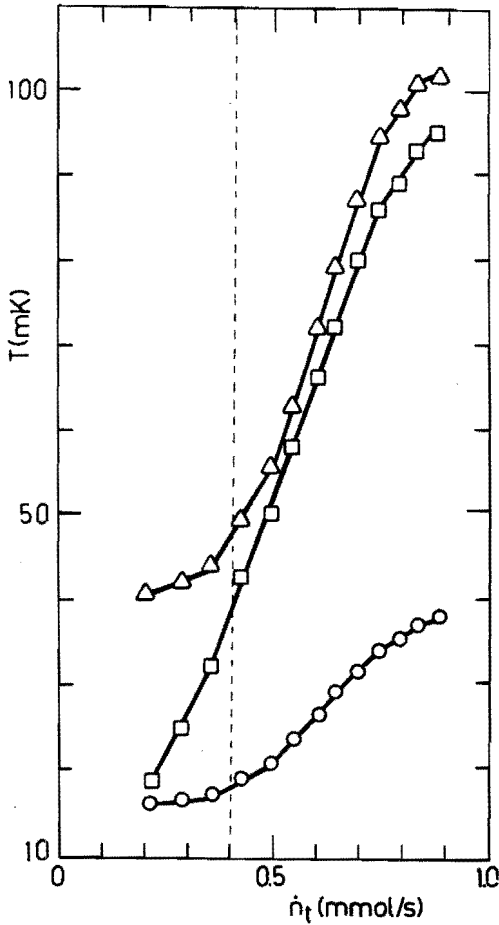
Fig. 4.4.1   Measured T-$\dot{n}_t$ dependences for a flow resistance with

L=10.5 mm and D= 1.2 mm, for $\dot{Q}_i=\dot{Q}_z=0$: ($\circ$), T_m;

($\square$), T_e; ($\triangle$), T_i.
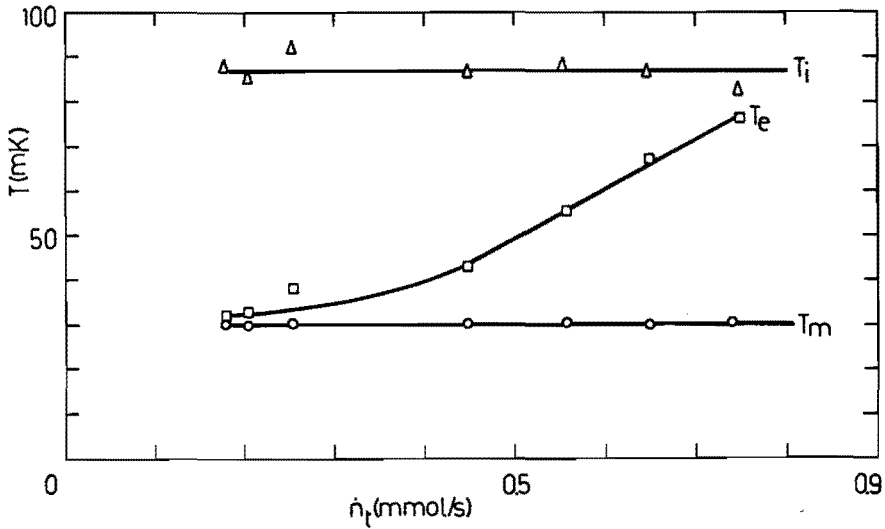
Fig. 4.4.2   The temperatures T_e and T_i as functions of $\dot{n}_t$ for a constant mixing chamber temperature T_m (30 mK). The flow resistance Z_m has $L=23$ mm and $D=1.6$ mm.
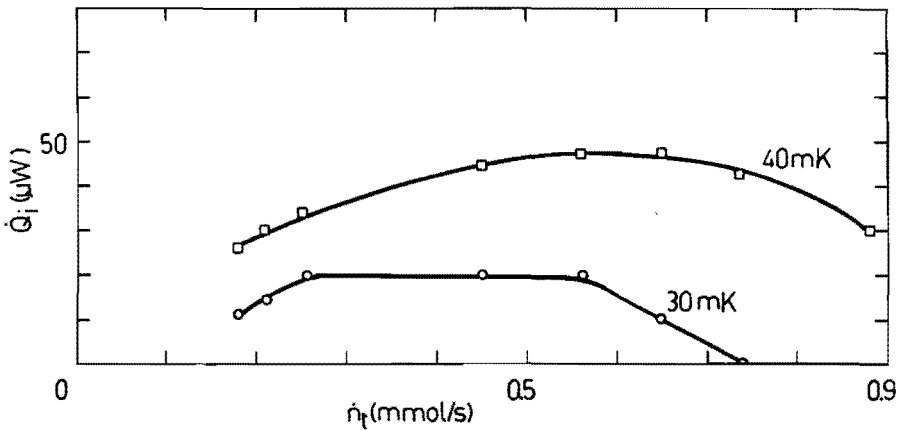
Fig. 4.4.3 $\dot{Q}_i$ versus $\dot{n}_t$ for two fixed values of T_m given in the figure. The flow resistance has $L=23$ mm and $D=1.6$ mm.

The transition from the low dissipation region to the high dissipation limit is illustrated in figure 4.4.1. It shows that for $\dot{n}_t < 0.4$ mmol/s holds that $T_e^4 \ll T_i^4$, which is the region of low dissipation. An increase of the circulation flow mainly increases T_e and hardly affects T_i and T_m. For these flow rates the temperature in the mixing chamber is determined by the performance of the heat exchangers. At higher flow rates, however, the dissipation in Z_m is so large that $T_e \simeq T_i$, and the high dissipation limit is reached. A further increase of $\dot{n}_t$ results in a rather strong increase of T_i and T_m. The mixing chamber temperature T_m is, under this condition, the minimum mixing chamber temperature which can be reached for the given Z_m and $\dot{n}_t$. This temperature would be reached, even with zero thermal resistance in the heat exchangers.

A similar behaviour is shown in case the mixing chamber temperature is fixed by adjusting $\dot{Q}_i$, for different circulation flow rates. An example of this type of experiments is depicted in figure 4.4.2. For low flow rates T_e is nearly equal to T_m. With increasing flow rate, $\dot{Q}_i$ has to be adjusted in order to keep T_m constant (see figure 4.4.3). For the higher flow rate values $\dot{Q}_i$ is a decreasing function of $\dot{n}_t$. In figure 4.4.3 it is shown that at a certain maximum flow rate $\dot{Q}_i$ is equal to zero. A further increase of $\dot{n}_t$ results in an increase of T_m. Again, the refrigerator operates in its high dissipation limit.

B $T_e - x_e$ dependence
The conservation of energy for a steady flow of ^{3}He through ^{4}He II is formulated in Eq.(2.2.5.). For adiabatic flow $\dot{Q}=0$, hence, H_3^{os}=constant. In the T-x region of interest for our experiments (10-150 mK, 2-7% ^{3}He), the enthalpy H_3^{os} is in good approximation a linear function of T^2 and x (Kue85):

$$H_3{}^{os} = 17.58 \, x + 84.06 \, T^2 \; . \qquad\qquad 4.4.1.$$

Hence, a change in x will give a corresponding change in T^2. This is shown in the double-logarithmic plot of ΔT^2 vs. $\dot{n}_t$ (figure 4.4.4), and in the plot showing the relation between ΔT^2 and L (figure 4.4.5), measured with the experimental set-up of figure 4.3.4. Both plots are similar to figures 4.3.3 and 4.3.5 showing Δx vs. $\dot{n}_t$ and Δx vs. L respectively.
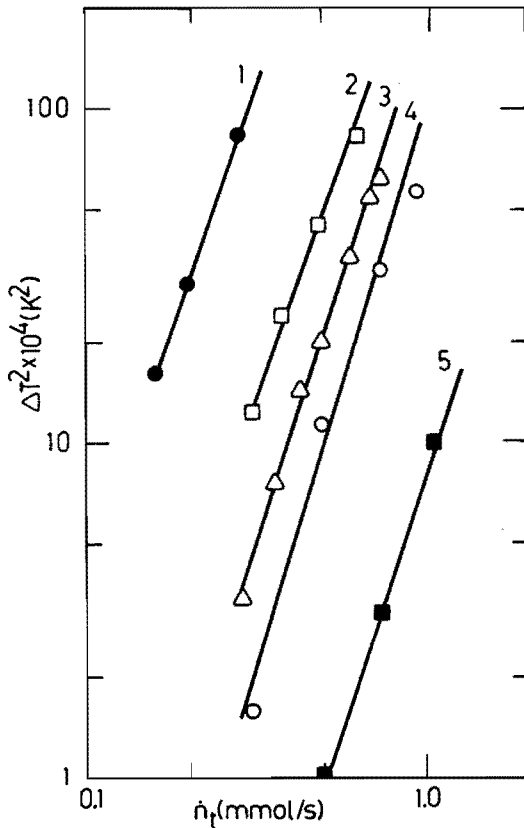
Fig· 4.4.4   Measured ΔT^2-$\dot{n}_t$ dependences for $\dot{Q}_i = \dot{Q}_z = 0$ for 5 different tube sizes (mm): 1, L=23, D=0.8; 2, L=130, D=1.6; 3, L=10.5, D=1.2; 4, L=23, D=1.6; and 5, L=23, D=2.3. The straight lines correspond with $\Delta T^2 \sim \dot{n}_t^{\alpha}$.
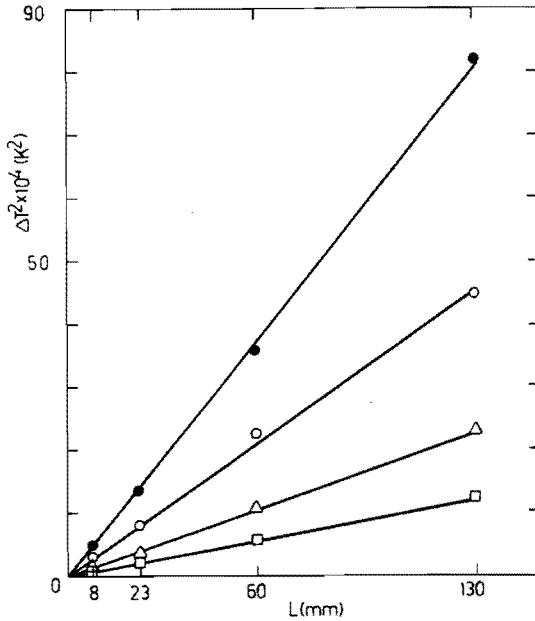
Fig. 4.4.5   *Measured ΔT^2-L dependences for four different values*

of $\dot{n}_t$(mmol/s): ($\bullet$), 0.64; ($\circ$), 0.49; ($\triangle$), 0.38;

($\square$), 0.31. T is measured at L=0, 8, 23, 60, and

130 mm respectively. D=1.6 mm.

Because of the linear dependence of $H_3{}^{os}$ in T^2 and x, it is convenient to plot the experimental data in a T^2-x diagram. In figure 4.4.6 measured T_e^2 -x_e dependences are plotted for two types of experiments.

In the first type $\dot{n}_t$ is varied while $\dot{Q}_i=0$ (compare figure 4.4.1). When large flow resistances, (and/or large flow rates) are used, the system is in its high dissipation limit $(T_e{\simeq}0.9T_i{\simeq}2.5T_m)$ as discussed above. Under these circumstances the T_e^2-x_e relation is represented by curve 2, given by

$$T_e^2 = 0.25(0.066 - x_e).   \qquad 4.4.2.$$

Fig.4.4.6 T^2-x diagram. Curves 1-4 have the following meaning:
1, phase separation line; 2, high dissipation limit;
3,and 4, least-squares fits of measured T^2_e-x_e points
with constant values of T_m=70 mK and 40 mK
respectively. The T^2_m-x_m points are indicated by •·

In the second type of experiments, $\dot{n}_t$ is varied while T_m is
fixed by adjusting $\dot{Q}_i$ (compare figure 4.4.2). In figure 4.4.6
curves 3 and 4 correspond to T_m=70 mk and T_m=40 mK respectively.
The measured T^2_e-x_e for this type of experiments are represented by
straight lines according to

$$T_e^2 + \alpha x_e = T_m^2 + \alpha x_m, \qquad\qquad 4.4.3.$$

where α is an experimentally determined parameter which is
independent of L, D, and $\dot{n}_t$. Its value varies slightly from
0.21 K^2, at low temperatures, to 0.19 K^2 at 70 mK. These values
are in agreement with Eq.(4.4.1.). Curves 3 and 4 are lines of
constant osmotic enthalpy. As already mentioned above, the heating
power $\dot{Q}_i$ is, at higher flow rates, a decreasing function of $\dot{n}_t$. At
a certain flow rate $\dot{Q}_i$ is zero. It is not possible to increase $\dot{n}_t$
above this maximum value without forcing T_i and T_m to rise. Again
the limit of high dissipation is reached. The corresponding $T_e^2-x_e$
data points are situated on curve 2 again. This can also be
demonstrated by the fact that Eq.(4.4.2.) follows from Eq.(4.4.3.)
by substitution of the low temperature values of α $(0.21$ $K^2)$ and
x_m (0.066), and by taking $T_m=0.4T_e$. A relation for the temperature
profile can be found by combining Eqs.(4.4.3.) and (4.3.6.),
yielding,

$$T_e^2 = T_m^2 + \alpha\gamma"Lj_3^\alpha. \qquad\qquad 4.4.4.$$

This relation is in agreement with the values of T_m and T_e,
measured in the experiments discussed above.

A third type of experiments is given in figure 4.4.7. In this
figure the phase-separation line is given by curve 1, and the high
dissipation line by curve 2. The curves 3-7 are obtained in
experiments in which $\dot{Q}_i$ (and thus T_m) is varied while $\dot{n}_t$ is fixed.
The $T_e^2-x_e$ curves are, in first order, parallel to the phase
separation line, reflecting the observation that Δx is constant
for different values of T_m (compare figure 4.3.1). For $\dot{Q}_i=0$, two
states of affairs can be reached:
1) $T_e<0.9T_i$. Under this condition the temperatures T_m, T_e, and T_i
are determined by the performance of the heat exchangers.
2) $T_e\simeq0.9T_i$. The refrigerator is in the high dissipation
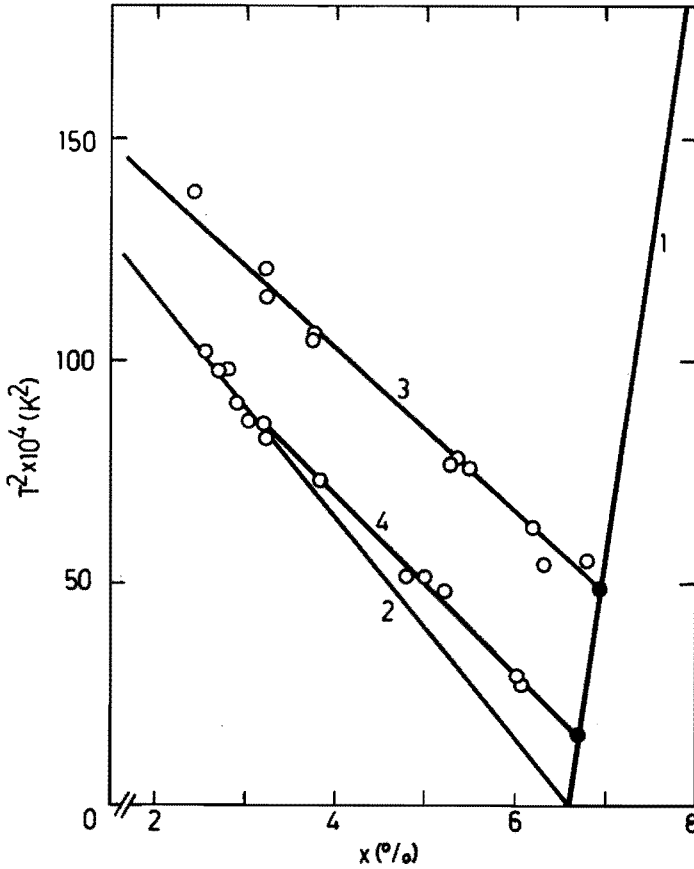limit. The corresponding data points are situated on curve 2.
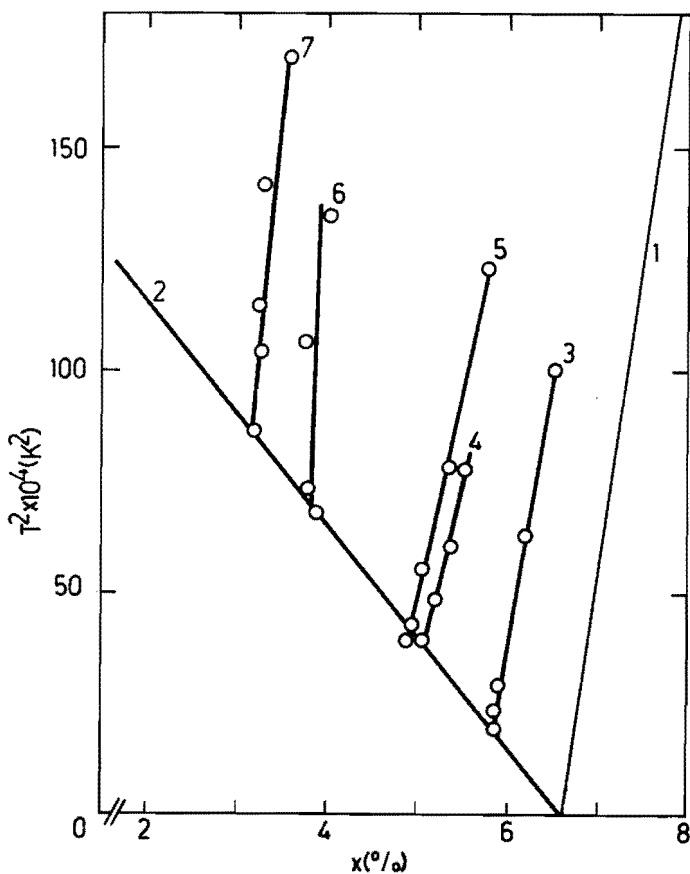
Fig.4.4.7 T^2-x diagram. Curves 1-7 have the following meaning:
1, phase separation line; 2, high dissipation limit;
3-7, measured $T_e^2-x_e$ dependences for constant $\dot{n}_t$ and
varying T_m.

When external heat loads are negligible, the minimum temperature
in the mixing chamber ($T_{m,min}$) in the second state, is determined
by the dissipation in Z_m only. This minimum temperature can be
calculated by substitution of $T_e=2.5T_m$ in Eq.(4.4.4.), leading to

$$T_{m,min} = \frac{1}{2.3}(\alpha\gamma''Lj_3^\alpha)^{1/2} \ .$$ 4.4.5.

Some typical $T_{m,min}-\dot{n}_t$ dependences calculated with Eq.(4.4.5.) are drawn in figure 4.4.8. The asterisks marking the ends of the curves correspond to the critical flow-rate densities derived from Eq.(4.3.7.).
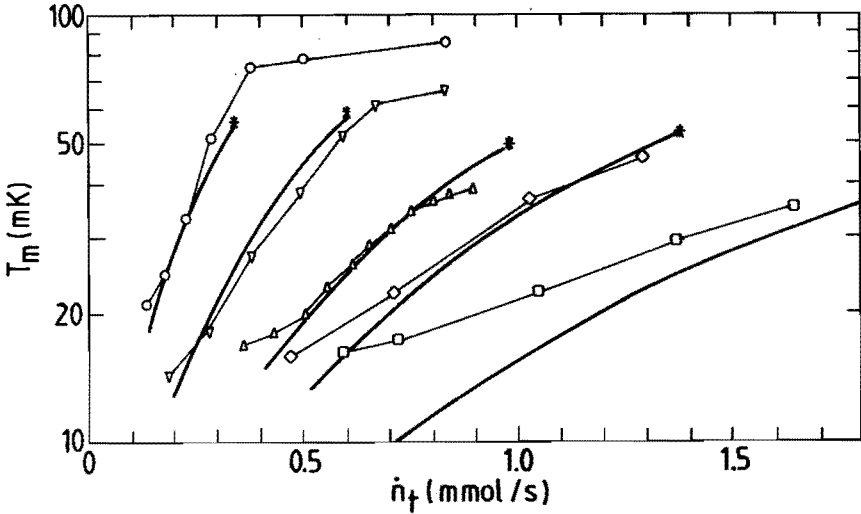
Fig. 4.4.8.   *Measured $T_m-\dot{n}_t$ dependences for $\dot{Q}_i=\dot{Q}_z=0$ for five different tubes (L and D in mm): ($\circ$), L=1382, D=1.6; (∇), L=280, D=1.6; ($\triangle$), L=10.5, D=1.2; ( ), L=23, D=1.6; and ($\square$), L=5, D=1.6. The solid curves are calculated with Eq.(4.4.5.). Critical flow rates, corresponding with Eq.(4.3.7.) are indicated with ✗. The lines connecting the measured points are to guide the eye only.*

The experimental $T_m-\dot{n}_t$ dependences with $\dot{Q}_i=\dot{Q}_z=0$ are also given in figure 4.4.8. At low flow-rate values, T_m is determined by the heat exchangers ($T_e<0.9T_i$). At high flow rates a high percentage of ^{4}He is circulated ($\dot{n}_t>\dot{n}_{tc}$). At intermediate flow rates the measured T_m values are in agreement with Eq.(4.4.5.).

C   Superleak shunt

With S//Z$_m$, the temperature rise in Z$_m$ is much smaller than in

58

case of no superleak shunt. Furthermore, there is a fairly good agreement between the measured $T_m - T_e$ dependences and the dependence according to Eq.(2.2.17.). In figure 4.4.9 a typical example of the measured temperatures with $S//Z_m$ is given. The value of T_e, calculated with Eq.(2.2.17.), is given in this figure also.
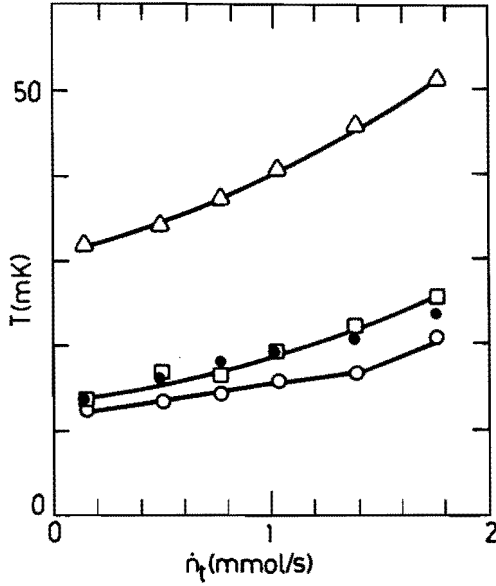
Fig. 4.4.9.   *Measured temperatures T_m (∘), Te (□), and Ti (△), as functions of $\dot{n}_t$, for a Z_m (L=33 mm, D=1.6 mm) shunted by a superleak (S//Z_m). The values of T_e calculated with the measured T_m and Eq.(2.2.17.) are indicated by •.*

4.5   *Experiments inside the flow impedance*

A   Temperatures

The expressions for the temperature rise (Eq.(4.4.4.)) and the concentration drop (Eq.(4.3.6.)) over a flow impedance with length L are derived from measurements performed in the liquid on both sides of Z_m. End effects (the creation and destruction of the flow profile in the tube), might cause disturbances in the

temperature and concentration profiles. Therefore, the possibility
exists that the given ΔT^2-L and Δx-L relationships are not valid
in the tube itself. An experiment where T or x are measured *inside*
the flow impedance will show the influence of end effects.
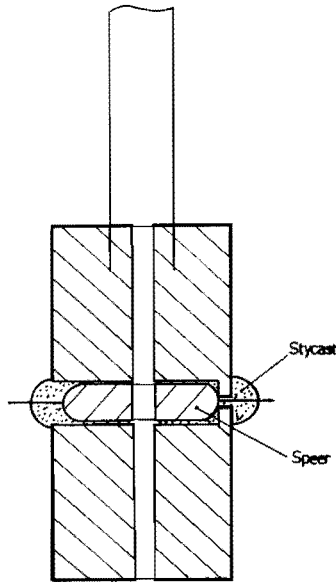
Fig. 4.5.1   *Flow impedance with built-in resistance thermometer.*
             The Z_m (L=23 mm, D=1.2 mm) is made of araldite. At
             half its length a Speer carbon resistor is fitted
             in. The flow channel perforates the carbon core of
             the resistor.

Unfortunately, an open capacitor for concentration measurements
inside the tube can not be constructed, with the necessary
accuracy. However, it is possible to measure a temperature in Z_m
locally, using the set-up depicted in figure 4.5.1. In this
experiment the main part of Z_m consists of an araldite cylinder
with a length L of 23 mm. In the middle a 220 Ω Speer resistor is
glued with Stycast 1266. A flow channel with a diameter of 1.2 mm
is drilled along the axis of the cylinder, going right through the
(1.8 mm diameter) carbon core of the Speer resistor. In this way a
good thermal contact between the liquid in the flow channel and

60

the resistance thermometer is established. By perforating the
resistor, its resistance value changes to 320 Ω. In order to
minimize heat transport from the mixing chamber to the resistor
along its electrical connections, 100 μm Niomax superconducting
wire is used. On top of the araldite cylinder a cupro-nickel tube
is glued, in order to attach the device to the dilute exit channel
of the mixing chamber. The flow impedance of this cupro-nickel
tube is negligible.
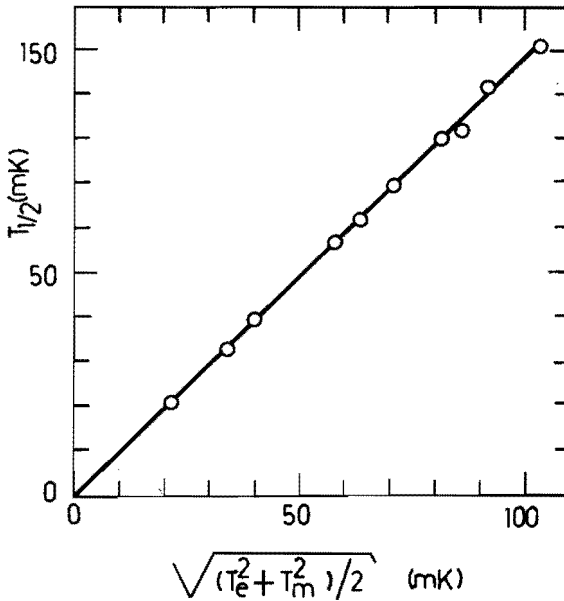
Fig. 4.5.2   *The measured values of $T_{1/2}$ plotted against*
     $\sqrt{(T_e^2 + T_m^2)/2}$, *for different flow rates and different*
     values of T_m. The drawn line connecting the point has
     slope 1, showing the validity of Eq.(4.5.2.).

When end effects are negligible, the temperature at half the
length of the impedance, $T_{1/2}$, will be given by Eq.(4.4.4.):

$$T_{1/2}^2 = T_m^2 + \frac{L}{2}\eta'' a j_3^\alpha \; ,$$

                 4.5.1.

which results in

$$T_{1/2}^2 = \frac{T_e^2 + T_m^2}{2} \ .$$
<div align="right">4.5.2.</div>

In figure 4.5.2 the measured values of $T_{1/2}$ are plotted against $\sqrt{(T_e^2 + T_m^2)/2}$ for several different flow rates and different values of T_m. This figure shows the validity of Eq.(4.5.2.) for our experimental region. This observation makes it plausible that, for our experiments, end effects are negligible and that Eq.(4.4.4.) can be written in a local form according:

$$2TdT = \gamma''aj_3^\alpha d\ell \ ,$$
<div align="right">4.5.3.</div>

where $d\ell$ is an infinitesimal part of length. Together with Eq.(4.4.3.)., we can write Eq.(4.3.6.) as

$$dx = -\gamma''j_3^\alpha d\ell \ .$$
<div align="right">4.5.4.</div>

Equations (4.5.3.) and (4.5.4.) now actually describe the temperature and [3]He concentration profile in the flow impedance.

B   Vibrating-wire experiment

The condition of the bulk liquid inside the flow impedance Z_m is investigated with a vibrating-wire technique. With this technique the forces working upon a small wire placed in a liquid can be measured. When a wire is vibrating in a liquid, the motion of the wire will be damped. The magnitude of damping will depend on the viscosity and the density of the liquid. Furthermore, it is possible that the motion of the liquid itself may have an influence on the motion of the wire. For instance, one might expect that a wire placed in a turbulent liquid is more strongly damped than a wire placed in a liquid of equal composition at the same temperature at rest.

The theory for a vibrating-wire detector placed in a liquid at rest has been described by several authors, e.g. Tough et al. (Tou64), Black et al. (Bla71), Alvesalo et al. (Alv75), Bruschi

and Santini (Bru75), Hojgaard Jensen et al. (Hoj80), Carless et al. (Car83), and Guenault et al. (Gue83). Here we will only give a brief description of the vibrating wire system. In principle it consists of a superconductive wire with radius r, bent into a loop of radius R. A magnetic field B is applied in the plane of the loop. An AC current through the wire generates a vibration due to the Lorentz forces. Magnetic flux changes cause an induced voltage over the loop. By steadily changing the frequency of the driving current, the resonance peak of the system can be registered. This peak is characterized by two parameters: the frequency shift Δf_1 equal to the difference between the resonance frequency in vacuum and the resonance frequency in a medium, and the half-height width of the peak Δf_2. The density and the viscosity of the liquid can be calculated from Δf_1 and Δf_2. If the density of the non-superfluid component of the liquid is known (as in ^{3}He-^{4}He mixtures at very low temperatures), the bulk viscosity of the liquid can be obtained from Δf_2.

The vibrating wire device (see figure 4.5.3) used in our experiment consists of a Nb wire (50 μm core, 5 μm insulation) bent into a loop with a radius of 1 mm. The leads to the loop are fed through a stainless steel capillary (inner diameter 0.15 mm, outer diameter 0.3 mm) in such a way that the wire loop is fixed on top of this capillary. The capillary is fixed to a support cap. On top of this cap a flow impedance (L=25 mm, D=2 mm) is attached, in such a way that the wire loop is situated at the axis of the impedance at 1/3 of its length. A permanent magnet is placed around the flow impedance, resulting in a magnetic field of 0.075 Tesla near the loop. Wide openings in the support cap assure a free access of the mixture to the flow impedance. In the mixing chamber this flow impedance can be shunted by a very small flow impedance (L=23 mm, D=5 mm), or by a superleak. When Z_m is shunted by a small flow impedance, most of the ^{3}He will leave the mixing chamber through this tube. Hence, the ^{3}He flow in Z_m will approach zero. In case of a superleak both the ^{4}He and the ^{3}He components can be moving. In this way measurements in three possibly different types of flow can be performed in order to investigate the influence of these flow types on the damping of the wire.

WIRE

MAGNET

SUPPORT CAP
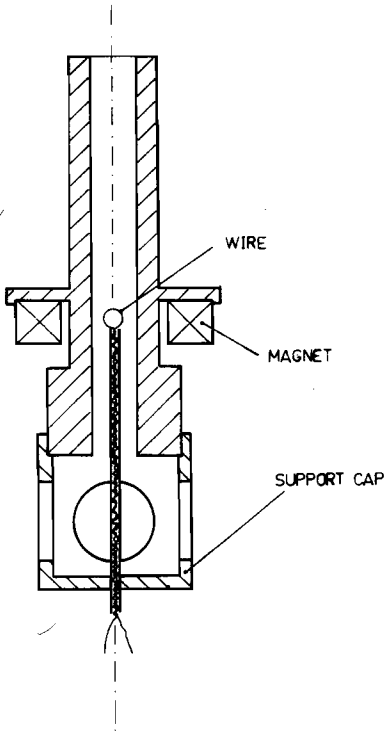
Fig. 4.5.3   Schematic drawing of the vibrating wire device. The flow impedance, the wire is placed in, has L=25 mm and D=2 mm. The wire consists of of Nb and has a core diameter of 50 μm. The permanent magnet gives a field of about 0.075 T at the wire position.

The measurements are performed at different flow rates and mixing chamber temperatures. In case of no superleak shunt, local temperatures at the position of the wire are calculated with Eq.(4.5.3.). With a superleak shunt the temperature rise in Z_m is negligible and the temperature near the wire can be set equal to T_m.

In figure 4.5.4 measurements of the half-height width of the peak are given as a function of the temperature for the three different types of flow in Z_m. For all three situations the damping of the wire in the liquid is equal, showing that there is no difference in the behaviour of the bulk liquid in a volume scanned by the vibrating wire. In our experiments the amplitude of vibration of the wire is on the order of 1 μm.
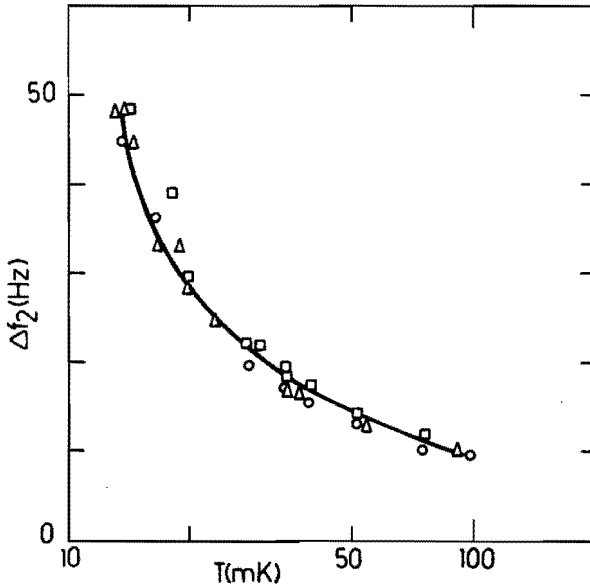
Fig. 4.5.4   The half-height width of the resonance peak Δf_2, as a
function of the temperature. Measurements are
performed for three different flow conditions:
($\circ$), $Z_m=0$; ($\triangle$), $L=25$ mm, $D=2$ mm; ($\square$), $S//Z_m$.

4.6   Pressure changes and osmotic pressure

In principle a pressure drop over Z_m will arise when ^{3}He
moves from M to E. This pressure drop will depend on the flow
rate, the size of Z_m, the temperature T_m, and the type of flow in
Z_m. Measurements of the pressure difference are performed with and
without $S//Z_m$.

For a laminar flow in cylindrical tubes the pressure drop is
given by Eq.(2.2.9.). At low temperatures, and in the situation of
constant H_3^{os} and μ_4 across the flow impedance, the pressure
difference can be expressed in terms of T_e and T_m, according to
Eq.(2.2.18.). In figure 4.6.1 some results are presented for
measurements with a superleak parallel to the flow impedance
($S//Z_m$), for different flow rates and different values of T_m. In
this figure the variation in the capacitance of the pressure gauge

is plotted against the right hand side of Eq.(2.2.18.), using the measured temperature values T_e and T_m. The points show a linear relationship with a slope of 460±15 aF/Pa, in good agreement with the calibration of the pressure gauge of 480±30 aF/Pa (see section 3.5.). In figure 4.6.2 the measured pressure differences, using the calibration of figure 4.6.1, are plotted against the ^{3}He flow rate for two values of T_m. This figure shows that the extrapolated pressure difference at zero flow rate has an offset value which is dependent on the mixing chamber temperature. No satisfactory explanation has been found yet for this phenomenon.
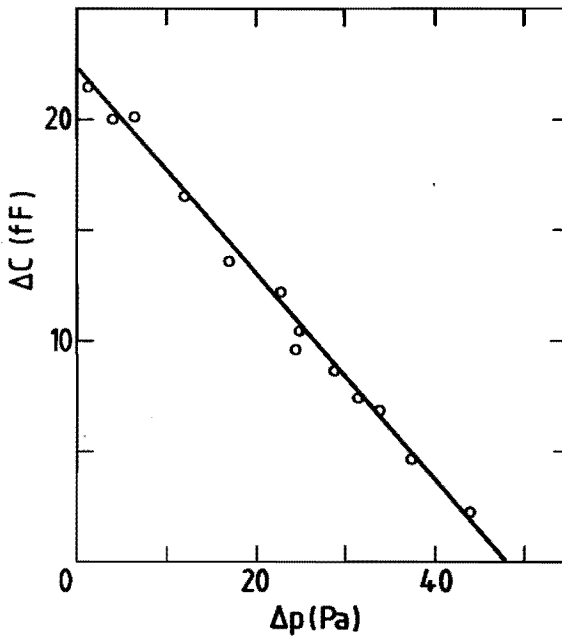
Fig. 4.6.1   Pressure changes across a tube shunted by a superleak
(S//Z). The variation ΔC of the capacitance C of the
pressure gauge (defined as ΔC=C−2450 fF) is plotted
versus the pressure difference Δp calculated from
the measured T_e and T_m with Eq.(2.2.18). The slope of
the line is 460±15 aF/Pa, in good agreement with the
calibration of the pressure gauge (480±30 aF/Pa).

From the slopes of the two lines at different T_m in figure 4.6.2 the values for the viscosity constant η_0 can be calculated with Eq.(2.2.9.) From the data for T_m=14 mK a value of 5.2×10^{-8} sPaK^2 is obtained, wich is in agreement with the value for η_0 given by Kuenhold et al. However, for T_m=20 mK one obtaines a very high value of 9.7×10^{-8} sPaK^2.

Apparently, the measured pressure differences across Z_m in the situation of a superleak shunt, are in agreement with Eq.(2.2.18.), derived from a thermodynamic consideration, but in disagreement with Eq.(2.2.9.), which results from a hydrodynamic description of the system. It is possible that the high ^{4}He flow rates, present in the superleak shunted system, are responsible for this effect. At the moment there is not enough experimental data to confirm this presumption.
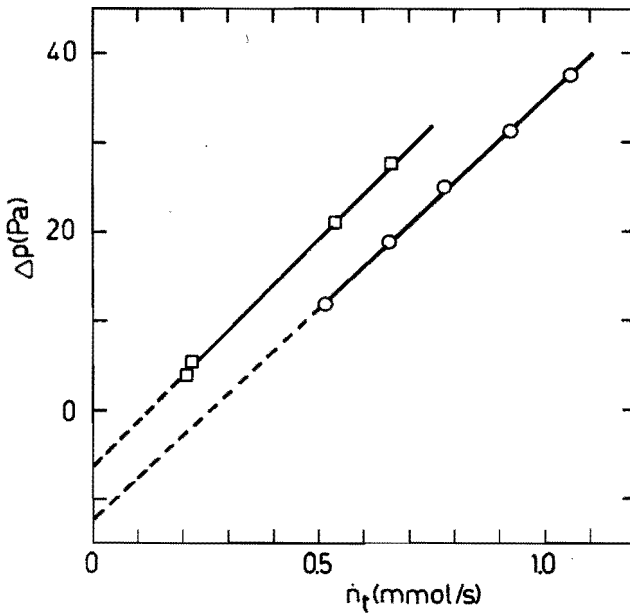
Fig. 4.6.2   Measured pressure differences Δp as functions of $\dot{n}_t$.
The pressure differences are obtained using the
calibration of the pressure gauge given in
Fig. 4.6.1. Measurements are performed at two mixing
chamber temperatures: ($\square$), 14 mK; ($\circ$), 20 mK. The
flow resistance has L=23 mm and D=1.2 mm.

In the absence of a superleak, the measured pressure
differences are no longer in agreement with the pressure drops
calculated with Eq.(2.2.18.). For the cylindrically shaped flow
impedances, as most commonly used in our measurements, the
pressure differences are on the order of 1 Pa. This is three
orders of magnitude smaller than the values of about 1000 Pa that
would result from Eq.(2.2.18.) and the measured T_e and T_m values.
This observation leads to the simple flow property that, within
about 1 Pa, the pressure drop due to the ^{3}He flow through ^{4}He II
is zero.
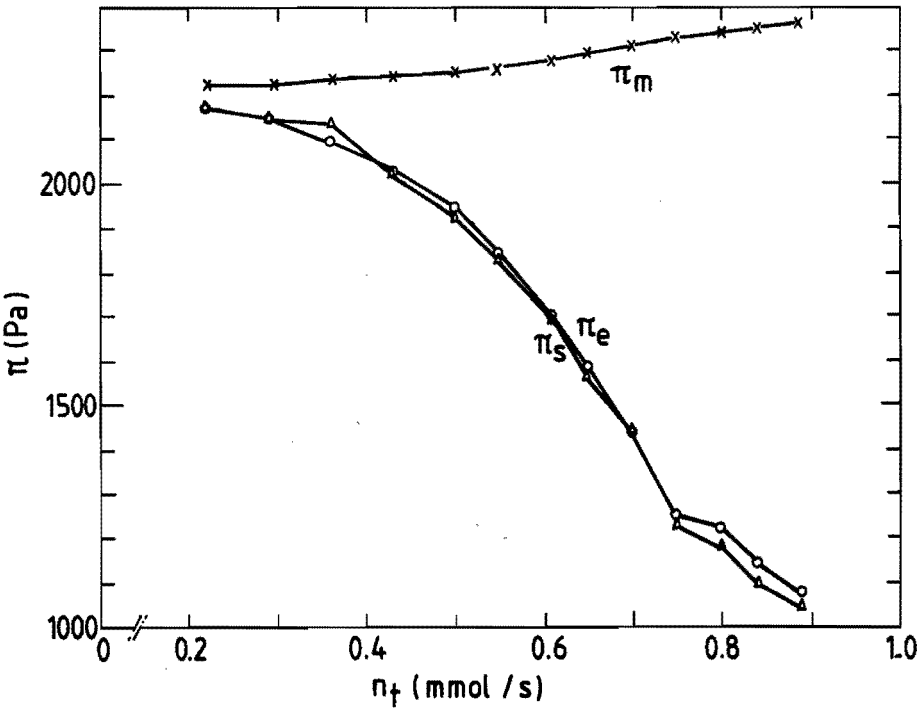
Fig. 4.6.3   Osmotic pressure in M, E, and in the still, plotted
versus $\dot{n}_t$ for a tube Z_m with L=10.5 mm and D=1.2 mm.
The osmotic pressures in M and E, represented by ×
and ○, respectively, are calculated from the values
of x and T measured. The osmotic pressure in the
still (△) was determined with the London device.

However, measurements performed in a later stadium of the investigation, show that when special types of flow impedances are chosen (i.e. several cylindrical tubes with a small inner diameter in parallel), pressure drops, substantially different from zero, are observed over Z_m. These measurements will be discussed in section 5.2.

The osmotic pressures Π_s and Π_e are determined as described in section 3.6. In figure 4.6.3 a typical example is given. The values of Π_s and Π_e are equal within the uncertainties of the calibration of the thermometers in the London device. Large differences between Π_e and Π_m are observed even though the pressure drop is zero (compare Eq.(2.2.19.)).

4.7 *Nonadiabatic flow measurements*

Until now only adiabatic flow experiments have been discussed.
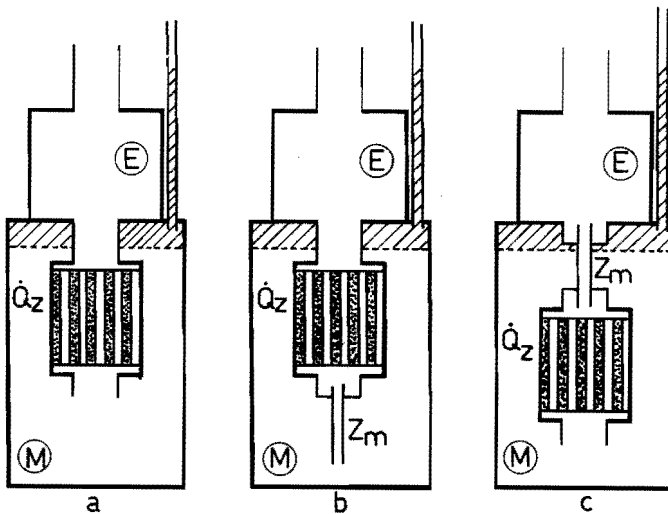
Fig. 4.7.1   Set-up used in nonadiabatic flow experiments.
(a) Heater connected between M and E without a flow resistance in series. (b) Series connection of Z_m and the heater. ^{3}He first passes Z_m and then the heater.
(c) Positions of Z_m and the heater are interchanged with respect to (b).

In this section we will discuss measurements where a heating power
$\dot{Q}_z$ is supplied to the liquid, flowing from M to E.
This heat is supplied by the heater described in section 3.2.
Three different types of nonadiabatic flow experiments are
performed. In the first type the ^{3}He flows through the heater with
no flow impedance in series ($Z_m=0$, figure 4.7.1.a). In figure
4.7.2 a T^2-x diagram is given in which lines of constant osmotic
pressure (isotones) are drawn (Kue85), together with three pairs
of measured T^2_e-x_e,T^2_m-x_m points.
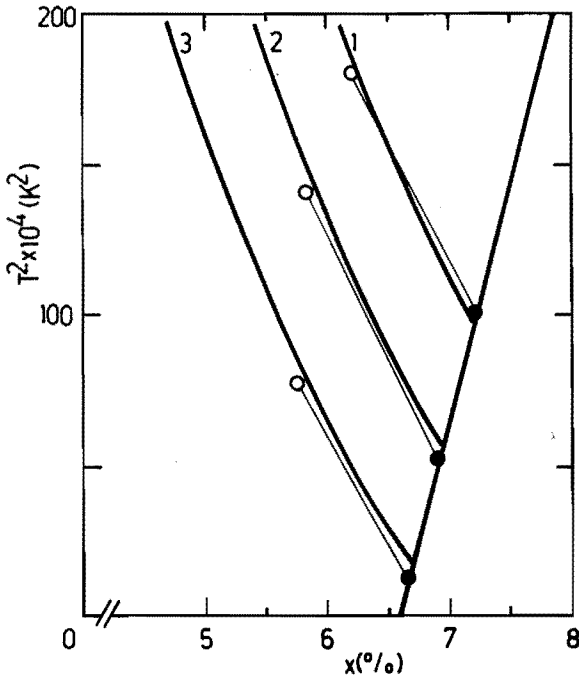
Fig. 4.7.2   Calculated lines of osmotic pressure: 1, $\Pi=3200$ Pa;
2, $\Pi=2800$ Pa; and 3, $\Pi=2400$ Pa. The points represent
the measured T^2_e-x_e (○) and corresponding T^2_m-x_m (●)
pairs in nonadiabatic flow measurements with $Z_m=0$
(Fig. 4.7.1.a).

It shows that the osmotic values of the corresponding $T_e^2-x_e$, $T_m^2-x_m$ pairs are equal. This demonstrates that for $Z_m=0$ holds:

$$\Pi_e = \Pi_m \; . \qquad\qquad\qquad 4.7.1.$$

In the temperature region of our experiments the fountain pressure is negligible and, since $Z_m=0$, the pressures in M and E will be equal, as confirmed by measurements with the pressure gauge. Therefore, Eq.(4.7.1.) can be transformed in the important flow property

$$\mu_{4_e} = \mu_{4_m} \; . \qquad\qquad\qquad 4.7.2.$$

This relation is the familiar steady state relation in the absence of mutual friction (see section 2.1).

In the experiments of the second type, a flow impedance Z_m is connected in series with the heater in such a way that the ^{3}He, leaving M, first passes Z_m, next passes the heater, and then enters E (figure 4.7.1.b). The $T_e^2-x_e$ relationships are determined by varying $\dot{Q}_z$ for certain, fixed, values of $\dot{n}_t$ and T_m. The mixing chamber temperature is fixed within 1 mK by adjusting $\dot{Q}_i$. In figure 4.7.3. some typical results are given for three different values of T_m. Like in the adiabatic flow experiments no pressure drop over Z_m could be detected. The measured $T_e^2-x_e$ relationships follow an isotone. Measurements with the London device confirmed this observation, by showing a constant Π_e. This means that not the ^{3}He concentration x_e but the ^{4}He chemical potential μ_4 is constant. As a consequence Eq.(4.3.6.) is no longer valid for nonadiabatic flow. In section 5.1 this will be discussed in more detail.

In the third set of experiments the positions of the heater and Z_m are interchanged. Hence, the ^{3}He first passes the heater and then Z_m (figure 4.7.1.c). Again the $T_e^2-x_e$ relationships are measured for fixed T_m and $\dot{n}_t$. These relationships turn out to be the same as in the experiments of the second type, showing that in

the region of our experiments the sequence of heater and flow
impedance is of no importance.
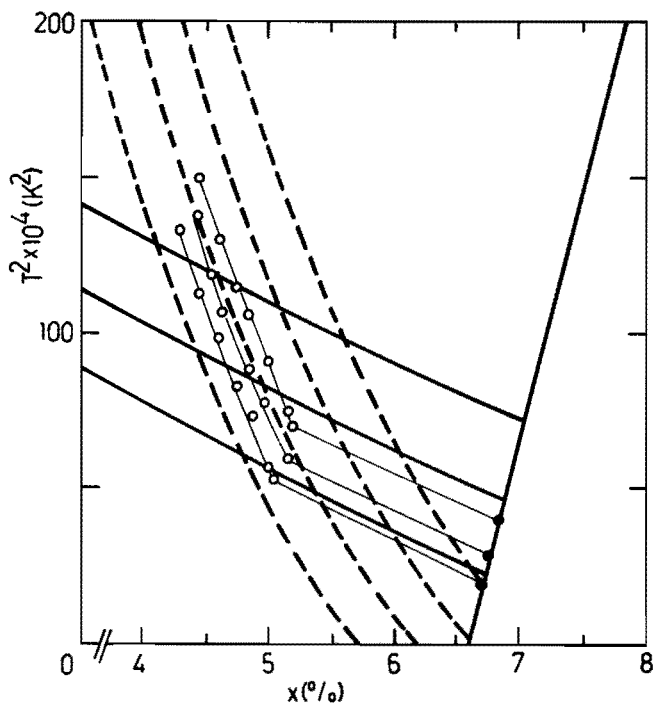
Fig. 4.7.3 Typical results of T_e^2-x_e relationship in
nonadiabatic flow experiment (○). The impedance Z_m
(L=23 mm, D=1.5 mm) and the heater are connected in
series according to Fig. 4.7.1.b. Measurements are
performed at three different, constant values of T_m
(●). The points are obtained by increasing $\dot{Q}_z$ while
adjusting $\dot{Q}_i$ to fix T_m. The solid lines are
isenthalps, the dashed lines represent isotones, and
the thin lines connecting the points are to guide the
eye only. The total flow rate used was 0.75 mmol/s.

V ^{3}HE-^{4}HE FLOW PROPERTIES; A NEW DESCRIPTION INCLUDING MUTUAL FRICTION.

5.1 *Summary of some empirical ^{3}He flow properties, and a comparison with related work*

A ^{3}He Flow properties

In chapter II a description was given of the Mechanical Vacuum model for ^{3}He flow in ^{3}He-^{4}He mixtures, at very low temperatures. In this model it is assumed that no mutual friction exists between the ^{3}He particles and the ^{4}He superfluid. As we have seen this would imply that, in the steady state, the ^{4}He chemical potential is constant. Using this result, together with energy conservation, and the Poiseuille equation, the temperature, ^{3}He concentration, and pressure profiles were deduced from the viscous force on the ^{3}He particles. The results of our experiments, however, were in disagreement with the MV-model, unless the flow impedance in use was shunted by a superleak. For adiabatic flow without a superleak, the flow properties can be summarized by:

$$p = \text{constant}, \qquad\qquad 5.1.1.$$

$$T^2 + ax = \text{constant}, \qquad\qquad 5.1.2.$$

and
$$x_e = x_m - \gamma"Lj_3^\alpha , \qquad\qquad 5.1.3.$$

with
$$j_3 = \left[\frac{4\dot{n}_3}{\pi D^2}\right] . \qquad\qquad 5.1.4.$$

The absence of an explicit temperature dependence in Eq.(5.1.3.) suggests that the ^{3}He flow is determined by the concentrationdrop, $x_m - x_e$, across the tube. However, it must be noted that, due to the validity of Eq.(5.1.2.), any linear combination of x and T^2 can be the factor determining the ^{3}He flow as well. The difference between the values in M and E of such a combination will also be proportional to Lj_3^α. Hence, no explicit conclusion about the ^{3}He-flow-determining quantity can be drawn

73

from the results of adiabatic flow experiments. From the experiments with nonadiabatic flow (see section 4.7) it can be seen that Δx changes with $\dot{Q}_z$, while the difference between the ^{4}He chemical potentials in M and E remains constant. Since, in the T-x region of our interest, μ_4 can be written as a linear combination of x and T^2 (Cas85, Kue85), Eq.(5.1.3.) can be generalized to

$$\mu_{4_e} = \mu_{4_m} + \Gamma L j_3^\alpha ,$$ 5.1.5.

where $$\Gamma = (32\pm4)\times10^{-9} \text{ (SI units).}$$ 5.1.6.

Equation (5.1.3.) can be regarded as a special case of Eq.(5.1.5.) for adiabatic flow. The validity of Eq.(5.1.5.) is shown in figure 5.1.1. where measured values of $\mu_{4_e}-\mu_{4_m}$ are plotted against $j_3^{2.8}$ for various tubes, and several values of T_m.
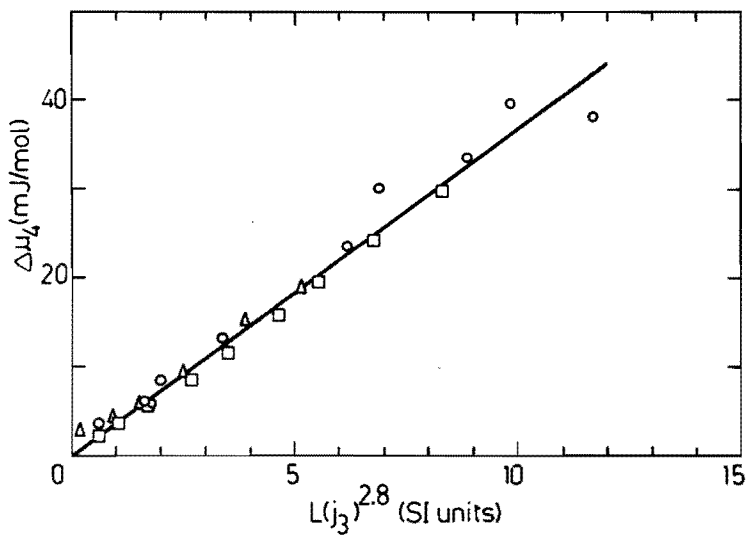
Fig. 5.1.1   Values of $\Delta\mu_4$ plotted versus $L(j_3)^{2.8}$ for 3 flow impedances (L and D in mm) and several mixing chamber temperatures in the range between 15 and 100 mK: (○), L=23, D=1.2; (□) L=10.5, D=1.2; (△) L=23, D=1.6. The drawn line corresponds with $\Gamma=36.5\times10^{-9}$.

74

The relations (5.1.1.) and (5.1.3.) differ from the analogous relations (2.2.9.) and (2.2.22.) obtained with the MV-model. However, when $S/\!/Z_m$ the experimental observations are in much better agreement with the predictions of the MV-model. This can be explained by assuming a mutual friction between the ^{3}He and the ^{4}He (Coo82). With $S/\!/Z_m$, the ^{4}He circulates between the mixing chamber, the tube, the experimental space and the superleak. When in Z_m the ^{4}He velocity is equal to the ^{3}He velocity, the mutual friction is zero. Furthermore, the ^{4}He chemical potential across the superleak is constant: $\mu_{4_e} = \mu_{4_m}$. Hence, two basic conditions for the MV-model are satisfied.

B.   Comparison with related work

    In 1971, Wheatley et al. (Whe71) measured the temperature increase resulting from a flow impedance consisting of an annular space (width 0.1 mm) between two cylinders (see figure 5.1.2).
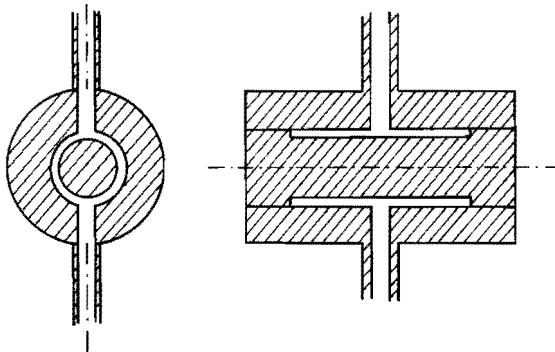
Fig. 5.1.2.   The flow impedance Z_m used by Wheatley et al. The flow channel consists of a slit, with a width of 0.1 mm and a length of 10 mm, between two concentric cylinders. The diameter of the inner cylinder is 6.35 mm.

The ^{3}He was flowing perpendicular to the cylinder axis. The mixing chamber temperature range was 12 to 40 mK; the ^{3}He flow rate varied between 10 and 53 μmol/s. Contrary to the observations described in the former part of this thesis, the experimental results of Wheatley's experiment were in good agreement with the MV-model.

In order to investigate this discrepancy we duplicated the flow impedance used by Wheatley. Unfortunately, it is not possible to operate our refrigerator at flow rates below 150 μmol/s. In figure 5.1.3 the Δx-$\dot{n}_t$ measurements with $\dot{Q}_z$=0 and $\dot{Q}_i$=0 are given.
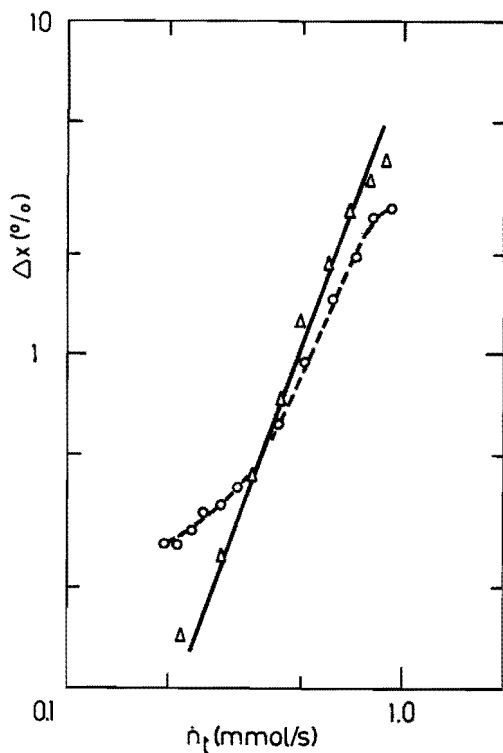
Fig. 5.1.3   Measured Δx-$\dot{n}_t$ dependences for two flow impedances:
(△) cylindrical tube, L=10.5 mm, D=1.2 mm;
(○) duplication of the impedance used by
Wheatley et al.

76

In this figure the Δx-$\dot{n}_t$ measurements for a cylindrical tube
(L=10.5 mm, D=1.2 mm) are presented also. For $\dot{n}_t$>0.4 mmol/s the
Δx-$\dot{n}_t$ dependences for both flow resistances are almost identical,
but for $\dot{n}_t$<0.4 mmol/s, Δx for the annular space impedance tends to
be larger. Furthermore, a dependence of Δx on T_m is found. The
agreement with Eq.(5.1.3.) is improved when T_m is increased, but
there are still deviations from the $\dot{n}_3^\alpha$-behaviour at lower flow
rates.

Our measurements with the annular space impedance,
extrapolated to lower flow rates, do not agree with the MV-model.
On the other hand, deviations from the empirical relation (5.1.3.)
as determined with long cylindrical tubes were observed for this
special type of flow impedance. Apparently the geometry of the
flow channel plays a role.

Niinikoski (Nii71) reported the observation of large osmotic
pressure differences between the mixing chamber and the still
(compare figure 4.6.3) which were not compensated by a fountain
pressure or by a pressure drop due to the viscosity of the
solution. From the flow impedance of Niinikoski's sintered heat
exchangers it can be estimated that the free passage in the heat
exchangers is a slit with dimensions 7 mm×0.4 mm. Using
Eq.(4.3.7.), with x_m=0.08, a critical flow rate of 800 µmol/s is
found. This value is in the flow-rate range of 50-1200 µmol/s, as
used by Niinikoski. According to our empirical relations large
deviations from the MV-model should be expected.

Frossati et al. (Fro77) observed anomalous $\dot{n}_3$-$\dot{Q}_s$ behaviour
similar to the phenomena described in section 4.2. With a tube in
the dilute channel with D=0.5 mm and an estimated length of 100
mm, a critical flow rate of about 60 µmol/s was found. From
Eq.(4.3.7.) a critical flow rate of 80 µmol/s would follow.
Furthermore, Frossati observed that with a tube with D=1.8 mm and
L=6 m, flow rates up to 300 µmol/s could be realized. This value
should be compared with the critical flow rate of 240 µmol/s
following from Eq.(4.3.7.).

In order to draw definite conclusions from the observations of Niinikoski and Frossati, more detailed information would be necessary. However, from the data available in (Nii71) and (Fro77), it seems justified to conclude that their observations are consistent with Eq.(4.3.7.).

5.2 *Hydrodynamic considerations*

A   Theoretical description

For ^{3}He flow through superfluid ^{4}He the gradient in the chemical potential of the ^{4}He is given by the empirical relation

$$\frac{d\mu_4}{d\ell} = \Gamma j_3^\alpha \quad , \qquad\qquad 5.2.1.$$

where $\alpha = 2.8 \pm 0.4$ and $\Gamma = (32 \pm 4) \times 10^{-9}$ (SI-units).

In section 2.3 it is discussed that in case of mutual friction between the normal and superfluid components in pure ^{4}He II, for axial flow in long cylindrical tubes holds

$$\frac{d\mu_4}{d\ell} = -V_{4_s} F_{sn}, \qquad\qquad 5.2.2.$$

where V_{4_s} is the volume of the liquid containing 1 mole of the superfluid component. According to Eq.(2.3.5.) the mutual-friction-force density $\vec{F}_{sn}$ is proportional to the cube of the relative velocities between the two components. At very low temperatures, as in dilution refrigerators, the ^{4}He consists of the superfluid component only. However, in ^{3}He-^{4}He mixtures the ^{3}He constitutes the normal fluid. Therefore, in accordance with Eq.(2.3.5.) we will introduce a mutual friction force density $\vec{F}_{43}$ between ^{3}He and ^{4}He, given by

$$\vec{F}_{43} = A_{43}\rho_4\rho_3(\vec{v}_4 - \vec{v}_3)^3 \quad . \qquad\qquad 5.2.3.$$

where $\vec{v}_4$, $\vec{v}_3$, ρ_4, and ρ_3 are the velocities and densities of the two helium isotopes respectively. The constant A_{43} is anologous to

the Gorter-Mellink constant A_{sn}. In agreement with relation
(5.2.2.), we can now write

$$\frac{d\mu_4}{d\ell} = -V_4 F_{43} .$$ 5.2.4.

where V_4 is the volume of the mixture containing 1 mole of ^{4}He.
In our experiments the average velocities of the ^{4}He equal zero
and Eq.(5.2.3.) yields

$$F_{43} = -A_{43}\rho_4\rho_3 v_3{}^3.$$ 5.2.5.

and thus $$\frac{d\mu_4}{d\ell} = A_{43}V_4\rho_4\rho_3 v_3{}^3 = \chi\left[\frac{\dot{n}_3}{A}\right]^3 .$$ 5.2.6.

where A is the cross-sectional surface area of the tube. Equation
(5.2.6.) coincides with the empirical relation (5.2.1.) for $\alpha=3$
and $\Gamma=\chi$. The value of 3 for α is in agreement with our experiments
were α was found to be 2.8 ± 0.4. Substituting $\alpha=3$, a best fit of
the experimental results is obtained for $\chi=(11\pm1)\times10^{-9}$ kgsm^{7}mol^{-1},
resulting in a value for A_{43} of 4500 ms/kg. Gorter and Mellink
(Gor49) found a value of 500 ms/kg for the factor A_{sn} in the
situation of counterflow on pure ^{4}He II. Due to the inaccuracy in
the value of α, the value of A_{43} can only be estimated roughly.
With a variation of α from 2.4 to 3.2, values of A_{43} are obtained
varying from 100 to 60000.

As shown above, the gradient in the ^{4}He chemical potential,
observed in our experiments, is in good agreement described by the
relation obtained by introducing a mutual friction force density
F_{43}, analogous to the description of mutual friction in ^{4}He II. In
analogy with section 2.2 the hydrodynamic relations for ^{3}He
flowing through superfluid ^{4}He can now be deduced. As the flow
channel we consider a long tube with length L and arbitrary
uniform cross section with area A. The total ^{4}He molar flow is
equal to zero (no superleak shunt). For adiabatic flow, energy
conservation yields

$$\dot{n}_3\mu_3 + \dot{n}_3TS_F + \dot{Q} = \text{constant} .\qquad 5.2.7.$$

Using the Gibbs–Duhem relation in Eq.(5.2.7.) gives

$$\frac{d\dot{Q}}{d\ell} + \dot{n}_3\left[T\frac{d(S_F)}{d\ell} + V_3\frac{dp}{d\ell} - \left[\frac{1-x}{x}\right]\frac{d\mu_4}{d\ell}\right] = 0 .\qquad 5.2.8.$$

Assuming Poiseuille flow and that the pressure drop is determined by the viscosity of the ^{3}He component, the pressure gradient $dp/d\ell$ is expressed by

$$\frac{dp}{d\ell} = -\eta\dot{n}_3V_3\zeta ,\qquad 5.2.9.$$

where ζ is a geometrical factor, called the impedance factor per unit length. For a single cylindrical tube $\zeta=128/(\pi D^4)$. By substitution of Eqs.(2.2.8.) and (5.2.6.) in Eq.(5.2.8.), and by using the low temperature approximations for κ, S_F, and η, for ^{3}He concentrations close to the value of a saturated mixture at absolute zero, x_0 as given in section 2.2, one obtains

$$-A\kappa_0\frac{d}{d\ell}\left[\frac{1}{T}\frac{dT}{d\ell}\right] + \dot{n}_3C_0T\frac{dT}{d\ell} - \eta_0\left[\frac{\dot{n}_3V_3}{T}\right]^2\zeta - \frac{1-x_0}{x_0}x\left[\frac{\dot{n}_3}{A}\right]^2 = 0\qquad 5.2.10.$$

This equation can be written in a dimensionless form by introducing the dimensionless parameters t, λ, and β, defined by

$$t = T/T_0' ,\qquad 5.2.11.$$
$$\lambda = \ell/L_0' ,\qquad 5.2.12.$$

$$\beta = \frac{\eta_0V_3{}^2C_0\kappa_0}{([1-x_0]x\kappa/x_0)^{3/2}} \times \left[\frac{A^4\zeta}{\dot{n}_3{}^3}\right] \simeq 1.03\left[\frac{A^4\zeta}{\dot{n}_3{}^3}\right] ,\qquad 5.2.13.$$

$$\text{where}\quad T_0' = \left[\frac{[1-x_0]x\kappa_0}{x_0C_0{}^2}\right]^{1/4} \times \left[\frac{\dot{n}_3}{A}\right]^{1/2} \simeq (2.5\times10^4)\left[\frac{\dot{n}_3}{A}\right]^{1/2} ,\qquad 5.2.14.$$

$$\text{and}\quad L_0' = \left[\frac{x_0\kappa_0}{[1-x_0]x}\right]^{1/2} \times \left[\frac{A}{\dot{n}_3}\right]^2 \simeq 46\left[\frac{A}{\dot{n}_3}\right]^2 .\qquad 5.2.15.$$

80

All quantities are expressed in SI-units. The quantities T_0' and L_0' are related to the quantities T_0 and L_0, defined in Eqs.(2.2.13.) and (2.2.14.), according to

$$T_0' = T_0(4\beta)^{-1/6} \qquad\qquad 5.2.16.$$

$$L_0' = L_0(\beta/2)^{-1/3} \; . \qquad\qquad 5.2.17.$$

Substitution of Eqs.(5.2.11-13.) in Eq.(5.2.10.) yields:

$$\frac{1}{2}\frac{dt^2}{d\lambda} - \frac{d}{d\lambda}\left[\frac{1}{t}\frac{dt}{d\lambda}\right] - 1 - \frac{\beta}{t^2} = 0 \; . \qquad\qquad 5.2.18.$$

In this equation the term β/t^2 is a measure for the ratio of the viscous force and the mutual friction force respectively (Kue86). In the limit in which mutual friction is neglected, Eq.(5.2.18.) simplifies to a form similar to Eq.(2.2.15.). The solution of this type of differential equations is described by Van Haeringen et al. (Hae79a, Hae80). Under the condition that viscosity is negligible one obtains Eq.(5.2.18.) without the β/t^2 term. This equation has also been solved by Van Haeringen et al. (Hae79b).[*]

We can now distinquish two limiting regions: $\beta/t^2 \gg 1$ and $\beta/t^2 \ll 1$. For large values of β/t^2, the viscous force is dominant, while for small values of β/t^2 the viscous force is negligible and the mutual friction force is dominant. The experiment performed by Wheatley et al. (Whe71), as described in section 5.1B, was performed in the region of dominant viscous force. From the data provided in their paper values of about 200 can be calculated for β/t^2 for their flow rate and temperature regions. As mentioned before, the temperature measurements were in good agreement with the MV-model. With Eq.(5.2.9.) one would expect a pressure difference Δp across the flow impedance on the order of 20 Pa.

[*] It is interesting to note that the energy balance near the mixing chamber of a ^{4}He circulating dilution refrigerator yields the same dimensionless equation.

Unfortunately, no report was given of pressure measurements in
this experiment. For the Δp experiments reported in section 4.4,
the values of β/t^2 were on the order of 0.004. In these
experiments the viscous force is negligible. Solution of
Eq.(5.2.18.) yields, in this region of small β/t^2, a large
temperature rise in the impedance, as observed in our experiments.
Since the viscosity decreases strongly with temperature,
Eq.(5.2.9.) gives pressure drops over the flow channel on the
order of 1 Pa. Pressure differences of this order are hard to
measure accurately because the pressure differences due to
concentration variations in the liquid are on the same order of
magnitude.

B   Experimental verification

     In the region where the value of β/t^2 is on the order of 1,
the viscous and the mutual friction forces play an equally
important role. The values of the characteristic temperature T_0'
and the characteristic length L_0' depend on the liquid parameters
and the average ^{3}He-flow-rate density j_3 only. On the other hand
the value of β/t^2 depends on the factor $A\zeta$, the ^{3}He-flow-rate
density j_3, and the temperature T according to

$$\frac{\beta}{t^2} = \left[\frac{A\zeta}{T^2}\right]\bar{j}_3^2 \quad . \qquad\qquad 5.2.14.$$

This opens the possibility to change the value of β by changing
the factor $A\zeta$, while keeping T_0' and L_0' constant. In this way the
validity of Eq.(5.2.18.) can be investigated experimentally. This
can be done by performing a series of experiments in which A is
constant and ζ is varied. This was achieved by taking a flow
impedance consisting of a bundle of N parallel tubes, each with
diameter D_N and length L, in such a way that the total area
$A=(N\pi D_N^2)/4$ was constant ($\simeq 2$ mm^2). The factor $A\zeta$ is equal to $8\pi N/A$.
Since A is constant, the value of ζ is proportional to the number
of tubes. The flow properties resulting from three different
bundles of tubes were investigated (compare figure 4.3.7). The ^{3}He
flow rates were in the range of 0.15 to 0.7 mmol/s. For a typical

82

value of $\dot{n}_3=0.5$ mmol/s, the values of T_o' and L_o' were 4 mK and 0.7 mm respectively. The pressure differences Δp were measured as functions of $\dot{n}_3$ for several values of the mixing chamber temperature T_m, varying between 30 and 60 mK. In table 5.2.1. the characteristics for the three flow impedances are given, together with the experimental ranges of β and β/t^2. The parameter Z given in this tabel is equal to the flow resistance according Poiseuille flow ($Z=\zeta L$).

Kind of impedance	N	L (mm)	D_N (mm)	$Z/10^{12}$ (m^{-3})	β	β/t^2 -range
single tube	1	23	1.6	0.14	0.83	0.002-0.1
bundle	9	23	0.5	1.7	5.8	0.015-0.7
bundle	28	23	0.3	5.4	17	0.04 -2.2

Table 5.2.1. *Properties of the flow impedances investigated.*
The Z-values of the tubes are calculated from
the tube dimensions assuming Poiseuille flow.
The β value is calculated for $\dot{n}_3 = 0.5$ mmol/s.
The β/t^2 ranges are given for $\dot{n}_3-T_m$ values of
0.7 mmol/s and T_m=60 mK, and 0.2 mmol/s
and T_m=30 mK respectively.

In figure 5.2.1 measured pressure differences as functions of the flow rate are given for the three flow impedances, for a mixing chamber temperature of 30 mK. In figure 5.2.2 the measured pressure differences across the impedance consisting of 28 parallel tubes are given as functions of $\dot{n}_t$ for various values of T_m between 30 and 60 mK. The values of the viscosity constant η_0 are derived from the linear parts of these figures at low flow rates. They varied from $(5\pm1)\times10^{-8}$ for T_m=30 mK to $(6.5\pm1)\times10^{-8}$ sPaK^2 for T_m=60 mK respectively. These values are in good agreement with the measurements of Kuenhold et al. (Kue72).

For the higher flow rates the increasing temperature in the tube
leads to a decreasing viscosity of the mixture. This effect
results in Δp values smaller than expected from the linear parts
in figures 5.2.1 and 5.2.2.
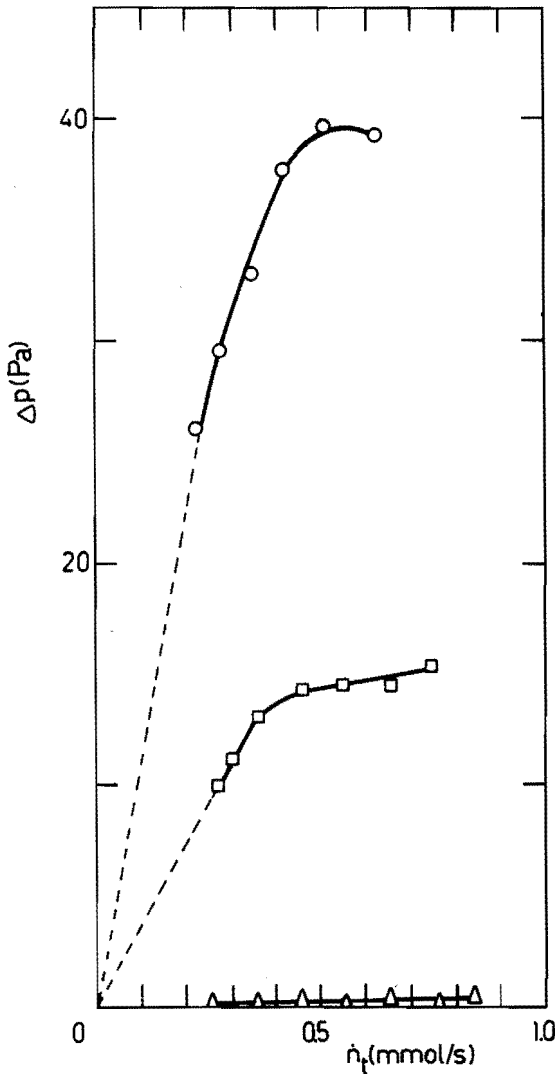
Fig. 5.2.1
Measured pressure
differences across
three different flow
resistances with a length
of 23 mm:
(o), 28 tubes parallel,
    D=0.3 mm;
(□), 9 tubes parallel,
    D=0.5 mm;
(△), 1 single tube,
    D=1.6 mm.
The experiments are
performed with T_m=30 mK.

In figure 5.2.3 differences in μ_4 across the three flow
impedances are plotted as functions of the circulation rate, for
two values of T_m. It is shown that the $\Delta\mu_4$-$\dot{n}_t$ dependences are
equal for the three impedances, indicating that $\Delta\mu_4$ depends on the

84

average ^{3}He flow rate j_3 only, as given by Eq.(5.2.6.). The observation of a pressure difference Δp and a difference in μ_4 confirms that both the viscous force and the mutual friction force are of importance in case of ^{3}He flow through superfluid ^{4}He.
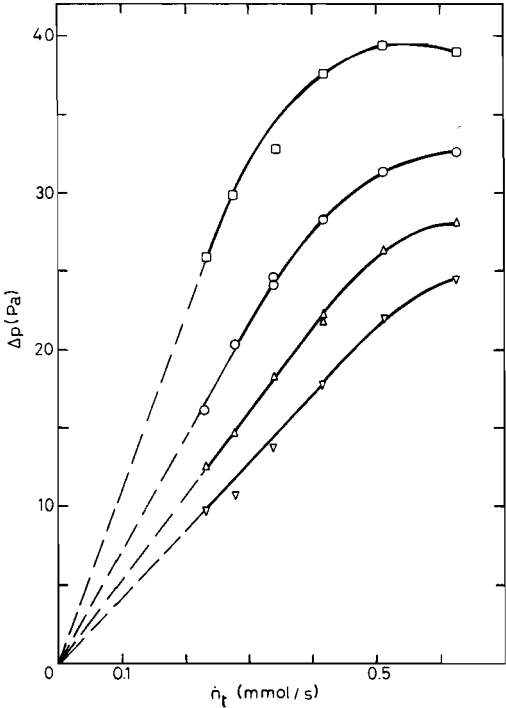
Fig. 5.2.2   *Measured pressure differences across the flow impedance consisting of 28 parallel tubes. The experiment was performed at several mixing chamber temperatures: (□), 30mK; (○), 40 mK; (△), 50 mK; (▽), 60 mK.*

Measurements with a porous plug as a flow impedance have also been performed. The plug had a length of 33.8 mm and a diameter of 8 mm. It consisted of a sintered bronze sponge. The spherical particals had a diameter varying from 30 to 90 μm. The pore size was irregular and varied from 0 to 100 μm. The filling factor was 74%. The values of the cross-sectional area A and the effective length L for this geometry are not well defined. From the results of the $\Delta\mu_4$ measurements an effective area of 1 mm^2 is found. A closed packed system of spheres would yield a free area on the order of 4 mm^2, thus the experimentally obtained effective area seems to be on the low side. Using the value of the impedance factor Z as determined at room temperature (183×10^{12} m^{-3}), the pressure measurement results are in good agreement with Eq.(5.2.9.). This result shows the validity of our analysis for flow-impedance factors which differ by three orders of magnitude.

86
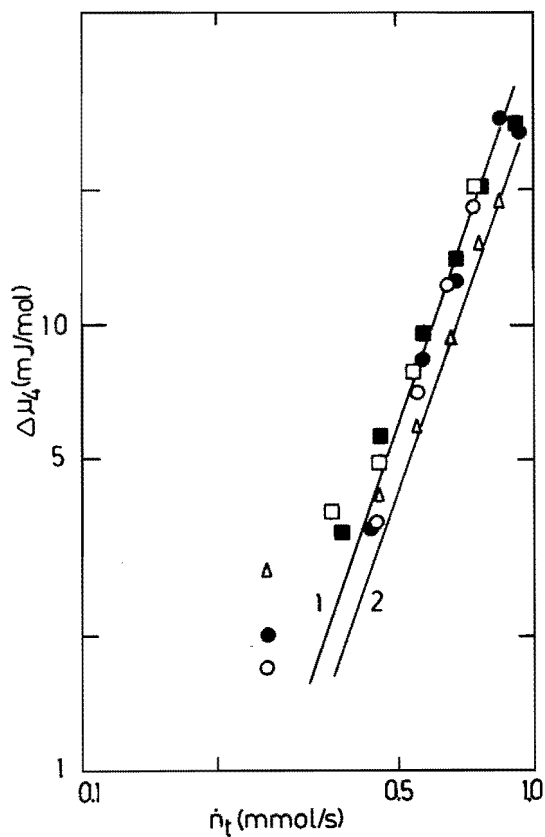
Fig. 5.2.3   Measured values of $\Delta\mu_4$ versus $\dot{n}_t$ for three flow
impedances: $(\circ,\bullet)$, 28 parallel tubes; $(\square,\blacksquare)$, 9
parallel tubes; $(\triangle)$, 1 single tube. Open symbols
correspond with $T_m=30$ mK, closed symbols with
$T_m=50$ mK. Both lines have slope 3. Line 1
corresponds with $\chi=1.1\pm10^{-8}$ for the area of the 9
tubes $(1.77$ mm$^2)$, line 2 with $\chi=1.2\times10^{-8}$ for a
area of 2 mm^2.

5.3 _Discussion_

In this chapter the hydrodynamics of ^{3}He-^{4}He mixtures has been described including both a viscous force and a mutual friction force. The mutual friction in ^{3}He-^{4}He mixtures was described analogous to mutual friction observed in counterflow experiments in pure ^{4}He II. Furthermore, it was assumed that the ^{3}He flow had a Poiseuille profile, and that this flow was accompanied by a pressure gradient determined by the viscosity of the ^{3}He. Under these conditions a hydrodynamic description could be given in agreement with experiments in which both the mutual friction force and the viscous force were important, as well as with experiments in which one force dominated the other.

Although the ^{3}He flow properties are well described by the new hydrodynamic equations, some aspects are open for discussion. As shown before, mutual friction in mixtures is analogous to mutual friction in pure ^{4}He II. It is likely that both forms of mutual friction are generated by a similar mechanism i.e. the interaction with a ^{4}He-vortex tangle (compare section 2.3). In ^{4}He counterflow experiments, mutual friction is accompanied by a critical relative velocity between the normal and superfluid components, below which no turbulence is created (Tou82). It is conceivable that a non-zero critical relative velocity between ^{3}He and ^{4}He exists in mixtures as well. This possibility has not been taken into account in our description, because the experimental data at very low flow rate densities, e.g. the values of $\Delta\mu_4$, could not be analysed with the necessary accuracy. In order to perform decisive experiments with concerning critical velocities, temperatures, ^{3}He-concentrations, pressure drops and flow rates have to be measured with a larger accuracy than present in our experimental set-up.

The values of the ^{3}He viscosity constant η_0, derived from the measurements of the pressure differences across the flow impedance as functions of the flow rate (figure 5.2.2) are in good agreement with the measuremunts of Kuenhold et al. (Kue72). This indicates the validity of the assumption that the pressure gradient in the flow tube is determined by the viscosity of the ^{3}He (Eq.(5.2.9.)). This implies that, in our experiments, the pressure gradient in

the tube, and thus the momentum transfer between different velocity layers in the liquid, is not to a great extend affected by the presence of a vortex tangle. Nevertheless, the possibility of an effect on the momentum transfer in the liquid by a vortex tangle can not be excluded and a thorough investigation of this possibility is commandable.

VI   THE DOUBLE MIXING CHAMBER

6.1   *Introduction*

A multiple mixing chamber, installed in the place of a single mixing chamber, is a reliable tool to decrease the minimum temperature of a dilution refrigerator, without the necessity of modifying the heat exchangers. The simplest form of a multiple mixing chamber is a double mixing chamber (DMC), in which the ^{3}He circulating through the dilution refrigerator is diluted in two steps (Coo79). A schematic drawing of the DMC is given in figure 6.1.1.
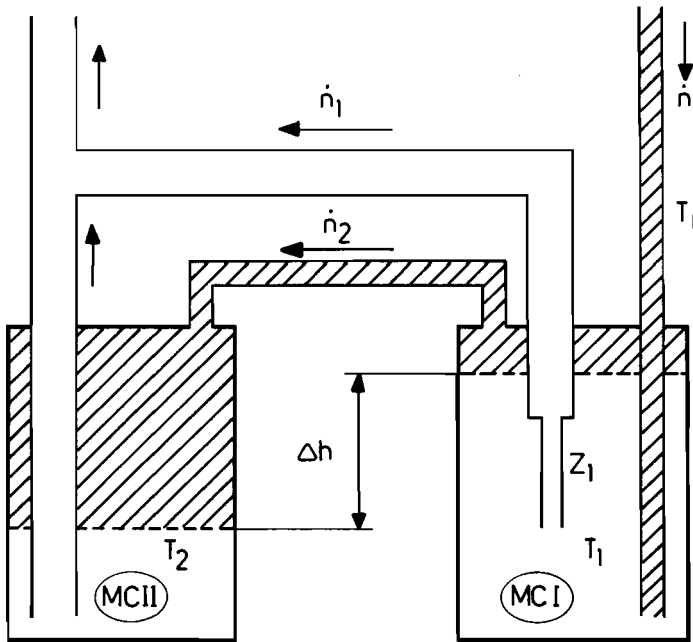
Fig. 6.1.1   *Schematic drawing of a double mixing chamber. The hatched regions represent ^{3}He in the concentrated phase. The first and second mixing chamber are represented by MCI and MCII, respectively. Per second $\dot{n}_1$ ($\dot{n}_2$) moles of ^{3}He are diluted in MCI (MCII). The inlet temperature T_i can be varied with a heater at the entrance tube.*

The concentrated ^{3}He is precooled in the first mixing chamber
before it enters the second mixing chamber. A full discussion of
the DMC in the framework of the MV-model is given by Coops et al.
(Coo79, Coo81). In this chapter a simplified discussion of the DMC
is presented, neglecting heat loads to the mixing chambers. It is
assumed that all the flow resistances in the DMC system can be
neglected, except the resistance of the dilute exit channel of the
first mixing chamber, Z_1 (length L, inner diameter D).
Furthermore, the circulation rate of the ^{4}He is assumed to be zero
$(\dot{n}_4=0, \dot{n}_t=\dot{n}_3)$.

In section 6.2 we will consider the DMC in the framework of
the MV-model. In section 6.3 the properties of the DMC are derived
according to the model including mutual friction. The experimental
set-up and experimental results are discussed in section 6.4.

6.2 *DMC properties according to the MV-model*

In a DMC the total ^{3}He flow rate, $\dot{n}_t$, is diluted in two
steps. A part, $\dot{n}_1$, is diluted in the first mixing chamber MCI; the
other part, $\dot{n}_2$, enters the concentrated side of the second mixing
chamber MCII, and is diluted therein. The temperatures of the
first and second mixing chamber, T_1 and T_2, and the flow rate $\dot{n}_1$
can be obtained from $\dot{n}_t$, T_i and Z_1 with the following relations,
resulting from Eqs.(1.2.1.), (2.2.9.) and (2.2.19):

$$\dot{n}_t H_{3_{cs}} T_i^2 = \dot{n}_1 H_{3_{ds}} T_1^2 + (\dot{n}_t - \dot{n}_1) H_{3_{cs}} T_1^2 , \qquad 6.2.1.$$

$$(\dot{n}_t - \dot{n}_1)(H_{3_{ds}} T_2^2 - H_{3_{cs}} T_1^2) = 0 , \qquad 6.2.2.$$

$$p_1 - p_2 = \frac{128L}{\pi D^4} \frac{\eta_0}{T_1^2} \dot{n}_1 V_3 , \qquad 6.2.3.$$

$$p_1 - p_2 = \Pi_s T_1^2 - \Pi_s T_2^2 , \qquad 6.2.4.$$

$$\Pi_s T_1^2 - \Pi_s T_2^2 = \frac{128L}{\pi D^4} \frac{\eta_0}{T_1} z \dot{n}_1 V_3 \, , \qquad\qquad 6.2.5.$$

where $H_{3_{cs}}$ ($=11.4$ J/molK^2) and $H_{3_{ds}}$ ($= 92.95$ J/molK^2) are the constants in the temperature dependent terms of the ^{3}He molar enthalpies in the concentrated and saturated dilute phase respectively. The expression $\Pi_s T^2$ is the temperature dependent part of the osmotic pressure along the phase separation curve ($\Pi_s = 104.4$ kPa/K^2). Equation (6.2.5.) follows from Eqs.(6.2.3.) and (6.2.4.).

Equations (6.2.1.)-(6.2.5.) can be written in a dimensionless form by introducing

$$t_1 = T_1/T_i, \quad t_2 = T_2/T_i, \quad r = \dot{n}_1/\dot{n}_t, \qquad\qquad 6.2.6.$$

and

$$A_1 = \frac{H_{3_{ds}}^3}{H_{3_{cs}}^2(H_{3_{ds}} - H_{3_{cs}})} \frac{\eta_0 V_3}{\Pi_s} \frac{128L}{\pi D^4} \frac{\dot{n}_t}{T_i^4} \, , \qquad\qquad 6.2.7.$$

resulting in

$$1 = \frac{H_{3_{ds}}}{H_{3_{cs}}} r t_1^2 + (1-r) t_1^2 \, , \qquad\qquad 6.2.8.$$

$$(1-r) \left[\frac{H_{3_{ds}}}{H_{3_{cs}}} t_2^2 - t_1^2 \right] = 0 \, , \qquad\qquad 6.2.9.$$

$$t_1^2 - t_2^2 = \frac{H_{3_{cs}}^2 (H_{3_{ds}} - H_{3_{cs}})}{H_{3_{ds}}^3} \frac{A_1 r}{t_1^2} \, . \qquad\qquad 6.2.10.$$

Equation (6.2.9.) is satisfied when $r=1$ or $H_{3_{cs}} t_1^2 = H_{3_{ds}} t_2^2$. The dimensionless parameter A_1 is chosen in such a way that $A_1 = 1$ when both factors in Eq.(6.2.9.) are zero. From the analysis as given by Coops (Coo81) it follows that for an optimal performance of the DMC, A_1 should be on the order of 2. When $A_1 < 1$, $t_2^2 \neq (H_{3_{cs}}/H_{3_{ds}}) t_1^2$ and there is no ^{3}He flow through MCII ($r=1$). This is a consequence of the fact that the heat loads to the mixing chambers are taken

equal to zero. Whenever there is a small, but finite, heat load to the second mixing chamber, there will be a small flow through MCII as well. For high values of T_i, and/or small values of $\dot{n}_t$, $A_1 \ll 1$, resulting in $T_1 \simeq T_2$. In this situation the DMC behaves as one single mixing chamber. When $A_1 > 1$ then $r < 1$ and $t_1^2 = (H_{3_{ds}}/H_{3_{cs}})t_2^2$. However, for $A_1 \gg 1$ the solutions of Eqs.(6.2.8-10) tend to $\dot{n}_1 = 0$ and $T_1 = T_i$, i.e. the temperature T_2 becomes equal to the temperature of a single mixing chamber.

The dimensionless equations lead to well defined t_1, t_2 vs. A_1 relationships, independent of specific values of $\dot{n}_t$, L, and D. Hence, the t_1, t_2 vs. A_1 dependences are universal for different tubes and flow rates.

The pressure difference, at equal heights in the dilute phases, between MCI and MCII is expressed in Eqs.(6.2.3.) and (6.2.4.). This pressure difference should result in a level difference Δh between the two phase boundaries, following from the condition for hydrostatic equilibrium:

$$\Delta\rho g\Delta h = p_1 - p_2 , \qquad\qquad 6.2.11.$$

where $\Delta\rho = 59$ kg/m^3 is the difference between the densities of the dilute and the concentrated phases, and g is the gravitational acceleration. With Eqs.(6.2.1-5.) and (6.2.11.), Δh can be expressed as a function of T_1, either in viscous or thermodynamic quantities:

$$\Delta h = \frac{128L}{\pi D^4} \frac{\eta_0 V_3}{\Delta\rho g} \frac{\dot{n}_t}{T_1^2} \qquad \text{for } A1 \lesssim 1 \qquad 6.2.12.$$

$$\Delta h = \frac{H_{3_{ds}} - H_{3_{cs}}}{H_{3_{ds}}} \frac{\Pi_s}{g\Delta\rho} T_1^2 \qquad \text{for } A1 \gtrsim 1 . \qquad 6.2.13.$$

A series of experiments with a DMC was performed by Coops, using the dilution refrigerator described in this thesis. The experimental results were analysed within the framework of the MV-model (Coo81). Coops reported that, contrary to the predicted values according Eqs.(6.2.12-13.), no significant level

94

differences were observed. Later experiments confirmed this deviation. However, in his report, Coops remarks that there was indirect evidence that in a small dilution refrigerator, with an average total flow rate of 50 μmols, the level differences Δh were in agreement with Eqs.(6.2.12-13.). These contradictory results could not be understood at that time, but in view of what has been discussed in the previous chapters, one might expect that the observed discrepancies with the theory were due to a mutual friction, not taken into account.

In the following paragraphs the DMC properties will be derived with the aid of the mutual friction equations of chapter five. Subsequently the experimental results are summarized and reanalysed.

6.3 DMC properties including mutual friction

In the previous section the DMC has been discussed with the assumption that the ^{4}He chemical potential is constant. However, in the previous chapters it was shown that a flow of ^{3}He through superfluid ^{4}He gives, due to mutual friction, a gradient in μ_4 in the tube, given by Eq.(5.2.1.). In the region where the mutual friction is dominant, the viscous pressure drop will be very small (see section 5.2). In this case the difference in the ^{4}He chemical potential across the tube is equal to the difference in μ_4 of the saturated dilute mixtures in MCI and MCII, in the low temperature limit given by (Kue85):

$$\mu_{41} - \mu_{42} = \mu_4{}_s(T_1{}^2 - T_2{}^2) \ , \qquad\qquad 6.3.1.$$

where $\mu_4{}_s = -2.882$ J/molK^2. Again T_1, T_2, and $\dot{n}_1$ can be obtained from $\dot{n}_t$, T_i and Z_1 (length L, diameter D) with the following relations corresponding Eqs.(1.2.1.), (5.2.1.) and (6.3.1.):

$$\dot{n}_t H_3{}_{cs} T_i{}^2 = \dot{n}_1 H_3{}_{ds} T_1{}^2 + (\dot{n}_t - \dot{n}_1) H_3{}_{cs} T_1{}^2 \ , \qquad\qquad 6.3.2.$$

$$(\dot{n}_t - \dot{n}_1)(H_3{}_{ds} T_2{}^2 - H_3{}_{cs} T_1{}^2) = 0 \ , \qquad\qquad 6.3.3.$$

$$\mu_{42} - \mu_{41} = \Gamma L \left[\frac{4\dot{n}_1}{\pi D^2}\right]^\alpha , \qquad\qquad 6.3.4.$$

$$(T_1{}^2 - T_2{}^2) = -\frac{\Gamma L}{\mu_{4_s}}\left[\frac{4\dot{n}_1}{\pi D^2}\right]^\alpha . \qquad\qquad 6.3.5.$$

Equation (6.3.5.) follows from Eqs.(6.3.1.) and (6.3.4.). The relations (6.3.2.)-(6.3.5.) can be transformed into a set of dimensionless equations using Eq.(6.2.6.) and the dimensionless parameter B defined by:

$$B^\alpha = \frac{H_{3_{ds}}{}^2}{H_{3_{cs}}(H_{3_{ds}}-H_{3_{cs}})} \frac{-\Gamma L}{\mu_{4_s}}\left[\frac{4\dot{n}_t}{\pi D^2}\right]^\alpha \frac{1}{T_i{}^2} , \qquad\qquad 6.3.6.$$

giving

$$1 = \frac{H_{3_{ds}}}{H_{3_{cs}}} r t_1{}^2 + (1-r) t_1{}^2 , \qquad\qquad 6.3.7.$$

$$(1-r)\left[\frac{H_{3_{ds}}}{H_{3_{cs}}}t_2{}^2 - t_1{}^2\right] = 0 , \qquad\qquad 6.3.8.$$

$$t_1{}^2 - t_2{}^2 = \frac{H_{3_{cs}}(H_{3_{ds}}-H_{3_{cs}})}{H_{3_{ds}}{}^2} B^\alpha r^\alpha . \qquad\qquad 6.3.9.$$

Again the factor B is chosen in such a way that

$$r=1 \qquad\qquad \text{for } B{\leq}1, \qquad\qquad 6.3.10.$$

and

$$H_{3_{ds}} t_2{}^2 = H_{3_{cs}} t_1{}^2 \qquad \text{for } B{\geq}1. \qquad\qquad 6.3.11.$$

The t_1, t_2 vs. B relationships show a similar behaviour as the t_1, t_2 vs. A_1 relationships discussed in section 6.2. However, the

definitions of the parameters A_1 and B are different, implying a different relation between L, D, $\dot{n}_t$, and T_i.

As stated before, the pressure difference p_1-p_2 will be negligible in the situation of dominant mutual friction. Hence, level differences between the two phase boundaries in MCI and MCII will be very small.

In accordance with section 5.2, the value of the term β/t^2 determines whether the viscous force or the mutual friction force is dominant. Using Eqs.(5.2.13.) and (5.2.14.), this ratio term can be calculated for the flow through Z_1, yielding

$$\beta/t^2 = 1.27\times10^{-6}\ [D/(\dot{n}_1 T_1)]^2\ .\qquad\qquad 6.3.12.$$

In the situation that $\beta/t^2 \ll 1$, mutual friction is the dominant force and the DMC properties are given by the set of equations (6.3.7-9.). For $\beta/t^2 \gg 1$ the viscous force plays the dominant role and the DMC properties are described by Eqs.(6.2.8-10.). When both the viscous and the mutual friction force are equally important, the DMC properties will be described by a set of equations similar to Eqs.(6.3.1-5.). However, in these situations both a gradient in pressure and in ^{4}He chemical potential will be present in Z_1, and Eqs.(6.2.5.) and (6.3.5.) have to be replaced by more complicated $T-\dot{n}_1$ relationships.

6.4 _Experimental set-up and results_

The experiments indicated at the end of section 6.2 were performed with a double mixing chamber installed in the dilution refrigerator described in section 3.1. The two mixing chambers were made of stainless steel cylinders (inner diameter 30 mm; length 100 mm), and were suspended at equal heights. The temperatures T_1, T_2, and T_i were measured in the liquid with calibrated resistance and CMN thermometers. The inlet temperature T_i could be varied by supplying heat to the inlet tube with the heater described in section 3.2. The flow impedance Z_1 usually was installed at the entrance of the dilute exit tube of the first mixing chamber (see figure 6.1.1). The exit tubes of the first and

second mixing chamber had an inner diameter of 4.6 mm.

The levels of the phase boundaries in the two mixing chambers could be determined by capacitive level meters (figure 6.4.1) attached vertically to the tops of the mixing chambers. They consisted of two concentric metal cylinders with an axial slit in order to give the liquids free access to the annular region. For calibration of the level meters, the levels of the phase boundaries were varied externally by varying the total amount of ^{3}He in the dilution refrigerator. The calibration is deduced from the capacitances, with the phase boundaries completely below and completely above the detectors, respectively. Level changes as small as 50 μm could be detected.
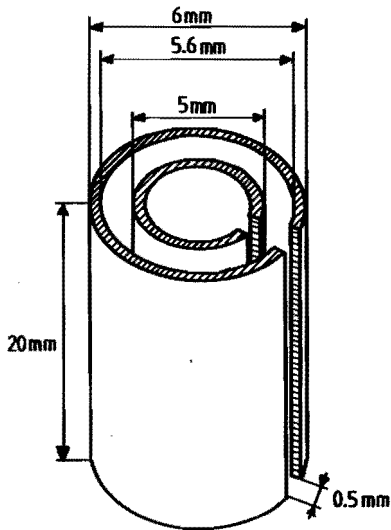
Fig. 6.4.1   Capacitor used for measuring the level of the phase
             boundary. The capacitance was about 10 pF.

The results obtained with this experimental set-up are reported here in terms of temperatures and level differences.

A   Temperatures
     The temperatures in the first and second mixing chamber, T_1

and T_2, were measured as functions of $\dot{n}_t$ and T_i, for various tube sizes. In the situation of a small flow resistance Z_1 (small L, large D), kinks in the $T-\dot{n}_t$ relationships could be observed. In figures 6.4.2 and 6.4.3 the measured values of the reduced temperatures t_1 and t_2 are plotted versus the dimensionless parameters A_1 and B respectively, for a tube Z_1 with L=5 mm and D=1.6 mm. Figure 6.4.2 shows that the experimental t_1, t_2 versus A_1 relationships are $\dot{n}_t$ dependent, contrary to the results obtained in section 6.2. On the other hand, figure 6.4.3 shows that the relationships between the

Fig. 6.4.2   *Measured t_1 (solid symbols) and t_2 (open symbols) for a tube Z_1 with L=5 mm and D=1.6 mm, plotted as functions of the parameter A_1. The value of T_i was varied at four different flow rates [0.14 (◊); 0.48 (○); 1.03 (□); 1.75 (△) in mmol/s].*

99

reduced temperatures and B are $\dot{n}_t$ independent, in agreement with the prediction for the situation of dominant mutual friction. The latter requires that the value of $\beta/t^2 < 1$ (with $t = T_1/T_\delta$ and $\dot{n}_3 = r\dot{n}_t$), for the experiments presented in figures 6.4.2 and 6.4.3. In table 6.4.1. the value ranges of B, β, and β/t^2 are given for the different points plotted in the figures.
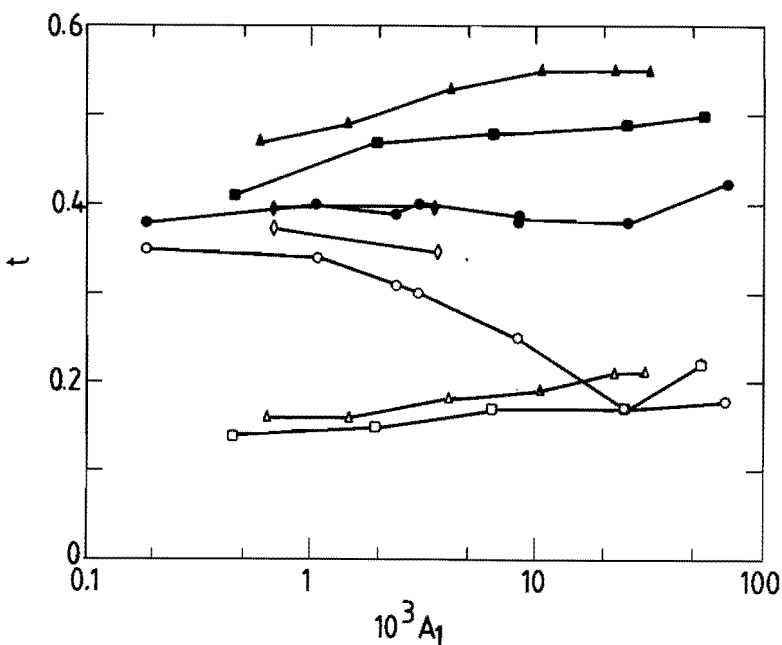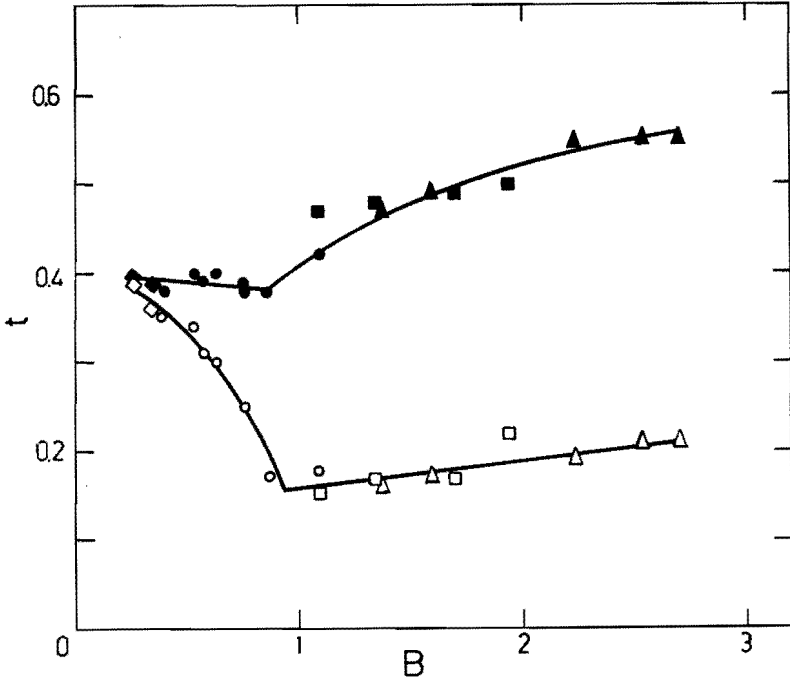

Fig. 6.4.3   Measured t_1 (solid symbols) and t_2 (open symbols) for a tube Z_1 with $L=5$ mm and $D=1.6$ mm, plotted as functions of the parameter B. The value of T_i was varied at four different flow rates [0.14 ($\lozenge$); 0.48 ($\circ$); 1.03 ($\square$); 1.75 ($\triangle$) in mmol/s].

$\dot{n}_t$	B	β	$\beta/t2$
0.14	0.2-0.4	80-100	0.2-1.2
0.48	0.6-1.1	1.6-3.6	0.004-0.1
1.04	0.8-2.0	0.3-1.3	0.001-0.02
1.75	1.4-2.7	0.2-0.6	0.0005-0.01

Table 6.4.1. *The value ranges of B, β, and $\beta/t_1{}^2$ for the different flow rates used (mmol/s).*

It is shown that indeed $\beta/t^2 \ll 1$ except for the points with

$\dot{n}_t = 0.14$ mmol/s. However for these points $B \ll 1$ and $t_1 \simeq t_2$. In this limit the two mixing chambers behave as one single mixing chamber in both models.

B   Level differences

The phase-boundary-level difference was measured as a

function of $\dot{n}_t$ and T_1 for a number of different tube dimensions and double-mixing-chamber geometries. In general, tubes were chosen resulting in values of A_1 on the order of 2 in the T_1 region. As mentioned in section 6.2, the measured Δh was usually of the order of 1 mm, much smaller than values on the order of 10 cm calculated from Eqs.(6.2.12.) and (6.2.13.). Sometimes even negative values of Δh were observed. Furthermore, the small Δh values were dependent on the place where Z_1 was mounted in the DMC system. The observed Δh values correspond to pressure differences across Z_1 of the order of 1 Pa, comparable with the observed pressure differences in a single mixing chamber system with no superleak shunt across the flow impedance. In figure 6.4.4

measured Δh-T_1 dependences for several values of $\dot{n}_t$ are given for the tube with L=5 mm and D=1.6 mm. In this figure the Δh-T_1 relationship, calculated with Eqs.(6.2.12.) and (6.2.13.) for this

tube with $\dot{n}_t = 1$ mmol/s, is also presented. From table 6.4.1. it can

be concluded that for this tube in our flow rate region mutual
friction is dominant and thus the pressure drops across Z_1 will be
smaller than expected from Eqs.(6.2.12.) and (6.2.13.).
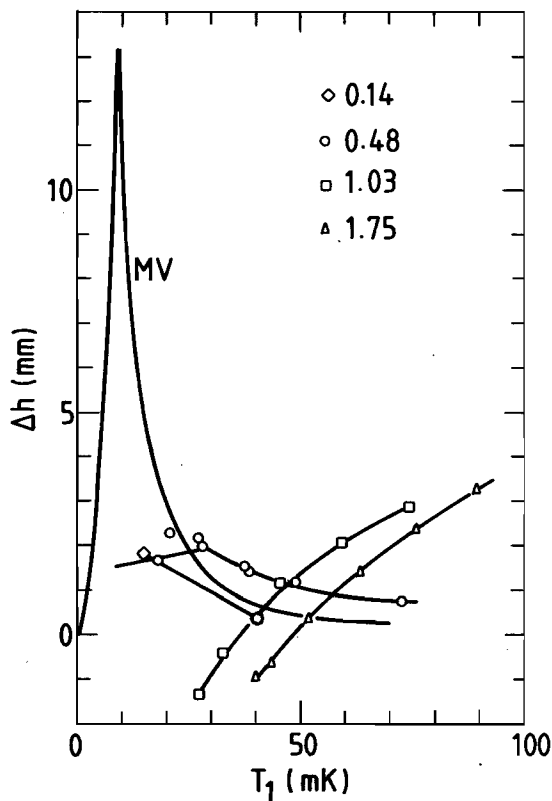
Fig. 6.4.4   *Results of Δh-T_1 dependences measured with a tube Z_1,*
with L=5 mm and D= 1.6 mm for four different values

of $\dot{n}_t$ given in the inset. The lines connecting the
points are to guide the eye only. The curve labeled
MV represents the Δh-T_1 dependence according to
Eq.(6.2.12.), calculated with $\dot{n}_t$=1mmol/s. It should
be compared with the squares in the figure.

Although no significant level differences were observed in a
DMC system installed in the dilution refrigerator described in

this thesis, there was indirect evidence that Δh had the correct value in a small dilution refrigerator with an average total flow rate of 50 μmol/s. The temperature reached in the first mixing chamber was 15 mK. The flow impedance Z_1 had a length of 140 mm and a diameter of 0.8 mm. With Eq.(6.3.12.) and the condition

$\dot{n}_1 \leq \dot{n}_t$, the value of β/t^2 can be estimated:

$\beta/t^2 \geq 1.27 \times 10^{-6} \ D^2/(\dot{n}_t T_1)^2 = 1.6$. This value of β/t^2 shows that in this experiment viscous forces dominated, hence, level differences according Eqs.(6.2.12.) and (6.2.13.) should be expected.

In conclusion, mutual friction determines the DMC flow properties in certain flow rate density and temperature regions. Similar to the single-mixing-chamber description, the value of the dimensionless parameter β/t^2 determines whether mutual friction or the viscous forces are dominant.

REFERENCES

Alv75   Alvesalo, T.A., Collan, H.K., Loponon, M.T.,
         Lounasmaa, O.V., and Veuro, M.C., J. Low Temp. Phys. **19**,
         1 (1975).

And66   Anderson, P.W., Rev. Mod. Phys. **38**, 298 (1966).

Bet76   Betts, D.S., *Refrigeration and Thermometry below 1K*,
         (Sussex Univ. Press., 1976).

Bla71   Black, M.A., Hall, H.E., and Thompson, K., J. Phys. C **4**,
         129 (1971).

Bru75   Bruschi, L. and Santini, M., Rev. Sci. Instrum. **46**,
         1560 (1975).

Car83   Carless, D.C., Hall, H.E., and Hook, J.R., J. Low Temp.
         Phys. **50**, 583 (1983).

Cas85   Castelijns, C.A.M., Kuerten, J.G.M., Waele, A.T.A.M. de,
         and Gijsman, H.M., Phys. Rev. B **32**, 2870 (1985).

Coo79   Coops, G.M., Waele, A.T.A.M. de, and Gijsman, H.M.,
         Cryogenics **19**, 659 (1979).

Coo81   Coops, G.M., Thesis, Eindhoven University of
         Technology, (1981).

Coo82   Coops, G.M., Waele, A.T.A.M. de, and Gijsman, H.M.,
         Phys. Rev. B **25**, 4879 (1982).

Das64   Das, P., Bruyn Ouboter, R. de, and Taconis, K.W., in
         *Proceedings of the IXth International Conference on Low
         Temperature Physics, Columbus, Ohio, 1964*, edited by
         J.G. Daunt, D.O. Edwards, F.J. Milford, and M. Yagub
         (Plenum, New York, 1965), p. 1253.

DeL71   DeLong. L.E., Symko, O.G., and Wheatley, J.C., Rev. Sci.
         Instrum. **42**, 147 (1971).

Ebn71   Ebner, C. and Edwards, D.O., Phys. Reports **2C**, 77
         (1971).

Fro77   Frossati, G., Godfrin, H., Hebral, B., Schumacher, G.,
         and Thoulouze, D., in *Physics at Ultralow Temperatures,
         Proceedings of the International Symposium at Hakone*,
         edited by P. Sugawara (Physical society of Japan, Tokyo,
         1977). p. 205.

Fro78   Frossati, G., Journal de Physique, Colloq. C6, suppl.8, **39**, 1578 (1978).

Gor49   Gorter, C.J. and Mellink, J.H., Physica **15**, 285 (1949).

Gue83   Guenault, A.M., Keith, V., Kennedy, C.J., and Pickett, G.R., Phys. Rev. Lett. **50**, 522 (1983).

Gug85   Guggenheim, E.A., *Thermodynamics*, (North-Holland Physics Publishing, Amsterdam, 1985).

Gho79   Ghozlan, A. and Varoquaux, E., Annales de Physique **4**, 384 (1979).

Hae79a   Haeringen, W. van, Staas, F.A., and Geurst, J.A., Philips J. Res. **34**, 107 (1979).

Hae79b   Haeringen, W. van, Staas, F.A., and Geurst, J.A., Philips J. Res. **34**, 127 (1979).

Hae80   Haeringen, W. van, Cryogenics **20**, 153 (1980).

Hoj80   Hojgaard Jensen, H., Smith, H., Wolfle, P., Nagai, K., and Maack Bisga T., J. Low Temp. Phys. **41**, 473 (1980).

Kha65   Khalatnikov, I.M., *An Introduction to the Theory of Superfluidity*, (Benjamin, New York, 1965).

Kie76   Kierstead, H.A., J. Low Temp. Phys. **24**, 497 (1976).

Kue72   Kuenhold, K.A., Crum, D.B., and Sarwinski, R.E., Phys. Lett. **41A**, 13 (1972).

Kue85   Kuerten, J.G.M., Castelijns, C.A.M., Waele, A.T.A.M. de, and Gijsman, H.M., Cryogenics **25**, 419 (1985).

Kue86   Kuerten, J.G.M., Castelijns, C.A.M., Waele, A.T.A.M. de, and Gijsman, H.M., Phys. Rev. Lett. **56**, 2288 (1986).

Lan48   Landau, L.D and Pomeranchuk, I., Dokl. Akad. Nauk SSR **59**, 668 (1948).

Lan59   Landau, L.D. and Lifshitz, E.M., *Fluid Mechanics*, (Pergamon, New York, 1959).

Lon51   London, H., in *Proceedings of the International Conference on Low Temperature Physics,Oxford, 1951*, (Clarendon Lab., 1951), p. 157.

Lon54   London, F., *Superfluids. Vol.I Superconductivity*, Vol.II, *Superfluid Helium*, (1954; reprinted, Dover, New York, 1964).

Lon62   London, H., Clarke, G.R., and Mendoza, E., Phys. Rev. **128**, 1992 (1962).

Lon68   London, H., Berks, H., Phillips, D., and Thomas, G.P., in *Proceedings of the IIth International Conference on Low Temperature Physics, St Andrews, 1968*, edited by J.F. Allen, D.M. Finlayson, and D.M. McCall (St. Andrews 1968), p. 649.

Lou74   Lounasmaa, O.V., *Experimental Principles and Methods below 1K*, (Acad. Press. London, 1974).

McC84   McClintock, P.V.E., Meredith, D.J., and Wigmore, J.K., *Matter at Low Temperatures*, (Blackie and Son, Glasgow, 1984).

Nii71   Niinikoski, T.O., Nucl. Instrum. Methods **97**, 95 (1971).

Put74   Putterman, S.J., *Superfluid Hydrodynamics*, (North-Holland Publishing Company, Amsterdam, 1974).

Rad67   Radebaugh, R., NBS Technical Note **362** (1967).

Ray64   Rayfield, G.W. and Reif, F., Phys. Rev. **136**, A1194 (1964).

Sch80   Schooley, J.F., Evans, G.A. Jr., and Soulen, R.J. Jr., Cryogenics **20**, 193 (1980).

Tac82   Taconis, K.W., Physica **109** & **110B**, 1753 (1982).

Tou64   Tough, J.T., McCormick, W.D., and Dash, J.G., Rev. Sci. Instrum. **35**, 1345 (1964).

Tou82   Tough, J.T., in *Progress in Low Temperature Physics VIII*, edited by D.F. Brewer (North-Holland, Amsterdam, 1982), p. 133.

Vin61   Vinen, W.F., in *Progress in Low Temperature Physics III*, edited by C.J. Gorter (North-Holland, Amsterdam, 1961), p. 1.

Wae76   Waele, A.T.A.M. de, Reekers, A.B., and Gijsman, H.M., in *Proceedings of the Sixth International Cryogenic Conference, Grenoble, 1976*, edited by K. Mendelsohn (IPC Science and Technology, Guildford, England, 1976), p. 112.

Wae77   Waele, A.T.A.M. de, Reekers, A.B., and Gijsman, H.M., in *Quantum Fluids and Solids*, edited by S.B. Trickey, E.D. Adams, and J.W. Dufty (Plenum, New York, 1977), p. 451.

Wae78   Waele, A.T.A.M. de, Coops, G.M., and Gijsman, H.M., Journal de Physique **8**, C6-1150 (1978).

Wae80   Waele, A.T.A.M. de, Coops, G.M., Satoh, T., and Gijsman, H.M., in *Proceedings of the Eighth International Cryogenic Engineering Conference, Genova 1980*, edited by C. Rizzuto (IPC Science and Technology, Guildford, England, 1980), p. 451.

Wae82   Waele, A.T.A.M. de, Geest, G.J. van der, Levels, H.P.L., and Gijsman, H.M., in *Proceedings of the Ninth International Cryogenic Engineering Conference, Kobe, Japan 1982*, edited by Yasukochi and Nagano (Butterworth, Guildford, England, 1982), p. 625.

Wae83   Waele, A.T.A.M. de, Keltjens, J.C.M., Castelijns, C.A.M., and Gijsman, H.M., Phys. Rev. B **28**, 5350 (1983).

Wat69   Watson,G.E., Reppy, J.D., and Richardson, R.C., Phys. Rev. **188**, 384 (1969).

Whe68a   Wheatley, J.C., Am. J. Phys. **36**, 181 (1968).

Whe68b   Wheatley, J.C., Vilches, O.E., and Abel, W.R., Physics **4**, 1 (1968).

Whe71   Wheatley, J.C., Rapp, R.E., and Johnson, R.T., J. Low Temp. Phys. **4**, 1 (1971).

Wil67   Wilks, J., *The properties of liquid and Solid Helium*, (Clarendon Press, Oxford,1967).

SUMMARY

The flow properties of ^{3}He, moving in dilute ^{3}He-^{4}He mixtures
at temperatures between 10 and 150 mK, are studied experimentally
in a ^{3}He circulating dilution refrigerator with a flow rate
ranging between 0.13 and 2.5 mmol/s. Temperature, pressure and
^{3}He-concentration variations across tubes are measured as
functions of the flow rate and the tube sizes. The flow tube
usually constitutes the dilute exit tube of the mixing chamber.
The diameter of the respective tubes under investigation varies
between 0.3 and 5 mm. In the experiments described the ^{3}He
velocities are limited to values ranging from 6 to 40 cm/s, far
below the Landau critical velocity for roton excitation
($\approx$140 m/s). Under these conditions, flow properties of dilute
^{3}He-^{4}He mixtures are usually described in the framework of the
mechanical vacuum (MV) model. In this model, outlined in chapter
II, the ^{4}He is treated as a vacuum in which ^{3}He moves as a fluid
with a certain viscosity but, without friction resulting from the
^{4}He background.

Experimental results, obtained with the set-up described in
chapter III, and discussed in chapter IV, yield a set of empirical
relations for the ^{3}He flow properties which is at variance with
the MV-model. This is most clearly visualized by the observation
of a non-zero gradient in the ^{4}He chemical potential in the liquid
in the tubes. The dependence of the gradient in μ_4 on the ^{3}He flow
rate density, is similar to μ_4-dependence observed in ^{4}He II
counterflow experiments.

In chapter V, the experimental results are analysed taking
into account a viscous force between the ^{3}He quasiparticles, as
well as a mutual friction force between ^{3}He and ^{4}He. The latter is
expressed by a relation which is similar to the Gorter-Mellink
relation, giving the mutual friction force density in pure ^{4}He II.
In this way, a good description of the observed phenomena can be
given.

Furthermore, experiments are discussed, simultaneously
showing the influences of the viscous force and the mutual

friction. Depending on the flow channel geometry, the ^{3}He flow rate and the temperature of the liquid, either one of the forces can dominate the other, or both forces can be of equal importance.

In the final chapter, the performance of a double mixing chamber system is discussed. Experimental results, which were obtained in a previous investigation, are reanalysed with the help of the relations derived in chapter V. Like the results discussed in chapters IV and V, these experimental results are in agreement with the description of the ^{3}He flow properties including mutual friction too.

In conclusion, the relations taking into account both a viscous force and a mutual friction force, give a good description of the ^{3}He flow properties in dilute ^{3}He-^{4}He mixtures. These relations are of crucial importance for the design of dilution refrigerators, and theoretical description of ^{3}He-^{4}He flow properties.

SAMENVATTING

De eigenschappen van ^{3}He stroming in verdunde ^{3}He-^{4}He
mengsels, bij temperaturen tussen 10 en 150 mK, zijn experimenteel
onderzocht in een ^{3}He circulerende mengkoeler met een
circulatiesnelheid tussen 0,13 en 2,5 mmol/s. Variaties in
temperatuur, druk en ^{3}He-concentratie over een stromingskanaal
zijn gemeten als functie van de stroomsnelheid en de afmetingen
van het kanaal. In de meeste gevallen is het kanaal tevens de
uitstroombuis voor het ^{3}He dat de mengkamer verlaat. De inwendige
diameter van de kanalen varieert van 0,3 tot 5 mm. In de hier
beschreven experimenten ligt de snelheid van het ^{3}He in de buis
tussen de waarden 6 en 40 cm/s. Deze liggen ver beneden de Landau
kritische snelheid voor roton exitatie ($\approx$140 m/s). Onder deze
omstandigheden worden de stromingseigenschappen in verdunde
^{3}He-^{4}He mengsels vaak beschreven met het mechanisch vacuüm (MV)
model. In dit model, beschreven in hoofdstuk II, wordt het ^{4}He
beschouwd als een vacuüm, waarin het ^{3}He zich als een viskueze
vloeistof beweegt, die echter geen wrijving van het ^{4}He
ondervindt.

Uit de meetresultaten, verkregen met de opstelling zoals
gegeven in hoofdstuk III, en die besproken worden in hoofdstuk IV,
volgen, voor de beschrijving van de ^{3}He stroming, empirische
relaties die strijdig zijn met het MV-model. Deze tegenspraak komt
het duidelijkst tot uiting in een waargenomen gradiënt in de
chemische potentiaal van het ^{4}He in het stromings- kanaal. De
afhankelijkheid van deze gradiënt van de ^{3}He-snelheid vertoont
overeenkomst met de μ_4-afhankelijkheid zoals is waargenomen in
experimenten waarin de superfluïde en de normale component in
zuiver ^{4}He II tegen elkaar in stromen.

In hoofdstuk V worden de meetresultaten geanalyseerd onder de
veronderstelling dat de stroming van het ^{3}He in verdunde mengsels
beïnvloed wordt door zowel een viskeuze kracht tussen de ^{3}He
deeltjes onderling, alsmede door een wederkerige wrijving tussen
^{3}He en ^{4}He. De aanwezigheid van wederkerige wrijving wordt tot
uitdrukking gebracht door een relatie analoog aan de
Gorter-Mellink vergelijking voor de wederkerige wrijvingskracht-

dichtheid in zuiver ^{4}He II. Het blijkt dat op deze manier een goede beschrijving van de waargenomen stromingsverschijnselen kan worden gegeven.

In hoofdstuk V worden ook enkele experimenten besproken waarmee zowel de viskeuze kracht als de wederkerige wrijving gelijktijdig kunnen worden aangetoond. Afhankelijk van de geometrie van het stromingskanaal, de snelheid van het ^{3}He en de temperatuur van de vloeistof, kan een van beide krachten de andere overheersen, of kunnen beide krachten een gelijkwaardige invloed op de stroming uitoefenen.

In het zesde en laatste hoofdstuk wordt de werking van een dubbele mengkamer besproken. Meetresultaten, verkregen in een eerder uitgevoerd onderzoek, worden opnieuw geanalyseerd, nu met behulp van de stromingsrelaties afgeleid in hoofdstuk V. Evenals de resultaten besproken in de hoofdstukken IV en V, zijn ook deze, experimenteel verkregen, gegevens in overeenstemming met de beschrijving van de stromingseigenschappen van het ^{3}He waarbij rekening is gehouden met de aanwezigheid van een wederkerige wrijving.

Geconcludeerd kan worden dat de stromingsrelaties, waarin zowel rekening wordt gehouden met viskeuze krachten als met wederkerige wrijvingskrachten, een goede beschrijving geven van de stroming van ^{3}He in verdunde ^{3}He-^{4}He mengsels. Deze relaties zijn van belang voor het ontwerp van mengkoelers, en de theoretische beschrijving van stroming van ^{3}He-^{4}He mengsels.

112

NAWOORD

Het in dit proefschrift beschreven werk is uitgevoerd in de groep Kryogene Technieken, o.l.v. Prof. Dr. H.M. Gijsman, van de afdeling der Technische Natuurkunde van de Technische Hogeschool Eindhoven. Aan het tot standkomen van dit proefschrift is een bijdrage geleverd door een groot aantal personen, van wie ik er op deze plaats graag enkele met name wil noemen, zonder hiermee volledigheid te betrachten.

-Dr. *A.T.A.M de Waele* heeft, als mijn direkte begeleider, mij steeds op stimulerende wijze bijgestaan. De samenwerking met hem heb ik als bijzonder prettig ervaren.
-Drs. *J.M.G. Kuerten* heeft met zijn kennis van de theoretische natuurkunde een grote bijdrage aan het onderzoek geleverd. Het was mij zeer aangenaam hem als kamergenoot te mogen hebben.
-Van *L.M.W. Penders en L.C. van Hout* heb ik de nodige technische ondersteuning gekregen, die mij steeds zeer welkom is geweest. Zij droegen in hoge mate bij tot de prettige werksfeer binnen de groep.
-Zonder de levering van de grote hoeveelheden vloeibaar helium en vloeibare stikstof, die *J.J.G.M. van Amelsvoort en W.C.T.H. Delissen* steeds op tijd verzorgden, had dit onderzoek nooit uitgevoerd kunnen worden. Ook de regelmatige verzorging van de inwendige mens was bij hen in goede handen.
-Dr. *G.R. Pickett and Dr. A.M. Guénault*, have made my two months visit at the Low Temperature Laboratory of the University of Lancaster a very instructive and enjoyable one.

Verder wil ik iedereen bedanken die mij op enigerlei wijze heeft geholpen tijdens mijn promotieonderzoek, met name alle stagiairs en afstudeerders waarmee ik heb samengewerkt.

CURRICULUM VITAE

04-12-1956   Geboren te Tilburg.

juni 1975   Eindexamen Atheneum B, aan de Rijksscholengemeenschap
              "Koning Willem II" te Tilburg.

sept. 1975   Aanvang studie Technische Natuurkunde aan de THE.

dec. 1979-   Student-assistentschap THE.
dec. 1980

juni 1982   Doctoraal examen natuurkundig ingenieur aan de THE.
              Afstudeerwerk verricht in de groep Cyclotron-
              toepassingen o.l.v. Prof. Dr. Ir. H.L. Hagedoorn.

aug. 1982-   Werkzaam als wetenschappelijk assistent aan de THE
aug. 1986   in de groep Kryogene Technieken o.l.v. Prof. Dr.
              H.M. Gijsman.

mei 1985-   Verblijf aan het Department of Physics, University of
juni 1985   Lancaster, Lancaster, UK.

114

STELLINGEN

behorende bij het proefschrift van

C.A.M. Castelijns

Eindhoven, 5 september 1986

1. De stromingseigenschappen van ^{3}He in verdunde ^{3}He-^{4}He
    mengsels kunnen bijdragen tot de bestudering van de
    eigenschappen van een ^{4}He vortex tangle.
    Castelijns, C.A.M., Kuerten, J.M.G., de Waele, A.T.A.M., en
    Gijsman, H.M., Phys. Rev. B, 32 2870 (1985).

2. Alhoewel de stroming in een ^{3}He circulerende mengkoeler
    beïnvloed wordt door zowel viskeuze als wederkerige
    wrijvingskrachten, wordt de theoretische intrinsieke lage
    temperatuur limiet beschreven met behulp van het
    mechanisch-vacuüm model.
    Waele, A.T.A.M. de, Keltjens, J.C.M., Castelijns, C.A.M.,
    en Gijsman, H.M., in Advances in Cryogenic Engineering,
    edited by R.W. Fast (Plenum, New York, 1984), Vol.29, p.625.

3. De werking van een ^{4}He circulerende mengkoeler kan niet
    op de juiste wijze beschreven worden zonder rekening te
    houden met een wederkerige wrijving tussen ^{3}He en ^{4}He.

4. De door Buchenauer en Jacobson voorgestelde methode voor het
    meten van snelle en grote variaties in de brekingsindex van
    gassen en plasma's m.b.v. een gemodificeerde Mach-Zehnder
    interferometer, is onnodig ingewikkeld.
    Buchenauer, C.J. en Jacobson, A.R., Rev. Sci. Instrum.
    48, 769 (1977).

5. Het feit dat Barenghi et al. bij hun experimenten, in
    tegenstelling tot anderen, geen hinder ondervinden van de
    eindige ontsnappingskans van elektronen uit een
    twee-dimensionale elektronenlaag onder een vloeibaar
    heliumoppervlak, gegenereerd m.b.v. een ondergedompelde
    veldemitterpunt, behoeft een nadere uitleg.
    Barenghi, C.F., Mellos, C.J., Muirhead, C.M., en Vinen,
    W.F., J. Phys. C, Solid State Phys. 19, 1136 (1986).

6. Ten onrechte suggereert Hansen dat, bij vaste frequentie, de minimale magneetveldwaarde voor cyclotronresonantie voor de niet-parabolische banen van het $E(1+E/E_g)$ type in bismuth, correspondeert met centrale overgangen.

   Hansen, O.P., Physica 138B, 7 (1986).

7. Bij het gebruik van een trillende-draad-viscositeitsmeter moet men bedacht zijn op acoustische effecten die de eigenschappen van het systeem kunnen beïnvloeden.

   Tough, J.T., McCormick, W.D., en Dash, J.G., Rev. Sci. Instrum. 35 1345 (1964).

8. Uit het gedrag van de soortelijke warmte van $Hg_{1-x}Mn_xTe$ en $Cd_{1-x}Mn_xTe$ trekken Nagata et al. en Galazka et al. de conclusie dat de Mn-ionen niet-statistisch verdeeld zijn. Ten onrechte hebben zij echter de long-range interaktie buiten beschouwing gelaten.

   Nagata, S., Galazka, R.R., Mullin, D.P., Akbarzadeh, H., Khattak, G.D., Furdyna, J.D., en Keesom, P.H., Phys. Rev. B22, 3331 (1980).

   Galazka, R.R., Shoichi Nagata, en Keesom, P.H., Phys. Rev. B22, 3344 (1980).

9. De uitgave van een compact disc met authentieke LP-ruis mag over enkele jaren verwacht worden.